ERDC/GSL TR-22-22

US Army Corps
of Engineers®
Engineer Research and
Development Center

ERDC
ENGINEER RESEARCH & DEVELOPMENT CENTER

Stability Analysis of Old River Low Sill Structure

Lucas A. Walshire, Joseph B. Dunbar,
and Benjamin R. Breland

September 2022

Geotechnical and Structures Laboratory

The U.S. Army Engineer Research and Development Center (ERDC) solves the nation's toughest engineering and environmental challenges. ERDC develops innovative solutions in civil and military engineering, geospatial sciences, water resources, and environmental sciences for the Army, the Department of Defense, civilian agencies, and our nation's public good. Find out more at www.erdc.usace.army.mil.

To search for other technical reports published by ERDC, visit the ERDC online library at https://erdclibrary.on.worldcat.org/discovery.

ERDC/GSL TR-22-22
September 2022

Stability Analysis of Old River Low Sill Structure

Lucas A. Walshire, Joseph B. Dunbar, and Benjamin R. Breland

Geotechnical and Structures Laboratory
U.S. Army Engineer Research and Development Center
3909 Halls Ferry Road
Vicksburg, MS 39180-6199

Final report

Prepared for New Orleans District (CEMVN)
New Orleans, LA 70160

Under Project 478533, "Old River Low Sill Structure Stability Investigation" (MIPR PA WI 1L8F7L)

Abstract

An updated stability analysis was performed on the Old River Low Sill Structure due to a change in the operating conditions from historic river sedimentation. Sedimentation of the Mississippi River channel since the 1973 spring flood has caused higher river stages at lower discharges. Numerical methods used included nonlinear analysis of pile group stability, seepage analyses, and limit equilibrium methods. The structure's foundation was compromised during the 1973 flood, and emergency repairs were conducted to prevent scouring and undermining of the foundation by the flood scour. Rehabilitation included the reconstruction of a failed wing wall on the left abutment, rock and riprap fill in the forebay channel, and emergency grouting to fill the scour hole beneath the structure. An operating restriction was emplaced to limit the differential head across the structure due to flood damage. Taking these conditions into account, results from an updated analysis showed that full headwater uplift caused increased tension in the piles, while the increased body load caused increased compressive loads in the piles. Review of piezometric monitoring and the seepage analyses showed that full headwater uplift is unlikely, indicating the foundation grouting adequately sealed the scour hole beneath the structure. Analysis results exhibited lower magnitude compression and tension loads in the piles with design load cases compared to previous analyses. Recommendations from these analyses indicate that increased monitoring and additional investigation may support increasing the differential head limitation.

Contents

Figures and Tables

Figures

Tables

Preface

This study was conducted for the U.S. Army Corps of Engineers New Orleans District (CEMVN-EDS) under Project Number 478533, MIPR PA WI 1L8F7L. The technical monitor was Mr. Craig B. Waugaman.

The work was performed by the Geotechnical Engineering and Geosciences Branch (GSG) of the Geosciences and Structures Division (GS), U.S. Army Engineer Research and Development Center, Geotechnical and Structures Laboratory (ERDC-GSL). At the time of publication, Mr. Christopher Price was Chief, GSG; Mr. James Davis was Chief, GS; and Dr. Michael K. Sharp, GZT, was the Technical Director for Civil Works. The Deputy Director of ERDC-GSL was Mr. Charles W. Ertle II, and the Director was Mr. Bartley P. Durst.

The Commander of ERDC was COL Christian Patterson, and the Director was Dr. David W. Pittman.

This report was revised 16 September 2022 for minor corrections. While it supersedes the previous version, the changes do not impact the reliability of the scholarly content.

1 Introduction

1.1 Background

The Old River Control Structure (ORCS) was authorized by the Flood Control Act of 1954, PL 780 under the 83rd Congress. Construction, initiated in October 1955, was accepted by the government in June 1959. Initially, the principal structures consisted of a low sill structure, an overbank structure, navigation lock, forebay and tailbay channels, earthen dam closing the Old River, main-line levee extensions, and bank stabilization along the Red and Atchafalaya rivers. An auxiliary structure was added to the ORCS in 1986 due to damage incurred at the low sill structure following a flood event in 1973.

A wet winter and subsequent flood in the spring of 1973 resulted in Mississippi River flows of 2,024,000 cfs* (project design flood is 2,720,000 cfs) and a maximum headwater elevation of 61.6 ft Mean Sea Level (msl) and tailwater elevation of 59.3 ft. Collapse of the left approach wing wall and a large scour hole on the upstream approach channel occurred. Rehabilitation of the structure included construction of a replacement approach wing wall with riprap and grouting the large void, which had scoured beneath the structure.

Following the 1973 flood and subsequent rehabilitation, a stability analysis was performed, and it found the stability of the structure was compromised; therefore, restrictions on the operating conditions were emplaced (USACE 1975a, 1975b). Through the following decades, this restriction was relaxed as subsequent inspection and monitoring showed adequate performance. Currently, the restriction consists of a 22-ft head differential between the headwater and tailwater. Originally, the structure was designed for a 35-ft head differential. Aggradation in the approach channel has resulted in increased headwater elevations during flooding,

* For a full list of the spelled-out forms of the units of measure used in this document, please refer to *U.S. Government Publishing Office Style Manual*, 31st ed. (Washington, DC: U.S Government Publishing Office, 2016), 248–252, https://www.govinfo.gov/content/pkg/GPO-STYLEMANUAL-2016/pdf/GPO-STYLEMANUAL-2016.pdf.

which has made maintaining flow distribution between the Mississippi and Atchafalaya river basins challenging.

The New Orleans District (CEMVN) is responsible for operating and maintaining the low sill structure, and the district requested personnel from the Engineer Research and Development Center (ERDC) to assess the stability of the Old River Low Sill Structure (ORLSS) under current-day conditions. Results of the ERDC geotechnical investigation are presented in this report.

1.2 Purpose and scope

The purpose of this investigation was to evaluate the existing stability analysis, perform a stability analysis using additional data, and recommend additional exploration and testing, or possible changes to the operating restrictions of ORLSS. This analysis is part of the periodic assessment of the structure's design due to changes in condition from historic channel aggradation, height restrictions imposed by the 1973 Flood, and nearly 60 yr of operational service since its construction. This report documents research results, summarizes activities performed to date in support of the investigation, and presents results obtained. An important focus of this effort was to accurately characterize the extent of scour damage beneath the structure resulting from the 1973 Flood and to determine the extent and properties of the grout volume in the area that was most affected.

An important effort of this study was to determine the number of piles affected by erosion and scouring, the horizontal and vertical extent of the pile exposure beneath the structure in the area of the scour hole, and the grouted properties of the repair section in relationship to the piles. This information was to be used in an updated stability analysis for various loading conditions.

1.3 Objectives

The objectives of this report were to provide a better understanding of the current level of stability of the LSS and how it compares to previous analyses performed. Results of this stability assessment will support modification of the current operating conditions for the differential head limitation currently in effect by the New Orleans District (MVN). An important goal of this study was to determine whether the possibility exists to increase or lift the differential head restriction in place to meet

the structure's original design objectives. The structure regulates flow from the Mississippi River such that 30% of the total flow passes down the Atchafalaya River and 70% down the Mississippi River. Additionally, MVN requested recommendations for further exploration and testing if there was information required to modify the current operating limitations.

1.4 Approach

Activities performed to support this effort involved a comprehensive literature review of ORCS documents to better understand the design of the structure and the extent of the repairs that were performed. Numerical analyses were performed to assess the stability of this structure with the currently understood foundation conditions. The numerical analyses included finite element seepage analysis, limit equilibrium stability analysis, finite difference seepage and stability, as well as a nonlinear analysis of pile response. Other studies involved review of the construction data and photographs, geologic data, design documents, periodic inspections, instruments including piezometer data and settlement gauges, data analysis, and preparation of this report.

1.5 Geographic setting, importance, and general history

The Old River Control Structure (ORCS) is located in Concordia Parish, LA, at Mississippi River mile 314.5 (Figure 1). The project was built between 1955 and 1958 and was fully operational by 1959 to prevent stream capture of the Lower Mississippi River by the Atchafalaya River. Full capture was estimated to have occurred when river flow into the Atchafalaya River basin was more than 40 percent of the Mississippi River's discharge. This event was predicted to occur by 1975 without construction of the ORCS (Latimer and Schweitzer 1951; Fisk 1952; Hardin 1958).

Figure 1. Location and primary features of the Old River Control Structure.

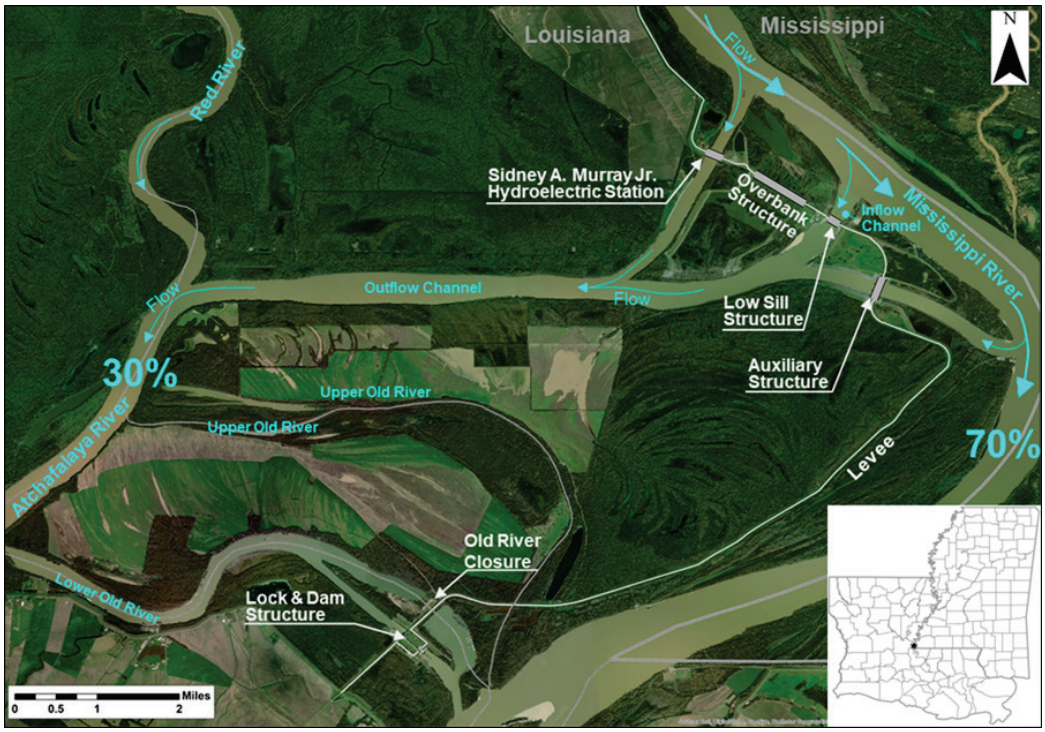

Geographically, the ORCS (low still structure, overbank structure, lock and dam, closure dams and levees) are strategically important structures because of their proximity and confluence to the Red, Atchafalaya, and the Mississippi rivers. Historically, this location has been an important entry point to these different rivers by steamship commerce since the early 1800s. The reach upstream of the mouth of the Red River was the focus of an intense effort to remove hundreds of miles of intermittent log jams otherwise known as “The Raft” beginning in 1821.

The raft was eventually removed by 1879 to permit steamship navigation upstream of Shreveport, LA. Work to remove the log jam was begun by Captain Shreve (USACE) and would take 58 yr to complete before a clear navigation channel was established above Shreveport (USACE 1910). Removal of the log jam on the Atchafalaya River for navigation purposes into the Atchafalaya basin would be accomplished much earlier, by 1860 (Reuss 1998). The cumulative effect of the raft removal and other improvements to navigation on the Red-Atchafalaya river systems would permanently enlarge the Atchafalaya River channel below Simmsport, LA, and eventually set the stage for increased stream capture of the Mississippi River by the Atchafalaya River unless preventative control measures were constructed (Figure 2).

Figure 2. Evolution of the ORCS by river migration and improvements to navigation (Fisk 1952).

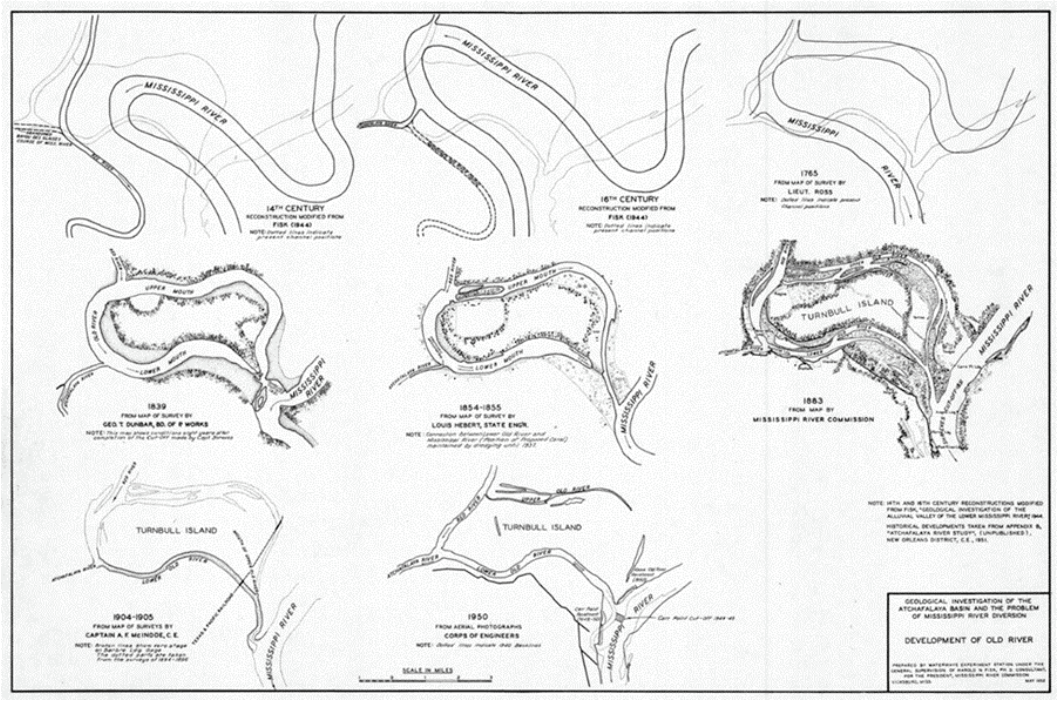

Reason for stream capture by the Atchafalaya River is due to the gradient advantage as compared to the longer course of the Mississippi River and the increased conveyance efficiency from raft removal and other improvements. The course through the Atchafalaya is 173 miles shorter than the current Mississippi River course. The distance to the Gulf of Mexico by way of the Atchafalaya River is 142 miles long as compared to 315 miles along the present-day course (USACE 2009). Currently, the ORCS regulates river flow into the Atchafalaya Basin to 30 percent of the combined Mississippi and Atchafalaya rivers' discharge.

Capture of the Mississippi River by the Atchafalaya River would be an economic and environmental disaster to river cities below Baton Rouge, as it would seriously affect navigation, freshwater supply to the city of New Orleans, utilities, and shipping along the industrial river corridor (Hardin 1958). A diversion of the river's course would create a salt-water estuary below Baton Rouge. Corporations have constructed billions of dollars of infrastructure consisting of manufacturing, petrochemical plants, refineries, grain elevators, fossil fuel, and nuclear power generating stations that are dependent on fresh water from the Mississippi River (USACE 2009).

1.6 1973 Flood and extent of emergency repairs

In April 1973, the Low Sill Structure (LSS) was seriously damaged by a major flood. Erosion and scouring in the approach channel resulted in the failure of the wing wall at the left abutment. Additionally, deep scouring along the left abutment extended beneath the foundation, resulting in the loss of sands beneath the structure and creation of a large void that exposed the steel piles supporting the structure. Damage to the structure also included the loss of the pressure relief systems in the foundation that were designed to help reduce uplift pressures that resulted from flood events.

Emergency repairs were immediately initiated. Repairs involved placing rock along the left abutment where the wing wall was located to prevent further erosion of the left abutment area. Additionally, the deep scour hole in the forebay was filled with stone to prevent the erosion from extending completely under the structure and connecting to the stilling basin. An emergency grouting program was subsequently initiated to fill the void beneath the structure, confined to gates 5 through 11. Repairs to the structure in 1973-74 have permitted the structure to operate safely but under a flow restriction based on a stability analysis conducted after the repairs (USACE 1975a, 1975b). Because of the economic and environmental consequences with the loss of this important structure, an auxiliary structure was authorized and constructed.

The auxiliary structure was built approximately one mile downstream of the LSS (Figure 1) to provide additional control in a design flood event and to provide backup capabilities in the event the LSS was closed due to maintenance and/or a navigation-related barge impact. Construction of the auxiliary structure was begun in July 1981 and completed in December 1986.

1.7 Historic channel aggradation

Channel aggradation has occurred in the Mississippi River reach adjacent to the LSS for as far back as reliable stage and discharge measurements are available (Winkley 1994). Consequently, LSS has witnessed higher water elevations for a given Mississippi River discharge. This channel aggradation is caused by a gradually decreasing slope in the river, which has a corresponding decline in the energy gradient available to carry coarse sediment.

The observed trend in higher water surfaces on the upstream side of the structure for a given discharge has further warranted a review of the stability analyses for the possible range of flow conditions. The following investigation is in support of the periodic stability evaluation. This evaluation updates previous analyses and specifically addresses the changes in loading conditions associated with higher river stages at lower discharges and the height restrictions imposed on the structure from the extensive foundation damage that occurred in 1973.

1.8 Previous stability reviews and analysis

Seven different seepage and slope stability analyses have been performed since ORLSS was designed and placed into operation (USACE 1954, 1967, 1969, 1971, 1975a, 1975b, and 1986). The current seepage and stability analysis will be the eighth analysis performed. The critical nature of this structure to prevent stream capture by the Atchafalaya River has necessitated periodic evaluations during its operational history to validate design loadings and any changes in condition through time.

Equally important for performing the periodic reviews is the technical advances that have occurred in geotechnical modeling and computational capabilities since the structure was designed and placed into service. Furthermore, an important part of the review process was to evaluate changes in the monitoring instruments that were added since the structure was placed into service, especially as many of the original instruments were damaged by the 1973 flood. Detailed summary of the different stability analyses performed is further described and summarized in Chapter 4 for better understanding of the different assumptions, computational models, and loading conditions that were used to evaluate the stability against a design event.

2 Geologic Setting

This chapter examines the foundation properties of the ORLSS site in terms of the underlying soils and geology. Maximum discharge capacity of ORLSS is 300,000 cfs or 135 million gpm. Table 1 shows the pertinent physical dimensions of the ORCS.

Table 1. Physical data involving the Old River Control Structures (USACE 2009).

Structure	Gates/Bays	Gate/Bay Width (ft)	Weir Crest Elevation (ft)	Total Length (ft)
Low Sill	11	44.0	-5.0 to 10.0	566.0
Overbank	73	44.0	52.0	3356.0
Auxiliary	6	62.0	5.0	442.0

The ORLSS and overflow structures were originally designed to accommodate a flow of 600,000 cfs from the Mississippi River during the project flood (Hardin 1958; Graves 1958). The addition of the Auxiliary structure and the Sidney A. Murray Jr. Hydroelectric Power Station to the ORLSS system is operated according to the hydraulic plan with the 30/70 regulated split distributed as required.

2.1 Geological investigation

The organization of this section is according to the original site exploration, geologic borings, and site selection.

2.1.1 Site exploration

The original site exploration plan was described by Mabrey and Steinreide (1949). Their report included geological mapping and a boring exploration program in the general vicinity of the Old River channel and Point Breeze to determine the optimal locations for the hydraulic structures identified in Figure 3.

Figure 3. ORCS candidate sites in comparison to the current location where locations A–D were candidate sites for the ORLSS (Mabrey and Steinreide 1949).

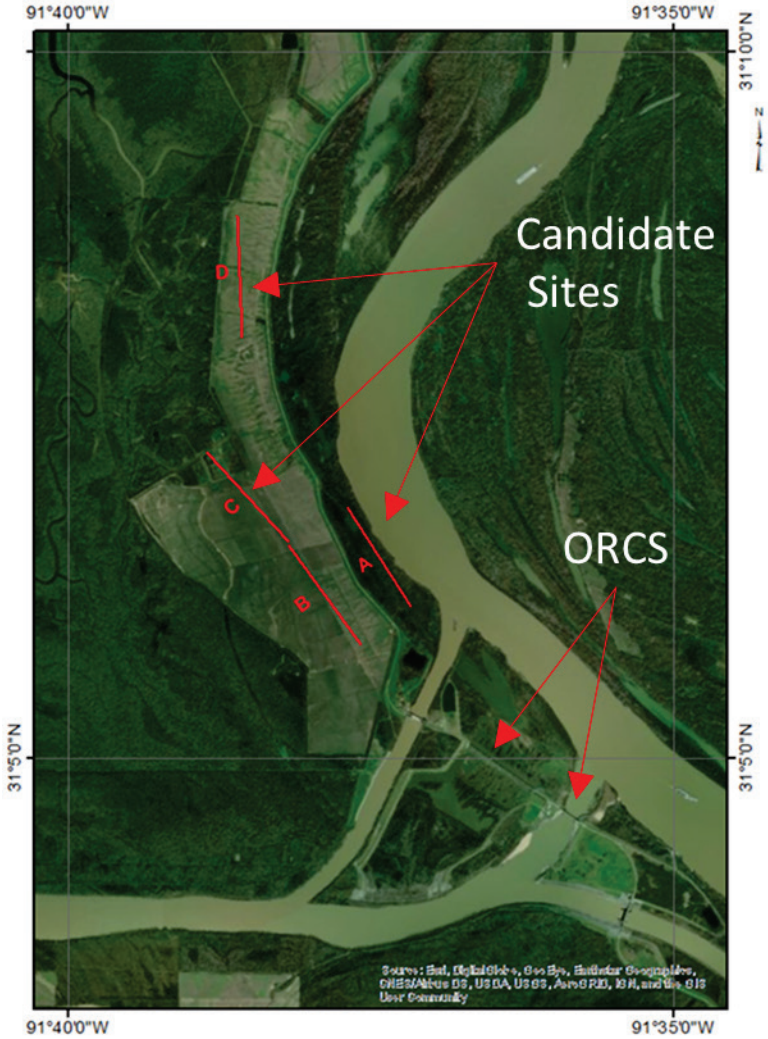

2.1.2 Geologic borings

The boring exploration program was performed by the Waterways Experient Station (WES), now known as ERDC, and MVN drill crews in 1949. The exploration program involved 78 exploratory borings comprised of 1 undisturbed type sample boring, general sample (split-spoon) type borings, and logs of 15 seismic shot holes. Their study was intended for siting the structures and not for design purposes. The foundation stratigraphy and depth to sand were important considerations in the site selection process. Also important was a stable site where bank caving by river migration was improbable (Graves 1958).

2.1.3 Site selection

Four locations (sites A through D) in Figure 3 were identified as candidate sites. However, the final site selected for the overbank structure and ORLSS was located further downstream from these locations (Figure 3). Moving the structure to its current position was based on geological and construction dewatering considerations (USACE 1954; Turnbull and Shockley 1958).

Fluvial depositional environments are identified in Figure 4 and show the spatial distribution of clay deposits at the surface. This sketch identifies point bar ridges, point bar swales, abandoned channels, and backswamp deposits. Turnbull and Shockley (1958) described this location as better suited for the final site because of the underlying soils in terms of dewatering during construction of the deep excavation and for controlling underseepage conditions after the structure was placed into service.

The structure was purposely located in the thick clay deposits (swale or abandoned channel), shown in Figure 4, so that the top of the pervious sands would be well below the bottom of the approach and outlet channels for the structure, thus avoiding potentially dangerous underseepage conditions and reducing the construction dewatering requirements (USACE 1953, 1954, 1963).

Figure 4. Clay deposits according to fluvial depositional environments and their spatial relationship to the Old River Control project structures (Turnbull and Shockley 1958).

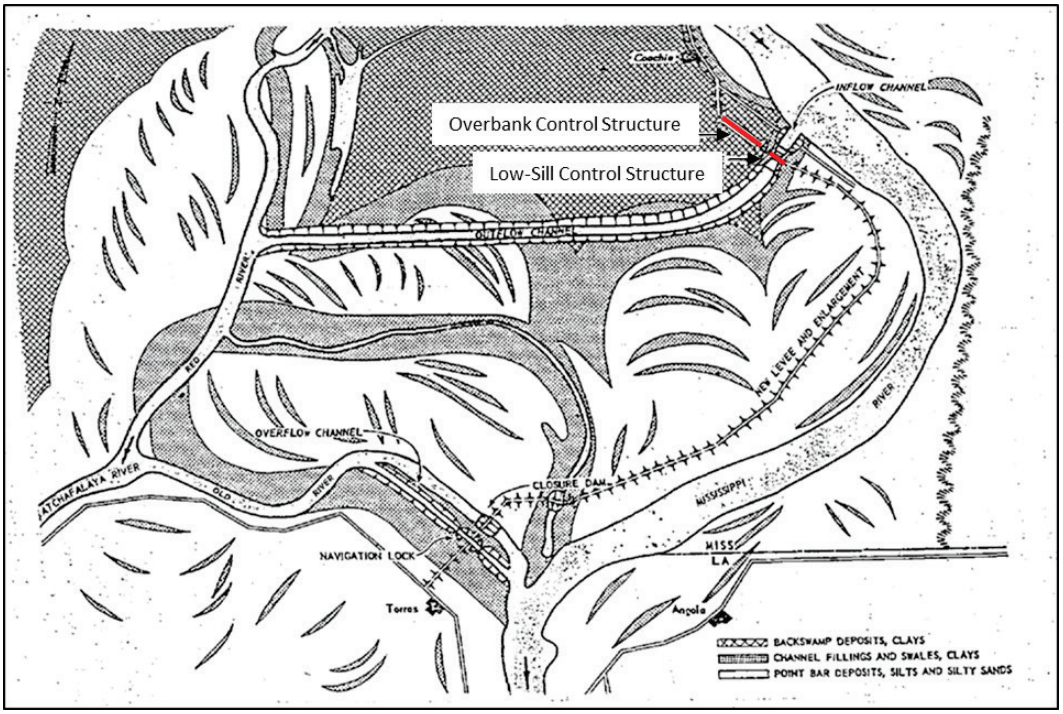

2.2 Geology of ORLSS and overbank foundation

The geology of the foundation of ORLSS is described in more detail in this section. This discussion focusses on the top stratum and substratum deposits described in the ORLSS design investigation.

2.2.1 Foundation cross sections

Geologic cross sections along the axis of the dam, the overbank structure, and the upstream approach channel and stilling basin are presented in Figures A-1 to A-4 (Appendix A). Profile sections in Figures A-1, A-2, and A-4 show Unified Soils Classification System (USCS) soil types beneath the structure and the limits of the deep excavation into the dam foundation. Figure A-3 identifies the different fluvial environments of deposition extending perpendicular to the dam axis, from the approach channel to the stilling basin, and the outlet channel.

2.2.2 Environments of deposition and engineering properties

Environments of deposition identified in Figure A-3 in descending order consist of 6.0 to 10.0 ft of natural levee silts, 10.0 to 20.0 ft of backswamp clay, 60.0 to 70.0 ft of alternating strata of silts, sandy silts, silty sands, and clay from an abandoned channel, 40.0 to 60.0 ft of medium substratum sands with gravel, and Tertiary clays at 110.0- to 120.0-ft depth (USACE 1963). These environments typically have characteristic soil types and engineering properties in terms of their grain size, Atterberg Limits, shear strength, water contents, and soil permeability.

2.2.3 Variability in engineering properties

Engineering properties of fluvial environments can vary due to local differences in water depth, current velocity, and the settling properties of the transported sediment from suspension. Additionally, post-depositional soil forming processes affect these sediments further with time through bioturbation (mixing of sediment by organisms affecting soil layering), oxidation, and weathering. These post-depositional processes impact soil layering and engineering properties (including cohesion, shear strength, and water content as examples). Relationships involving fluvial depositional environment, USCS soil type, and engineering properties have been studied and described by Fisk (1944, 1947); Kolb (1957, 1962); Montgomery (1974); and Saucier (1994).

2.2.4 Point bar and abandoned channel deposits

The base of ORLSS in Figure A-3 is identified as being in channel fill, comprised of alternating strata of silts, sandy silts, and silty sands. In Figure 4, ORLSS is shown and described on channel fill and swales. Surface features in Figure 4 show a classic point bar environment slightly southeast of ORLSS, involving ridge and swale topography. This undulating topography is typical of a point bar landform where sandy point bar ridges are separated by low-lying clay-filled swales. Point bars are formed by river channel migration across its floodplain through time. The horizontal extent of the point bar environment along its longitudinal profile on the floodplain surface forms distinct meander belt deposits and marks the spatial limits of the respective river course that created them.

Conventional practice for mapping of abandoned channel deposits by WES geologists (Fisk 1944; Kolb and Shockley 1957; Saucier 1969, 1994) have traditionally identified abandoned oxbows and courses because of clearly discernable bank line boundaries on aerial photography and topographic maps, and the presence of fine-grained, organic-rich, clay-dominated sediments or "clay plugs" in these oxbow settings. Sediments beneath ORLSS do not exactly match the definition of an abandoned channel section that has been traditionally used by WES geologists for purposes of engineering geology mapping in the Lower Mississippi Valley (LMV) (Kolb and Shockley 1957). Foundation conditions beneath ORLSS are more closely related to point bar deposits, containing ridge (sand bars) and swale (clay-filled low areas) topography as identified by Figure 4.

Point bar ridges correspond to the arcuate-shaped sandbars that form on the convex side of the river bank as the river migrates and deposits new sediment in the channel along the convex bar. Swales are topographically low-lying, wetland areas containing silt and clay-rich deposits that occur between adjoining sandbars. Swales develop and thicken by overbank flooding and deposition of fine-grained sediment from suspension (vertical accretion).

Point bar deposits become finer, in terms of sediment grain-size, vertically upward (decreasing depth). Point bar deposits extend to the thalweg (maximum depth) of the river channel. Comparison of the foundation sections for the ORLSS and overbank structure in Figures A-1, A-2, and A-4 indicates the lower, fine-grained, sands (SP) occur deeper beneath ORLSS. These fine-grained sands occupy the basal part and/or extend to the thalweg of the river channel under which they were deposited.

The Artonish 15-min. engineering geology quadrangle by Saucier (1969) identifies ORLSS as being within the point bar environment and the Overbank Structure as being in backswamp deposits (Figure 5). These surficial environments are underlain by undifferentiated meander belt deposits as shown by the generalized cross section in Figure 6. As the name implies, undifferentiated meander belt deposits incorporate natural levee, point bar, abandoned channel, and abandoned course (two or more connected abandoned channels or oxbows) environments (Kolb and Shockley 1957). Together, these different depositional environments spatially identify the horizontal extent of a laterally migrating river course across its floodplain surface through time.

Figure 5. Part of Artonish 15-min. engineering geology map showing distribution of environments of deposition (Saucier 1969). Note portion of cross section A′ on left bank of ORLSS showing point bar deposits and backswamp on right bank of ORLSS and overbank structure.

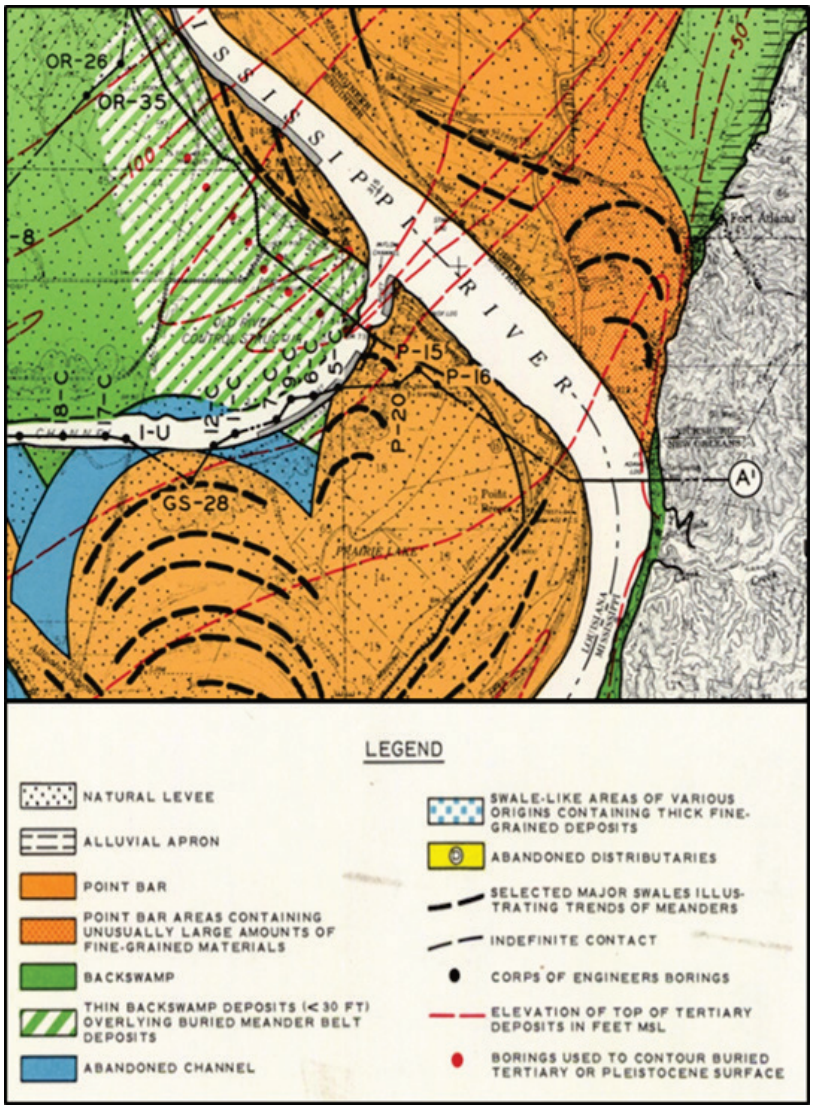

Figure 6. Part of geologic cross section from left abutment of ORLSS (Saucier 1969). Boring P-15 is at the left abutment.

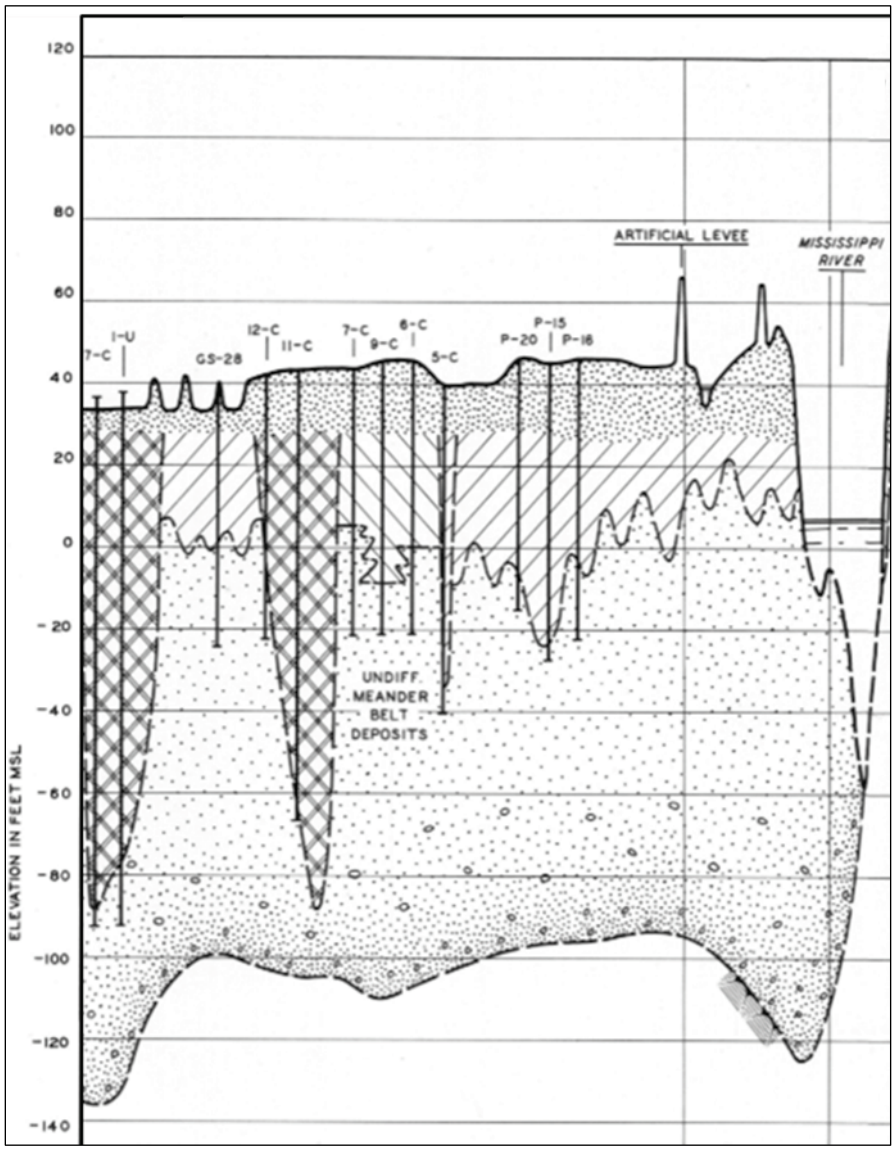

2.2.5 Backswamp

Backswamps are tree-covered, low-lying, wetland areas situated between different meander belt complexes and/or upland (Tertiary) valley walls. Backswamps are typically clay-dominated settings, as they receive only fine-grained sediment during annual flooding cycles, when the river overtops its banks and carries suspended sediment to distal parts of the floodplain. Low-lying backswamp areas in close proximity to the river are often favored locations for a crevasse or break in the levee and will form a sandy crevasse splay (or localized inland delta).

2.2.6 Substratum deposits

Substratum deposits occur below the thalweg and are typically associated with Late Pleistocene to Early Holocene braided stream conditions, when glacial melting was transporting an excess quantity of coarse sediment through the river system. Braided stream deposits contain fine to coarse gravel within a sand matrix. Braided stream conditions in the study area occurred during a period of lower eustatic sea level conditions, prior to the transition to a meandering river regime. Saucier (1994) estimates the transition to a meandering river regime to have occurred some 8,000 to 10,000 years before present.

2.2.7 Summary of foundation geology

Sediments forming the ORLSS foundation contain a fine-grained, top stratum (10 to 30 ft thick), developed by vertical accretion of natural levee silt and clay deposits. A lower point bar sand unit occurs beneath this fine-grained layer, comprised of silty sand (SM) and fine sand (SP). The lower point sand unit extends to the thalweg of fluvial scour by the river channel.

Underlying the lower point bar sand unit at a depth of 100.0 to 125.0 ft below the ORLSS foundation are substratum deposits that contain medium to coarse sand and fine gravel (Figures A1 to A4, Appendix A and Figure 6). A clay layer is present between the point bar substratum and the lower substratum deposits (Figure A3, Appendix A). The lower substratum deposits are associated with braided stream conditions during much lower sea level stages in the Pleistocene.

Geological mapping by Saucier (1969) shows buried meander belt deposits below the natural levee and point bar top stratum for the overbank structure and ORLSS (Figure 5). This undifferentiated classification incorporates several fluvial environments consisting of natural levee, point bar, abandoned channel (single oxbow loop), and abandoned course (multiple connected oxbow loops) deposits (Kolb 1957). Thus, silty and silty sand sediments beneath ORLSS are typically more representative of the lower sand unit of a point bar as compared to fine-grained channel fill.

2.3 Summary of soil engineering properties

Laboratory soil test data are shown on the cross sections in Figures A-1, A-2, and A-4. Tests performed involved visual classification, natural water content, mechanical analyses, Atterberg limits on selected samples, permeability, density, shear strength, and consolidation on undisturbed

samples. Test data for soil classification, compaction, shear strength, and consolidation are summarized by the selected graphs and tables in Figures A-5 to A-8. These data are further described by topic in the sections that follow.

2.3.1 Water content

Foundation soils beneath the ORLSS site are generalized using the centerline channel profile with presentation of depositional environments in Figure A-3 (USACE 1963). Water contents of the natural levee deposits varied between 14 to 33 percent with an average value of 30 percent. Backswamp clays varied from 35 to 45 percent, while the underlying fine-grained silty to sandy point bar deposits (originally identified as channel fill) have water contents from 25 to 33 percent.

2.3.2 Penetrative resistance

Logs of split-spoon resistance (standard split-spoon, 140-lb hammer, and 30-in. dropped weight) are included on the selected cross sections in Figures A-1 and A-4. Values vary from 25 to over 50 blows per ft. Below elevation -40.0, the penetrative resistance varies from 50 to over 100 blows per ft. Based on driving resistance from foundation borings, a boundary between looser and denser materials occurs at elevations -35.0 ft and -55.0 ft in borings N-14 and N-16, respectively (USACE 1954).

2.3.3 Shear strength clay

Shear strength of the clay samples was determined from unconfined compression tests, unconsolidated-undrained triaxial tests, and consolidated-undrained triaxial tests (Figure A-6). Average shear strength of the clays based on Coulomb empirical equation was computed to be Ø = 13° and c = 0.1 ton per sq ft. This value closely agrees with the results of the consolidated undrained triaxial tests on clays.

2.3.3.1 Shear strength point bar silts and sands

A design shear strength of Ø = 28° and c = 0.1 ton per sq ft was selected based on consolidated undrained triaxial tests on silts and sands in (Figure A-6). Because of the high degree of stratification of silty sand samples, the same design shear strength was assigned. It was recognized that consolidated undrained triaxial tests on silty sands are generally higher than those obtained from silts and sandy silts. Furthermore, it was thought that complete saturation of the triaxial test specimens was not effective,

and test results in the laboratory would be much higher than realized in the field if sheared quickly under conditions of no drainage (USACE 1954).

2.3.3.2 Shear strength substratum sands

Shear strengths of the sand samples were determined from consolidated-drained triaxial tests. A design value of Ø = 33° and c = 0 were used for estimating pile capacities (USACE 1954). This value was based on several tests, including freezing and thawing samples in the undisturbed state prior to sample test preparation, and on remolded samples prepared at the estimated natural void ratio.

Shear strength of the silts, sandy silts, and silty sands (point bar deposits) is plotted versus elevation on Figure A-6. Values computed from Coulomb's equation and average test results were Ø = 30° and c = 0.2 ton per sq ft. The design shear strength was Ø = 28° and c = 0.1 ton per sq ft.

2.3.4 Consolidation tests

Consolidation tests were performed on the top stratum and substratum deposits to predict settlements. Tests were performed for the upper backswamp clays (above EL 30.0 ft), the natural levee deposits (above EL -5.0), silty sand deposits below EL -5.0, and the deep sands at EL -70.0 ft. Test data are summarized in Figure A-7. It was determined that clay soils above EL 30.0 are pre-consolidated more than the present overburden pressure. Silty sands are somewhat more compressible than the deep sands. However, based on the recompression curves, which are probably representative of actual settlement characteristics, the two sands are fairly similar in nature. It was determined that top stratum silts and sandy silts are substantially more compressible than the underlying silty sands.

2.3.4.1 Deep clay

The consolidation test on the sample from the deep clay stratum above the substratum deposits (Figure A-3) indicates this stratum is relatively compressible and could result in significant settlement unless the piling is driven through the stratum (USACE 1954). The deep clay unit probably corresponds to fine-grained sedimentation associated with flooding of the Mississippi River embayment during sea level rise in the Late Pleistocene and/or Early Holocene. Pile lengths identified by the as-built plans indicate all the tips extended through the clay stratum and were founded in substratum sands.

2.3.5 Compaction

Compaction tests were performed on natural levee silts and fat clays above EL 20.0 ft. Fat clays were used in construction for the preload fills, cofferdams, guide levees, and the upstream impervious blanket in the forebay channel and upstream abutment slopes (Figure A-3). Excavated silts were used as backfill material behind training walls and stilling basin walls.

Results of the compaction tests are shown in Figure A-5. Compaction data were based on the Standard Proctor Test, but the tests did not follow the specified blows per layer. Tests were based on 15 blows per layer rather than the standard 25 blows. The explanation given for this variation was that preload fills, cofferdams, and guide levees were constructed using semi-compacted fill.

Maximum dry density averaged 103 pcf for silts and 80 pcf for clay. Optimum water content of the silts averaged 18 percent and for clays, it was 36 percent. Unconfined compression tests were performed on two of the compacted fat clay samples. A design shear strength of 0.3 tons per sq ft was assigned to the compacted clays. Assignment of this shear strength for the cofferdam and embankment fills permitted placement of fill materials by semi-compaction at approximately the natural water content.

2.3.6 Permeability of point bar silts and silty sands

Laboratory permeability tests were performed on selected undisturbed samples of the foundation between EL -5.0 and EL -65.0. Results of permeability tests in the vertical direction are shown with the boring logs in Figure A-8. Vertical permeabilities ranged from 0.26 x 10^{-4} cm/sec for a silt with clay laminations to 34 x 10^{-4} cm/sec for a relatively uniform silty sand. A vertical permeability of 2 x 10^{-4} cm/sec was used for design purposes for the foundation between EL -5.0 and EL -65.0 ft. This interval was assigned a horizontal permeability for design of 18 x 10^{-4} cm/sec, which is 9 times the vertical permeability from laboratory testing of samples (USACE 1954).

2.3.7 Permeability of deep substratum sands

Values for vertical permeability of deep sands were determined by tests on remolded samples. Samples used for testing involved undisturbed borings (N-13 and N-18), a split-spoon boring (T-1), and a bailer sample from the test well (W-2). Samples tested were cleaned of any drilling fluids prior to testing. The relationship between void ratio and permeability was determined from

five 3-in. Shelby tube samples (Figure A-8). The slope of these curves was used to estimate the natural void ratio obtained from the grain size (D10) density plots in Figure A-8. Average permeability of the deep sands based on a D10 of 0.25 mm was estimated to be 500 x 10^{-4} cm/sec.

Permeability values from lab testing were approximately half of the permeability values from of the field pumping tests for horizontal permeability in well W-2, which were calculated to be 1,000 x 10^{-4} cm/sec (described next). As noted by the subject design memorandum (USACE 1954), this value matches empirical relationships determined from laboratory permeability and field pumping tests from the St. Louis District's Alton to Gale Underseepage Investigation (USACE 1956a), which found that horizontal permeability values from pump tests were about twice those determined from remolded laboratory tests.

2.3.7.1 Comparison to pump test data

Test well W-2 was used to determine aquifer permeability values for the design. The 8.1-in. well was located on the centerline of the ORLSS at station 63+25. The well was screened between EL -86.1 to -115.4 ft. and fully penetrated the pervious aquifer beneath the lower clay layer in Figure A-4. The log of the test well W-2 is presented in Figure A-8 along with a split-spoon boring 10.0-ft distant. Pump tests involved pumping the well at three different flow rates for an extended time until equilibrium was reached in the well and surrounding piezometers.

Flow into the well screen at different depths was measured using a flow meter. The distribution of flow into the well screen in percent flow is shown on Figure A-8 (note the curve next to the boring log for test well W-2). The lower flow rate with depth was attributed to the presence of drill-mud residual in the substratum formation despite the increase in permeability with the coarse nature of the substratum sand and gravel with depth. Permeability values for each pumping flow rate based on an aquifer thickness of 40.0 ft are shown in Table 2.

Table 2. Permeability values computed for different flow rates from pump test at well W-2.

Pumping Rate, GPM	k_{20} x 10^{-4} cm/sec*
57	990
118	1052
223	1080
Average	**1040**

*k_{20} = coefficient of permeability at natural void ratio

3 1973 Flood Damage and Rehabilitation Chronology

In April 1973, ORLSS was seriously damaged by a major flood with deep scouring into the foundation, loss of foundation material beneath the structure, and formation of a large void. During the 1973 flood event, flow through the ORLSS exceeded the design flow by 50 kfs when scouring took place. Scouring also resulted in the failure of the wing wall at the left abutment, which was the first sign of distress and observed damage to the structure. Emergency repairs involved first placing rock along the left abutment where the wing wall had been located to prevent further erosion of the abutment area (Figure 7).

Figure 7. Construction of rock dike on left abutment on 18 April 1973.

Construction of the rock dike was begun 14 April, and the dike was completed 7 May, requiring 98,000 tons of rock (USACE 1975a). Rock placement was performed with the gates open on the ORLSS. The overbank structure was opened on 14 April after the wing wall collapsed

to relieve pressure on the structure and was gradually closed, beginning 2 June and completely by 15 June.

Completion of the rock dike on the left abutment was followed next by filling the deep scour channel in the forebay area and in front of the structure with stone to prevent further erosion and prevent channel scouring under the structure and connecting directly to the stilling basin (Figure 8). Rock was placed in the hole by a derrick barge, which was anchored to a winch-barge from a revetment mat sinking unit (Figure 8). Rock placement began 9 May and was completed 31 May, requiring 118,000 tons of rock (USACE 1975a). Rock placement was performed with the gates fully open on the ORLSS.

Figure 8. Rock being placed in forebay on 18 May 1973.

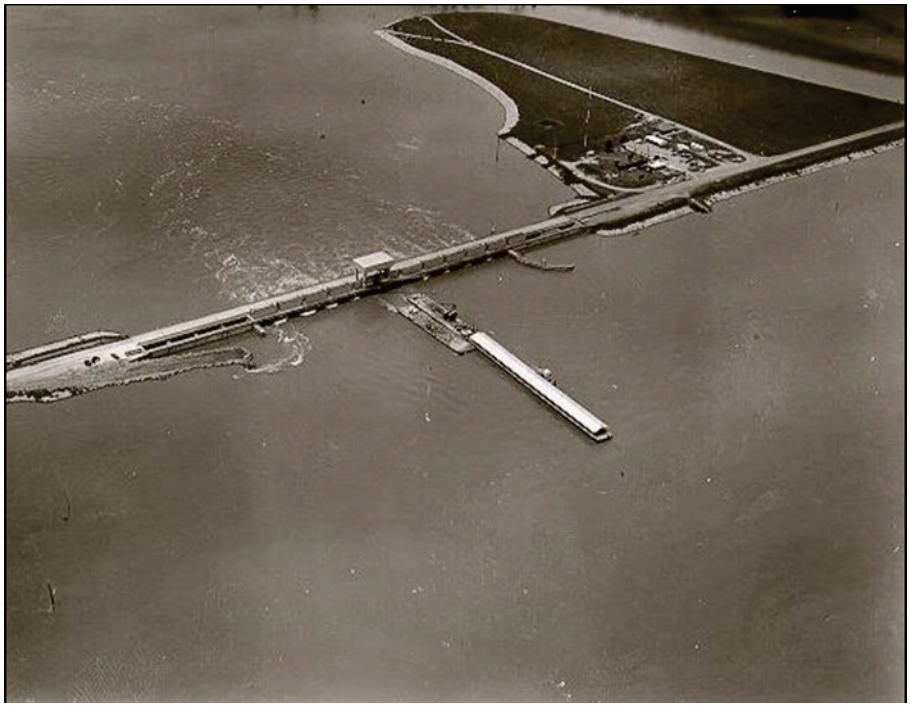

Surveys were performed to determine the full extent of the flood damage in the forebay area next to the structure. These surveys were initially done by a lightweight 100.0-ft boom and a fathometer suspended from the boom crane located on the structure. Because of the void extent beneath the south end of the structure, the crane was not permitted to fully traverse this area to map void limits in detail. Mapped limits of final rock and stone placement in the forebay area are shown by Figure 9.

Figure 9. Rock and stone placement in forebay with bottom elevations (USACE 1973a).

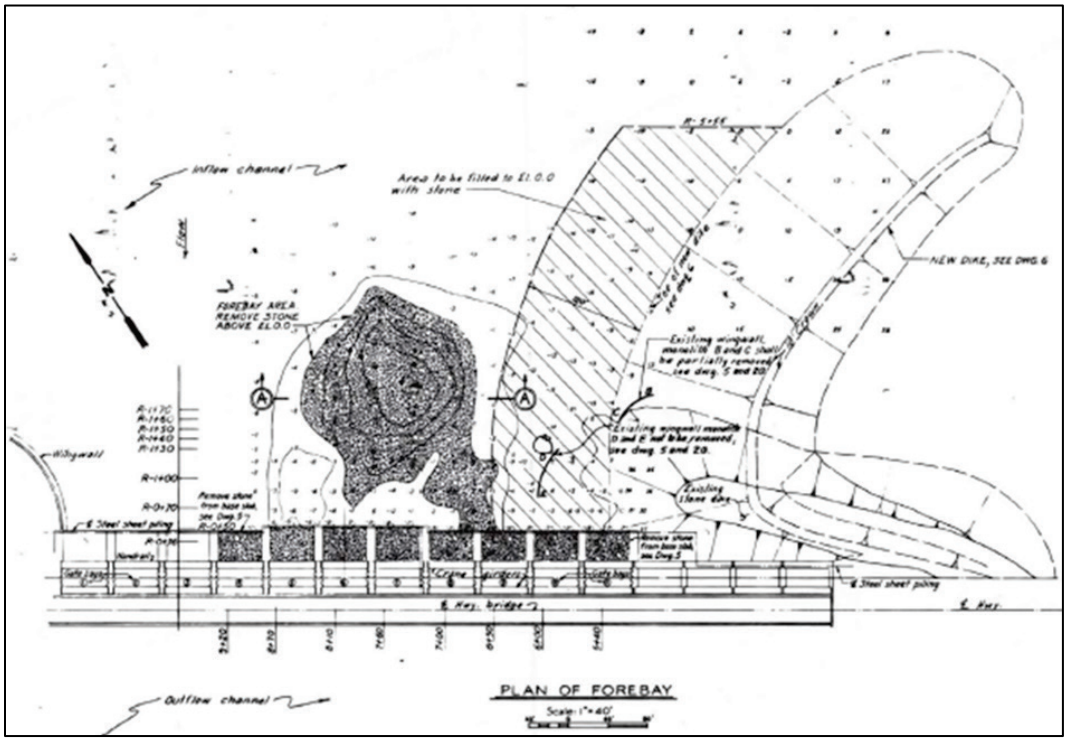

An exploratory boring program was subsequently initiated from the structure to determine the extent of the void under the structure as part of the grouting program (Wilson 1978). The large void beneath the structure was confined to gates 5 through 11 (Figure 10). MVN decided to fill the void with cement grout as quickly as possible. MVN and WES designed and evaluated various grout mixtures for the repair (Wilson 1978).

Figure 10. Scour limits under the ORLSS (USACE 1973a).

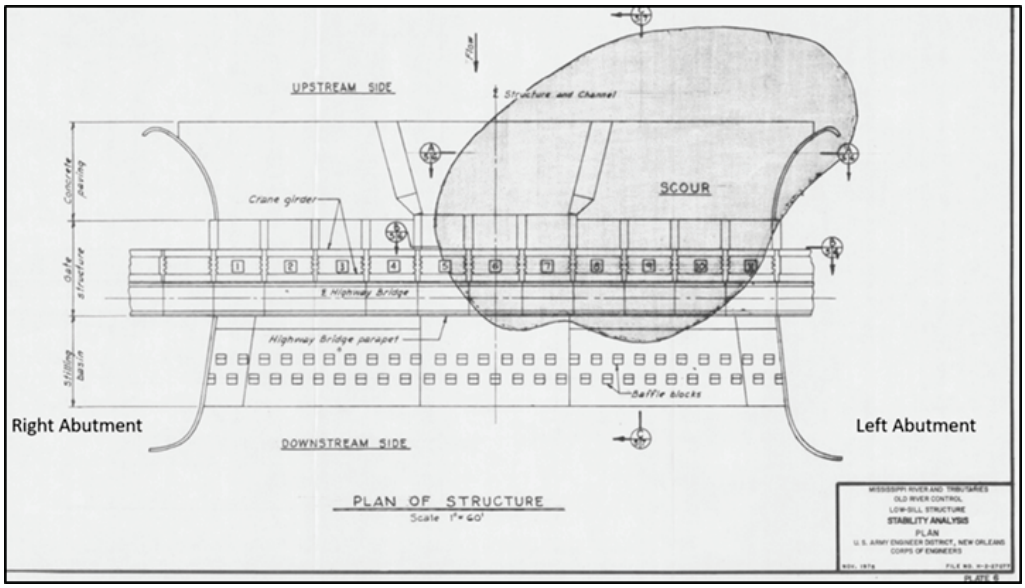

An emergency grouting program was subsequently initiated in November of 1973 to fill the void using a commercial grouting company. The specialized grout mixture was developed by the WES Concrete Laboratory and was designed to closely match the engineering properties of the eroded foundation soils. Major grouting was completed by February 1974, but intermittent grouting by Mobile District continued to September 1974. Approximately 33,000 yd^3 of grout were used to fill the void beneath the structure and the stilling basin (USACE 1975a).

Damage by fluvial scouring of the foundation and subsequent grouting of the void area using the specialized grout mixture resulted in the loss of the horizontal pressure relief system beneath the front half of the stilling basin. This pressure relief system was designed to reduce hydraulic uplift under the structure from extreme flood loadings.

A change to the gate operation plan was initiated after the repairs to provide for a more uniform flow distribution through the structure to reduce the potential for concentrated deep scouring at the left abutment. The ORLSS has been successfully operated since the 1973 flood damage occurred. However, restrictions have been placed on its operation to limit the maximum head differential between the headwater and tailwater because of stability concerns within the repaired section. Currently, the head differential restriction is 22.0 ft, which was increased from the 13.0-ft differential restriction imposed following the 1973 scour event. The original design head differential restriction was 35.0 ft.

For further perspective on the magnitude of flood conditions during the 1973 flood, the high water was the largest flood experience by the Old River Project. Maximum recorded headwater stage was 61.6 ft on 15 May 1973. The corresponding tail water was at 59.3 ft. Observed flow at Natchez was at 2,024,000 cfs on 18 May 1973. For the sake of comparison, the design project flow is 2,720,000 cfs at Natchez (USACE 1975a).

3.1 Forebay rock placement

The limits of rock and stone placement in the forebay area following the emergency stone placement are summarized by Figure 9 (USACE 1973a). This figure identifies spot elevations in the forebay area and the limits where maximum rock placement occurred (identified by the gravel symbol pattern). The gravel extends to gates 8 and 9, where maximum scour activity was concentrated based on the void limits determined by boom surveys and exploratory borings.

Maximum stone size was specified in USACE 1973b as being less than 8 tons. The purpose for this summary of stone size is to better understand their size and how they would potentially move into the void and pass through the front row of H-piles that would have been exposed by scouring at the peak of emergency repairs. A dense network of H-piles and batter piles is used to support the structure resting on the deep alluvial foundation. A central question is whether rock was able to pass beneath the structure into the void area.

To address this question in more detail, it was first necessary to better understand the rock dimensions that were likely used. Limestone rock has an average unit weight of 150 lbs/ft^3; thus, the approximate stone dimensions per ton are estimated for different sized pieces (assumed to be cubic in shape) are shown in Table 3.

Table 3. Assumed volumes and weights of stone for scour stabilization.

Weight (tons)	Volume (ft^3)	Assumed Cube Dimension (ft)
1	13.3	2.4
2	26.7	3.0
3	40.0	3.4
4	53.3	3.8
5	66.7	4.0
6	80.0	4.3

The description of stone placement above indicates the rock was lowered and adjusted into position before being released. Based on the various sizes identified above and the prevailing current conditions in the forebay with the gates open, it is likely that large derrick stone was not able to travel any appreciable distance downstream on release. Further hindering this downstream movement would be the sheet pile directly in front of the structure and the dense network of H-piles behind the sheet pile. Vertical H-pile spacing is 9.0 ft apart along the centerline axis and 4.5 ft apart perpendicular to the centerline axis with 5 rows of vertical piles at the upstream slab, shown in Figure 11.

Figure 11. Pile layout and arrangement beneath the ORLSS monoliths (Sherman 1962).

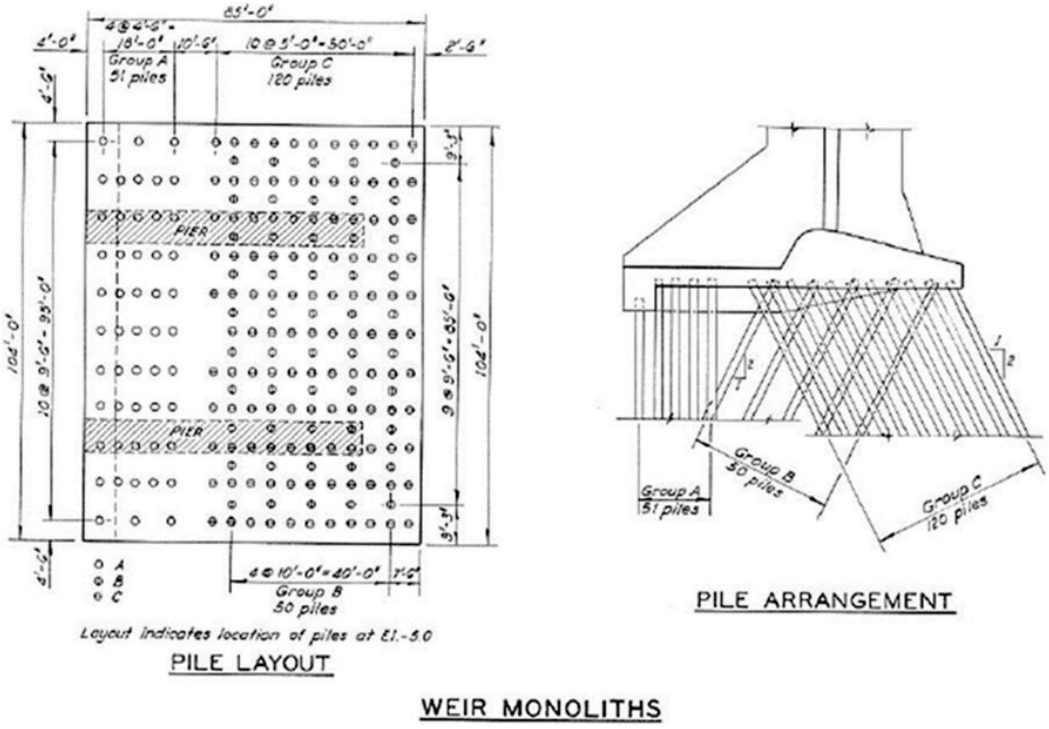

This spacing arrangement and the size of the stone used would indicate that the stone was likely confined to the first few rows of the vertical piles. A drawing that portrays this viewpoint from the 1975 stability analysis (USACE 1975a) is shown in Figure 12. This illustration shows limited penetration of the stone past the vertical H-piles and directly below the structure.

Figure 12. Scour hole limits along forebay profile and hypothetical rock extent beneath the structure (USACE 1976, Plate 8).

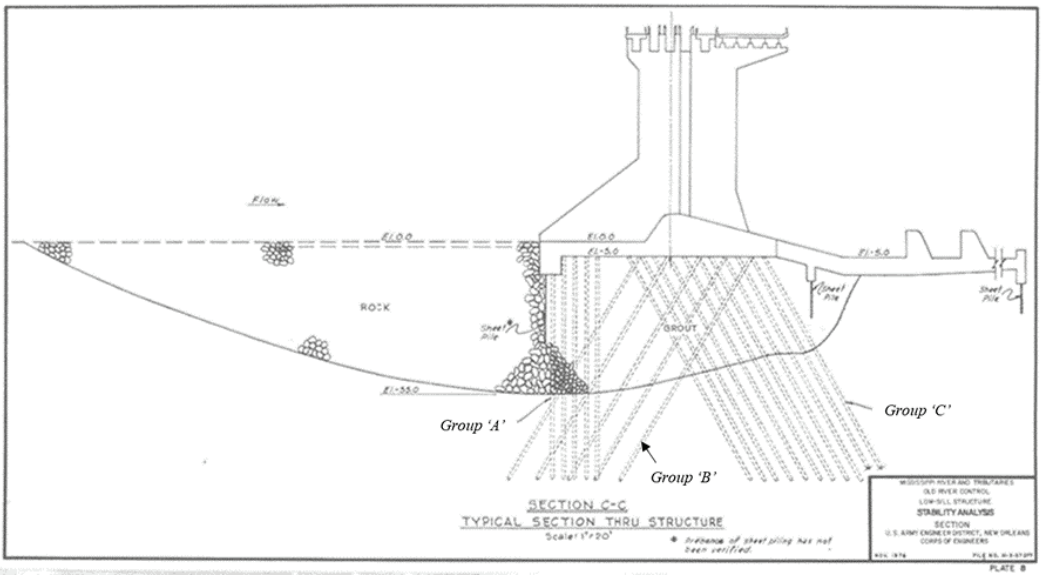

Cross sections showing the void extent and scour limits directly in front of the structure in the forebay area are shown in Figure 13. These drawings are based on measurements of the forebay scour pool and boring data below the structure, which are described next in discussion of the grouting program.

Figure 13. Scour hole limits in front of the structure (USACE 1976).

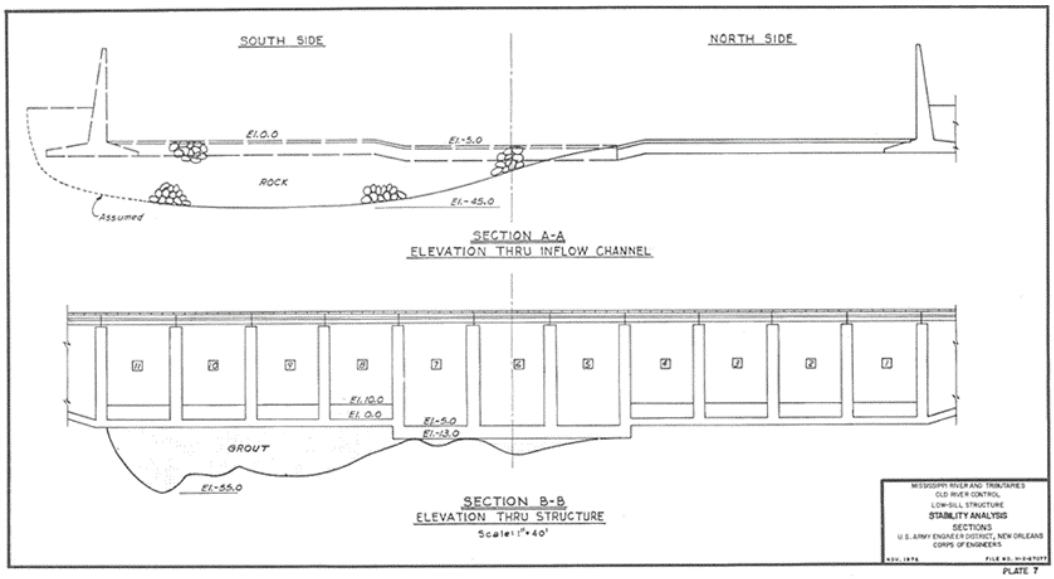

3.2 Grout boring investigation

The boring investigation program to define the extent of the void beneath the structure and to deliver grout was begun in September 1973 and

completed by early February 1974 (Wilson 1978). Forty-eight borings were drilled to determine the limits of the void beneath the structure (Figures 13 and 14). Borings were drilled along three lines across the zone of maximum scour with B-line borings upstream of the gates, C-line borings in the spillway upstream of the center or tailbay sheet pile, and D-line borings downstream of the tailbay sheet pile (Figure 14). These borings were used to determine the depths and dimensions of the scour pool. Results from the boring program are presented as cross sections in Figures A-9 to A-11 for the B, C, and D-lines, respectively. A profile of the dam showing the grout lines in relation to the forebay, tailbay, and stilling basin is presented in Figure A-12.

Figure 14. Boring locations to determine void limits based on 3 lines of borings (Wilson 1978).

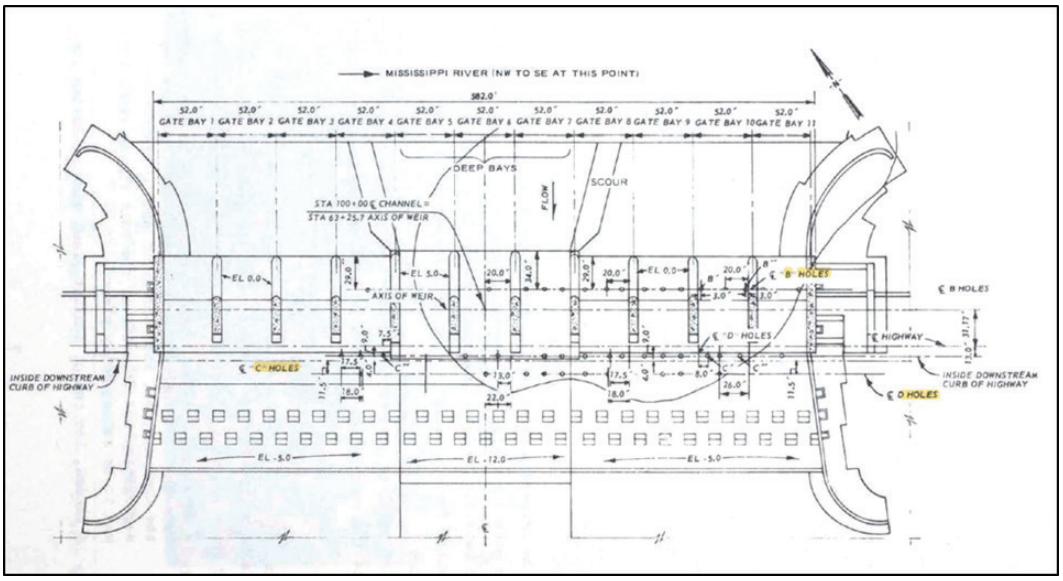

3.3 Void limits

The elevation values for the B, C, and D lines presented in Figures A-9 to A-11 were used to derive a contour map of the void area. These elevations were augmented with point data from the forebay area from published cross sections (Figures 12 and 13). Measured elevation points used to derive the void limits are shown in Figure 15, and a contour map from these values is presented in Figure 16. Maximum scour limits occur in front of and beneath gates 8 through 11. A concentrated zone of scour occurred beneath gates 8 and 9 that almost reached into the stilling basin based on the D-line boring data. The foundation scouring reached slightly past the tailbay sheet pile in these gates (see Figure A-12 for sheet pile location). A close-up view of the rock placement map (Figure 9) is shown with the contour map of the

void area in Figure 17. This illustration shows the close relationship between the zone of maximum scour in front of the structure and areas where rock placement was likely thickest (gravel pattern). Note that the plan view in Figure 17 is looking upstream toward the forebay.

Figure 15. Measured spot elevations used to determine void limits (Wilson 1978). Plan view is looking downstream from forebay.

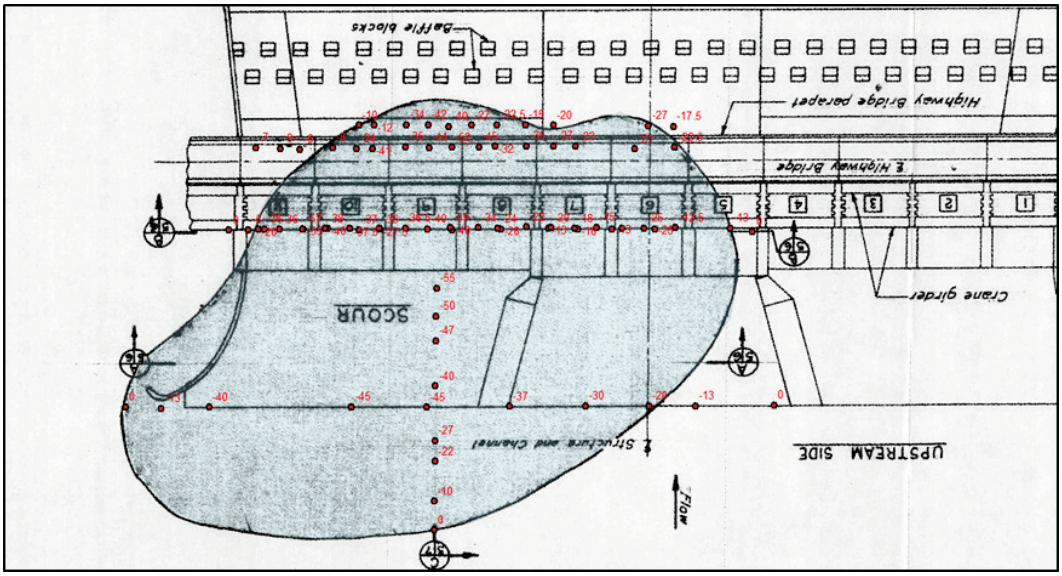

Figure 16. Elevation contour map of the scour zone in the forebay and beneath the structure. Plan view is looking downstream from forebay.

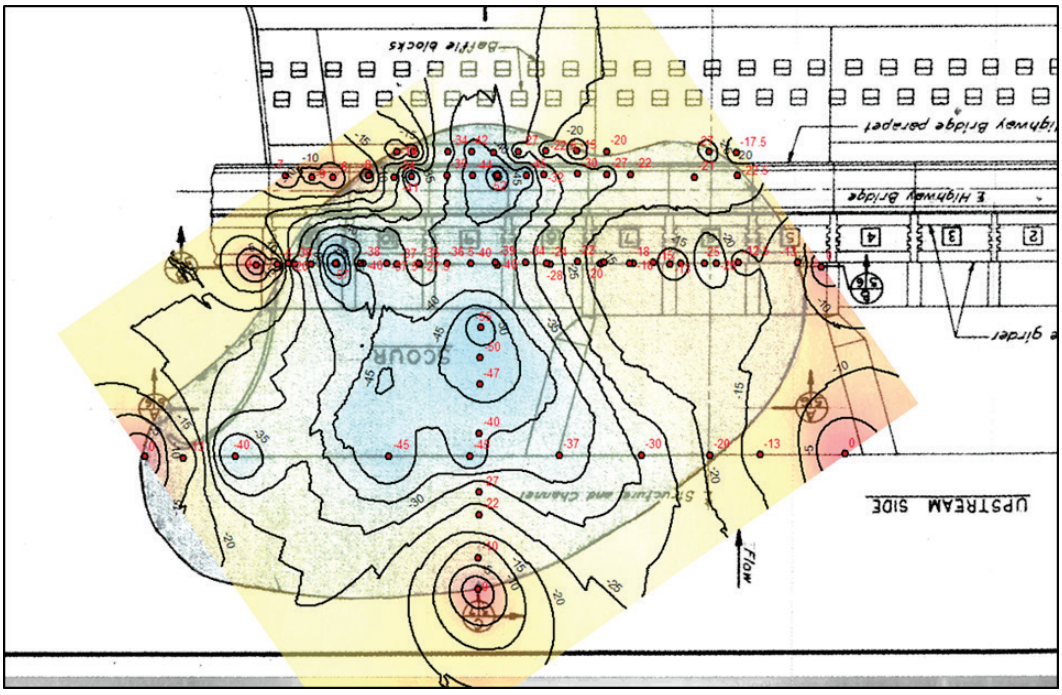

Figure 17. Elevation contour map superimposed onto the rock placement map in the forebay area. Plan view is looking upstream toward Mississippi River. Note the close agreement between deepest scour area and rock placement in front of the structure.

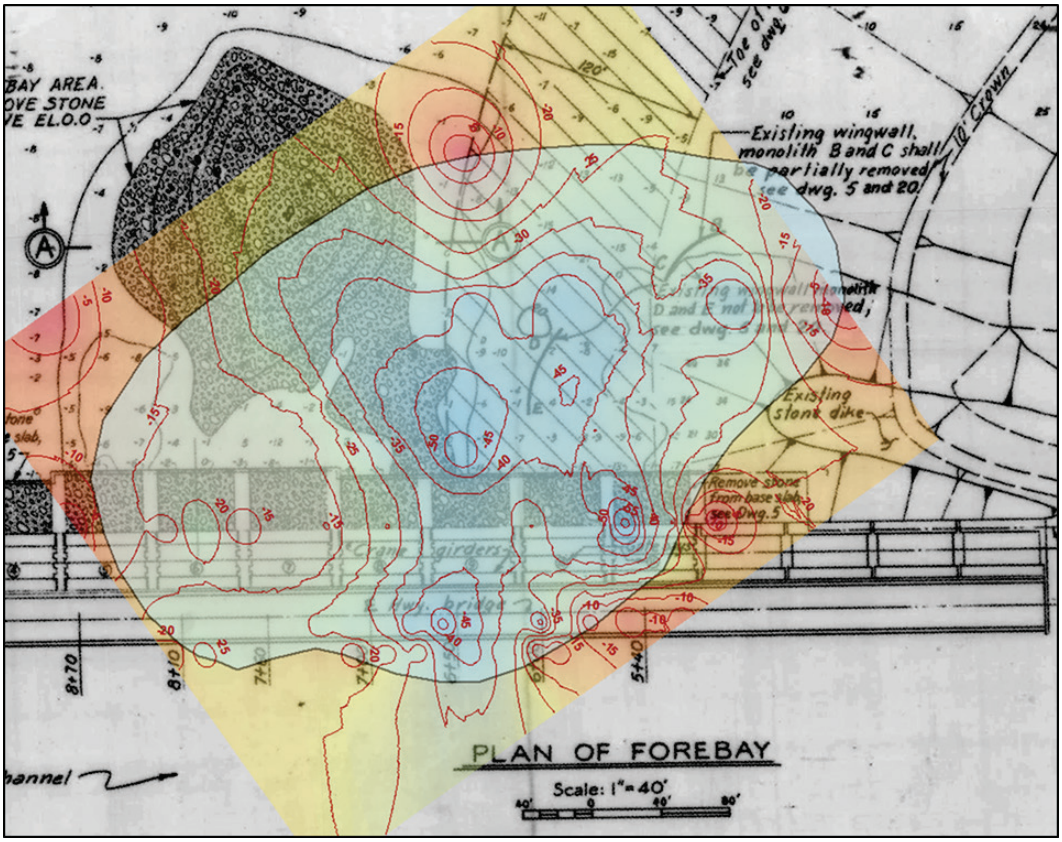

Published elevation data from beneath the structure and the forebay area make possible an accurate map of the damaged area. This map is in general agreement with the rock placement in the forebay area in terms of the maximum fill areas identified. Furthermore, close attention has been drawn to the downstream extent of the scour hole limits beneath the structure where the tailbay sheetpile is present. As described by the next section, grouting operations will be noticeably impacted by the extent of the void area under gates 8 and 9.

3.4 Grout mixtures

Specialized grouts were developed by WES to ensure maximum effectiveness for filling the void and matching the engineering properties of the lost soils beneath the structure. A summary of the engineering properties of the grouts used are presented in Table 4.

Table 4. Grout mixtures used for LSS remediation for dry batch (Wilson 1978).

Materials	Units	Mixtures (SSD)		
		OR-5	OR-13	OR-23
Cement, Type I Portland,	lb/yd^3	281.61	563.49	1088.1
Sand	lb/yd^3	875.07	-	-
Barite	lb/yd^3	851.85	-	892.89
Bentonite	lb/yd^3	75.6	59.94	92.34
Water	lb/yd^3	1028.97	1199.8	1088.1
Theoretical Unit Weight	lb/ft^3	115.4	111.3	117.1
Theoretical Cement Factor	bags/yd^3	3	6	11.6
Water-Cement ratio (by weight)	-	3.65	2.13	1

The theoretical unit weights for these different mixtures were designed to closely match the in situ densities of the underlying soil strata that were lost.

3.5 Grouting program

Grouting operations, begun in late November 1973 and completed by early February 1974, were monitored with borehole sensors that measured the conductivity of the fluid in the void during the grouting program. Conductivity sensors were calibrated to readings in air, water, muck, and then grout to determine the effectiveness of the void-filling process. Conductivity sensors placed in the void area were able to determine the grout elevations across the void zone. Uplift pressures using strain gauges were monitored during grouting to ensure the foundation structure was not uplifted (Wilson 1978).

The deepest areas, which contained the most muck, were grouted first with a special blend to mix with the muck. The sequence for grouting was to first agitate the muck at the bottom of the void with water to place the muck into suspension. Grout mixture OR-13 was then placed in the void after agitation to mix with the suspended muck to create a soil cement. This mixture was immediately followed with grout mixture OR-5 to EL -23.0 ft. A five-day cure time followed to permit the combined (OR-13 and OR-5) grout mix to set up. Grouting was continued five days later with a second treatment of OR-5 to EL -18.0, and a second cure period occurred for 5 days. A third grouting treatment of OR-5 was resumed five days later to 1.0 ft below the concrete base, which was EL -14.0 ft in gates 5-7 and EL -6.0 in gates 6-11. The final

stage of grouting involved a high water-cement ratio of OR-23 to fill the remaining void space and to create a tight bond to the bottom of the concrete.

Boring 8C in Figure 18 was the focus of intense attention during the grouting process. This grout hole is in gate 8 and is the leftmost (based on perspective of looking downstream or south) borehole in this gate bay. During the grouting process, it was noticed that the grout level in this boring had not risen in the same manner as the other borings. The D-line borings revealed no grout buildup in these borings since the initial grout injection. Wilson (1978) reports that different attempts were made to place this borehole in compliance: adding an accelerator (SIKA 4A) and regulated-set cement to the OR-5 mixture, pumping the mix at a rapid rate and then followed by the regular OR-5 mixture, and using tracer dye to locate the grout placed. However, no traces of the dye were found.

Figure 18. Scour depth in feet beneath the concrete portion of the structure from behind the first row of sheet pile. Plan view is looking upstream.

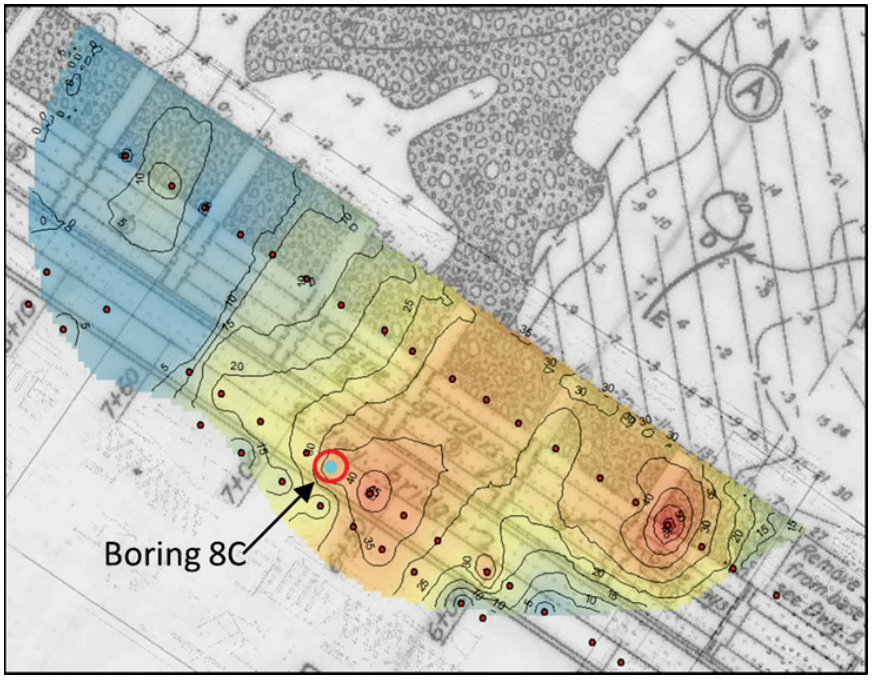

The next action performed was to bring the grout level up along the D-line borings to equalize the pressure along the downstream sheet pile between the C- and D-lines. The grout level was brought to 1.0 ft below the stilling basin slab with the OR-5 grout mixture. With the grout levels at -13.0 ft along the D-line, uplift pressures under the stilling basin slab dropped to and remained at tail water pressures (Wilson 1978).

Grouting was then moved back to the C-line borings to fill 8C. To facilitate grout into 8C, 400 to 500 ft^3 of foam rubber square (1 ft x 1 ft x 6 in.) were forced down boring 8C, and a special mixture of diesel fuel, cement, bentonite, and cellophane flakes (lost circulation material) were placed immediately following the foam rubber cubes. The cellophane flakes were dispersed into blender pots to get as much into the grout as possible. Wilson (1978) reports that about 30 yd^3 of this mixture were placed and followed immediately by placement of OR-5. This sequence of steps was successful as the grout in 8C began to rise.

Close examination of Figure 18 and the location of 8C in relation to the maximum scour hole extent in gates 8 and 9 show the presence of a scour hole at this location, which extends past the D-Line area on the downstream side of the tailbay sheet pile. The tip elevation of the tailbay sheet pile is at -27.0 ft for gates 8-11 (Figure A-12). Thus, the depth of scour was between 13.0 and 18.0 ft below the bottom of the tailbay sheet pile, and this explains the problems that were encountered with the grouting of boring 8C.

The placement of grout in the D-line borings most probably filled the void behind the sheet pile as evidenced by the report of uplift pressures returning to tail water pressures after grout was pumped into this area to EL -13.0 ft. The return of tail water pressures in the D-Line borings is evidence of the success in filling the void area behind the tailbay sheet pile, which permitted the successful filling of the void space between the tailbay and forebay sheet piles (Figure A-12).

3.6 Pile exposure

This section examines the impact of the 1973 scour on exposing the piles that support the structure. For this study, the drawings of the pile locations were digitized and georeferenced to their geospatial coordinates. Accurate placement of the piles under the structure permits evaluation and understanding of the exposure extent caused by the scour. Previously referenced Figure 11 shows both plan and profile views of the piles beneath the weir monolith. Piles were driven vertically (Group A) and battered at a 2V:1H slope in both the upstream (Group B) and downstream (Group C) directions as shown by Figure 11. Figure 12 shows the interpretation of the rock extent and the exposure of the piles beneath the structure. It should be noted that Figure 12 was updated from the original to provide continuity in this report with that in USACE (1976); pile groups B and C

were opposite from the original design. The focus of this discussion is how much of the pile lengths were exposed by the 1973 flood scour, not the identification of the battered pile groups, which is not fully resolved here.

Figure 19 shows the location of all the piles and those affected by the 1973 flood. There are 1,920 piles supporting the structure, and 683 were exposed to some degree by scouring during the 1973 flood. A close-up view of those piles directly affected is shown in Figure 20. The underlying contour map and color shading corresponds to the depth of scour beneath the concrete base. Maximum scour areas are shown by the red-colored areas. The severity of scour in Figure 20 can be broken into three general categories: minor (blue-colored areas), moderate (yellow), and severe (red).

Figure 19. View looking upstream of ORLSS showing locations of monoliths (blue) and the piles (green) across the structure. Piles affected by the 1973 scour are shown in red.

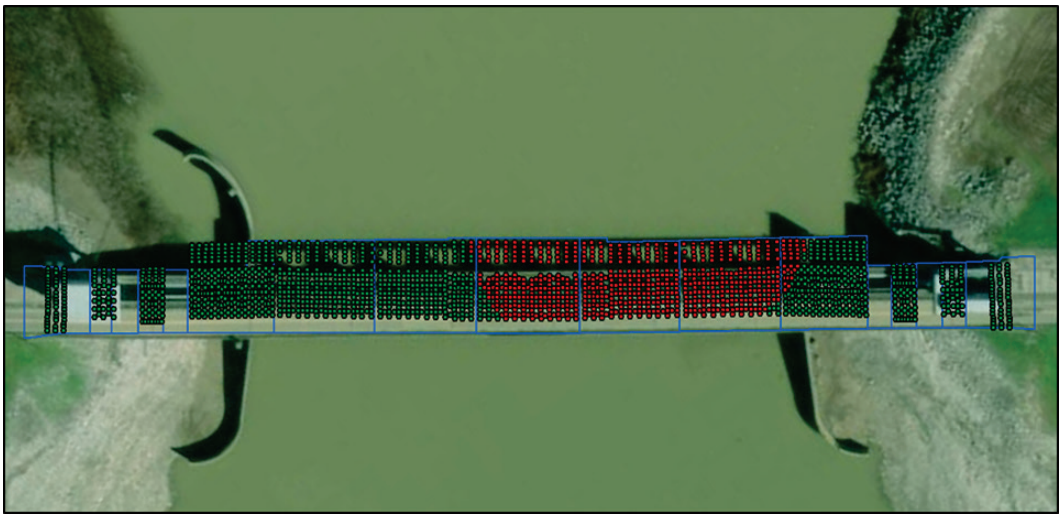

Figure 20. Close-up view of piles impacted by the scour in relationship to the depth of scour beneath the structure. Maximum scour and pile exposure are in the red-colored areas. Scour contours are in depth (feet) below the base of the concrete as it varies across the structure.

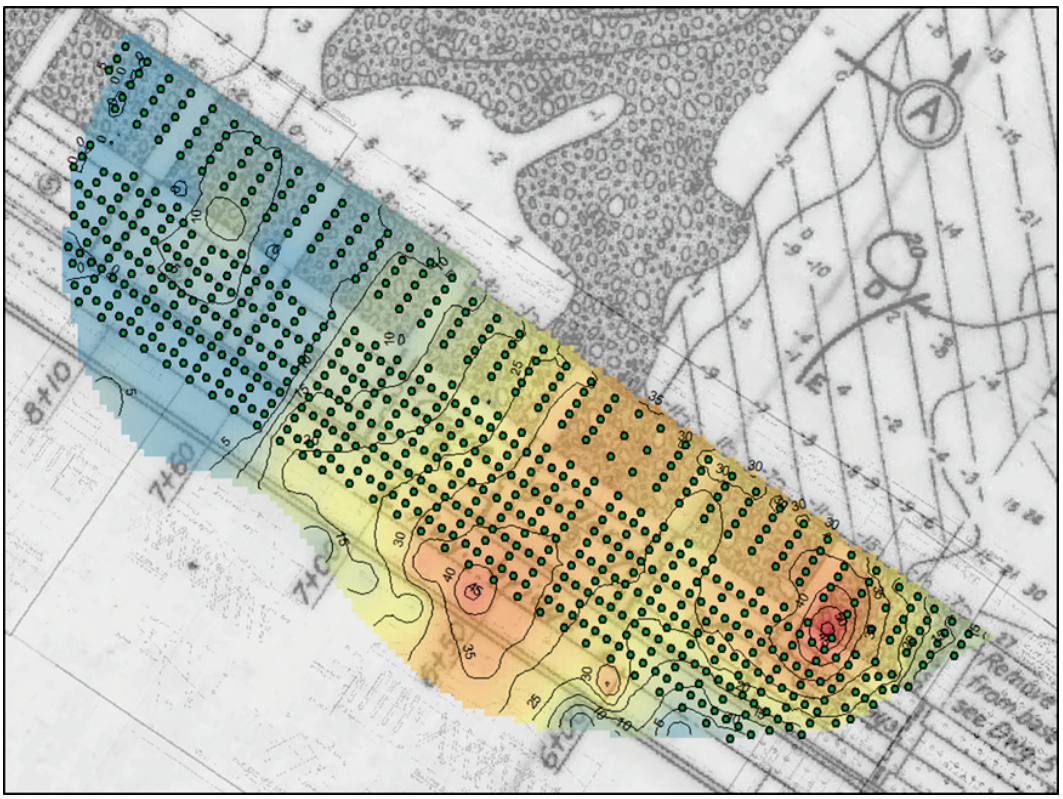

The exposed pile lengths on the vertical piles were a simple matter to calculate. However, the battered piles are affected differently by the scour depth because of their 63-deg batter angles in both upstream and downstream directions. Thus, the relative exposure length can be more significant in the deeper scour areas of the structure's foundation, as the exposure length of the pile affects its ability to support the structure. Fortunately, the maximum exposure areas are limited to the red-colored areas in Figures 20 and 21. Figure 21 shows the location of the piles exposed by their length, and they are delineated by 10-ft increments of exposure. Maximum exposure is again limited to areas of deepest scour.

Figure 21. Location of piles exposed and classified by 10-ft exposure increments.

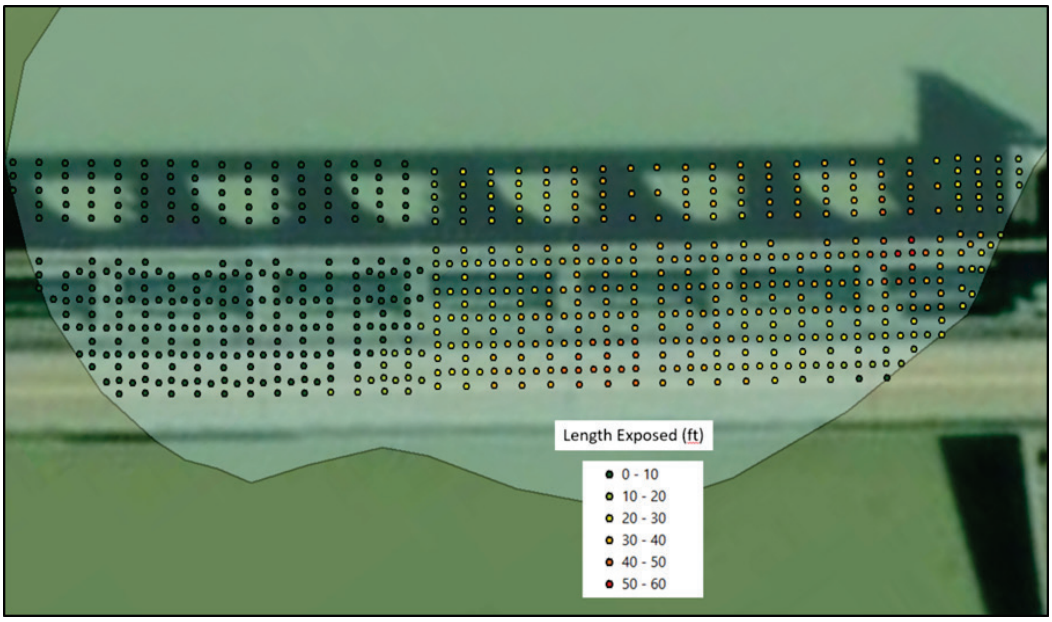

Pile exposure by 5-ft lengths is presented in Table 4. Included in this table is the percent exposed (amount exposed/total length) for the 5-ft classification scheme. The length of the piles varies in each classification band and is expressed as a range for percent exposed. Maximum exposure is limited to those piles at the 35-ft boundary and above where there are about 126 piles directly impacted. Piles exposure in the 20- to 35-ft range accounts for 243 piles and varies from 21 to 36 percent of the pile length exposed. The 10- to 20-ft exposure band represents 54 piles and 11 to 24 percent of the pile length exposed. The exposed category from 0 to 10 ft represents 260 piles with less than 10 percent of the pile length exposed.

Table 5. Pile lengths exposed and percent of exposed.

Exposed Length (ft)	Number of Piles	% Exposed
0 to 5	94	< 5
5 to 10	166	5 to 10
10 to 15	26	11 to 18
15 to 20	28	17 to 24
20 to 25	54	21 to 28
25 to 30	66	27 to 36
30 to 35	123	31 to 42
35 to 40	95	37 to 45
40 to 45	25	41 to 52
45 to 50	3	48 to 56
50 to 55	3	53 to 57

3.7 Volume of void

The estimated volume of the void beneath the structure was calculated from the elevation data presented in Figure 18 and 19. A raster grid was developed from the elevation data to produce the contour maps presented in Figures 19 through 21. A raster grid was developed from the construction drawings to define the base of the concrete. Elevations from this surface were subtracted from the elevation grid of the void beneath the structure. The estimated volume calculated for the void beneath the structure and stilling basin is 601,384 ft^3. To fill this void space would require 22,273 yd of grout assuming no loss to the forebay area and a 27 yd^3 mix. A 25 yd^3 grout mix and no loss to the forebay area results in 24,055 yd^3 of grout to fill the void.

The volume of grout reported to fill the void was estimated at 33,000 cubic yards (Wilson 1978). The volume estimated to fill the void compared to the amount used to fill the void space varies from 67 percent (27 cubic yard mix) to 72 percent (25 cubic yard mix) of the amount reported. Thus, 28 to 33 percent of the grout was lost into the forebay and surrounding area. The volume reported to fill the estimated void space is considered reasonable as grout leakage into the porous rock fill in the forebay is likely to have occurred in addition to the losses in grout hole 8c discussed previously.

Another factor that bears mention is the concept of stone entering and partially filling the void during the rock placement in the forebay. The minimum volume of grout required to fill the void space would support the idea that large stone described in an early section of this chapter was prevented from completely passing through the vertical piles in front of the structure because of the volume of grout that was needed for the repairs.

4 Pile Stability Analysis

4.1 Introduction

An analysis of the pile foundation of ORLSS was conducted to assess the response of the pile foundation to various loadings. Two periods of time were considered for this analysis: the design conditions and the post-1973 flood rehabilitated condition. The time prior to the 1973 scour event is considered in line with the original design. The post-flood condition incorporates possible increased uplift and grout loads. A numerical simulation of a pile load test, performed prior to construction of the structure, was conducted to ascertain the appropriate properties for use in a larger three-dimensional (3-D) pile group analysis. The 3-D analysis was conducted using the software GROUP distributed by ENSOFT. This software is capable of performing nonlinear analysis of the pile group and pile cap. Three different material property cases were considered with regard to the axial load versus settlement properties: Case 1 was based on recommended design values, Case 2 was calibrated to the load test results, and Case 3 was performed as a conservative case.

4.2 Foundation conditions

Selection of the site for ORLSS considered ease of dewatering during construction as well as consideration of uplift and stability of the structure. The chosen site consists of both historic and prehistoric meander loops of the Mississippi River across the site. Major landforms of the site consist of natural levee deposits, point bar deposits, backswamp clays, and channel fillings consisting of clays and silts. In the vicinity of ORLSS, foundation soils consist of a thin layer of natural levee, which are mainly silts, underlain by backswamp clays. Beneath the backswamp clays are alternating sandy silt and silty sand deposits to approximately -80.0 ft, msl. Figure 22 shows a general profile of the foundation.

Figure 22. General foundation geology of ORLSS (Turnbull and Shockley 1958).

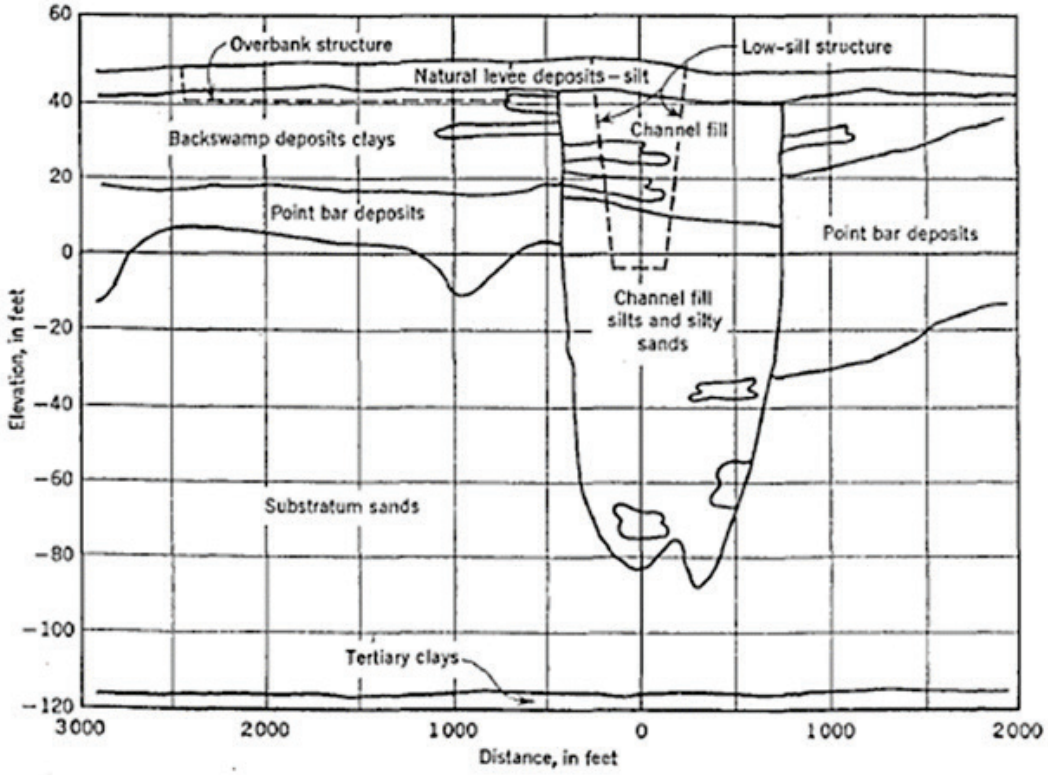

A foundation exploration was conducted to assess the consolidation, shear strength, density, and hydraulic conductivity of the foundation and borrow materials. Soil borings were performed along the centerline of the structure and inflow/outflow channel. In addition, standard penetration tests (SPT) were conducted in granular soils, and the foundation exploration was performed by CEMVN and WES (USACE 1954). The results of the 1950s' foundation exploration and laboratory testing were reviewed for the current stability analysis to attain a representative foundation profile and to derive material properties.

SPTs were performed using a standard split spoon sampler (1 3/8-in. inside diameter and 2-in. outside diameters) and a 140-lb hammer dropped 30 in. Uncorrected SPT N-values (blow counts) were reported in USACE (1954); for this analysis, they were corrected for overburden and rod length as described in McGregor and Duncan (1998). The corrected values for SPT performed along the centerline of the inflow/outflow channel are shown in Figure 23. It is apparent from Figure 23 that there is a general trend of increasing penetration resistance with increasing depth, although with considerable scatter. SPT blow counts are well-correlated with shear strength; therefore, Figure 23 shows a definite increase in shear

resistance with depth (McGregor and Duncan 1998). Figure 24 shows the locations of the SPTs used to prepare Figure 23.

Figure 23. Corrected SPT values versus elevation (ft, msl) along the centerline of the channel.

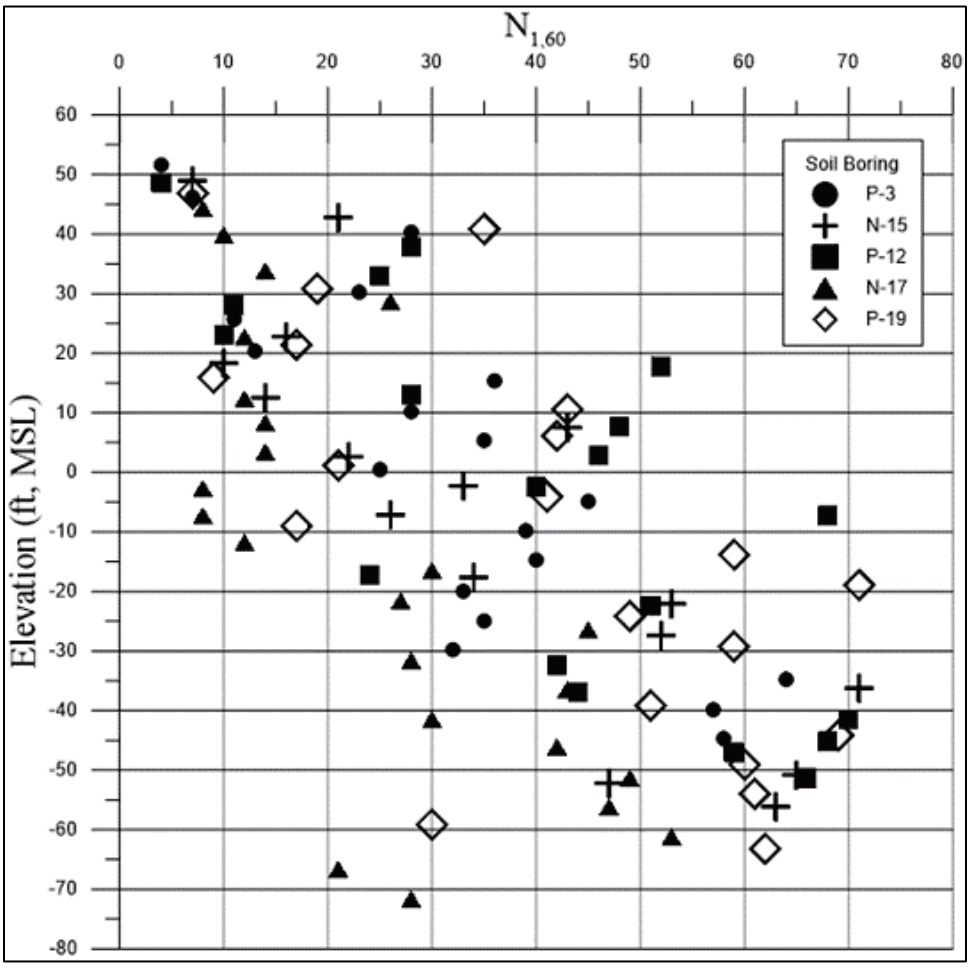

Figure 24. SPT locations.

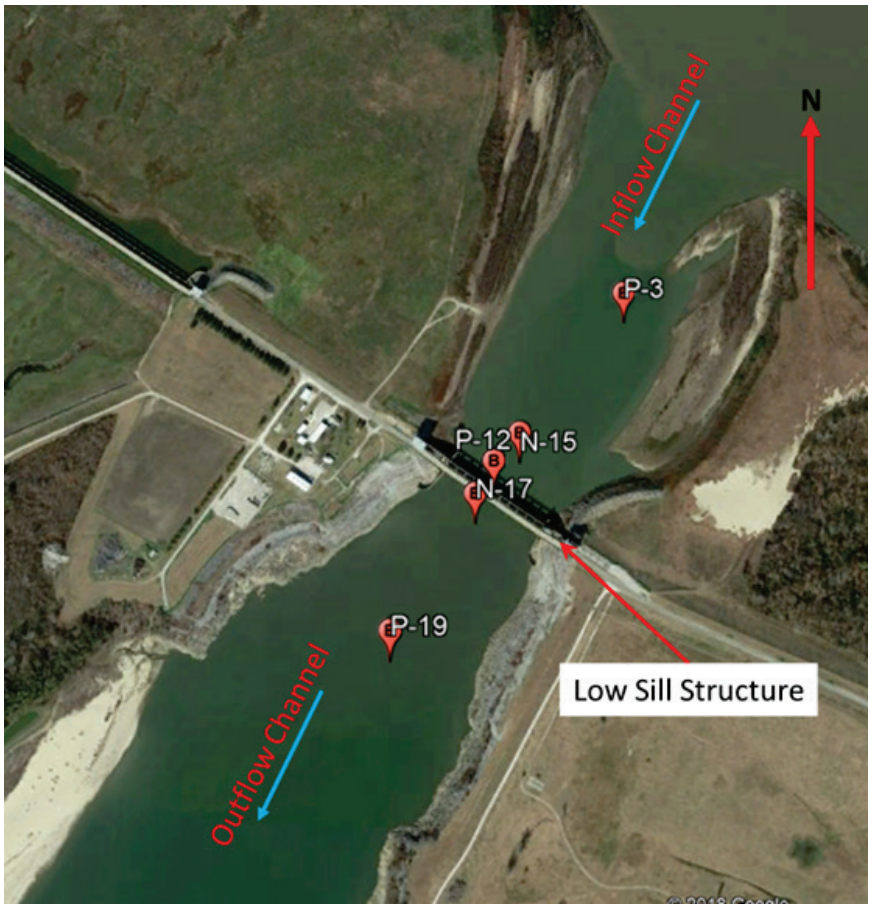

During the general design and exploration phase, laboratory testing was conducted to assess the shear strength using direct shear and triaxial testing. The tests performed consisted of consolidated undrained (CU), unconsolidated undrained (UC), and consolidated drained (CD) testing (USACE 1954). The results of CD tests on the silts, sandy silts, and silty sands resulted in a friction angle of 34 deg and for the clean sands, a friction angle of 36 deg was measured (Turnbull and Shockley 1958). Undisturbed samples of the sands were collected by freezing the samples, and these results were compared to remolded samples with good agreement between the two samples (USACE 1954).

After review of the boring logs and laboratory data, a simplified interpretation was derived (Table 6). The simplified interpretation in Table 6 was used in the numerical model and is considered representative of the ORLSS foundation prior to the scour event. Table 3 shows a comparison of laboratory measured shear strengths and those derived from the corrected SPT blow counts. The shear strengths derived from SPTs used the

relationship presented in McGregor and Duncan (1998). There is very good agreement between the laboratory and field-derived friction angles.

Table 6. Representative properties selected for pile analysis.

Elevation (ft, msl)	Layer	Blow Count, N (blows/ft)	σ' (psf)	Corrected Blow count, N' (blows/ft)	φ' (deg)		USCS
					SPT	Lab	
-0.8	1	5	90.0	10	32	33	ML
-5.7	2	17	1406.7	20	33	33	ML
-45.4	3	40	2836.5	36	35	33	ML
-55.5	4	78	3932	62	40	36	SP

4.3 Pile foundation

The ORLSS was founded on piles to ensure stability of the structure with respect to horizontal sliding and to prevent excessive settlement. A total of 1,920 H-piles were driven with 454 of these driven vertically and 1,466 battered either upstream or downstream (USACE 1959). The piles were grouped according to orientation, Group A is oriented vertically, Group B are battered upstream, and Group C are battered downstream. Group B piles were fitted with tension connectors. Figure 25 shows the piles in section view for the weir and low-flow monoliths. The pile-driving criteria were set to ensure that the piles were driven to a minimum and maximum of 25.0 ft and 35.0 ft, respectively, into the sand aquifer underlying the silts and silty sands.

Figure 25. Pile layout for weir and low-flow monoliths (USACE 1954).

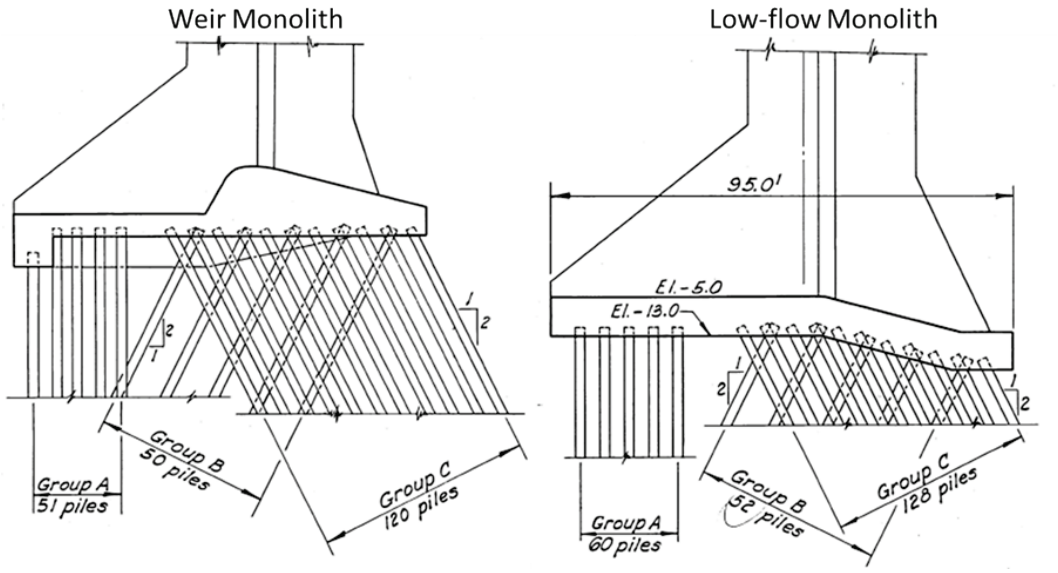

Pile-driving criteria were selected based on results of a pile-load test performed in January to March of 1955 (USACE 1959). The load test was performed by loading the piles vertically and measuring the displacement of the pile under each load. The pile load tests were conducted in an excavation to relieve overburden pressure from the foundation soils and better simulate actual conditions to which the piles would be subjected to during their service life. Seven different piles were tested during the load test. Due to the sensitivity of the structure to differential settlement and the compressibility of the silty foundation soils, it was deemed necessary to determine the load on the pile that could be carried by the clean sand and underlying silty soils (USACE 1956). Strain rods were installed on six of the seven piles tested to determine the distribution of load in the pile during testing. Results of the load tests were presented to the pile driving contractor and H-piles were selected as the most cost-effective option (USACE 1959). Two different configurations of the H-pile were tested during the load test, one with a bottom plate and the other without a bottom plate. The piles selected for driving were the option without a bottom plate.

Results of the pile load test are shown in Figure 26 in the form of the axial load versus settlement curve. During design of the low sill structure, it was assumed that the piles would be capable of carrying 200 kips in compression and 80 kips in tension, although only Group B piles were fitted with tension connectors. Results of the pile load test showed that for a pile load of 200 kips, the factor of safety against plunging would be 1.35.

It was predicted that the structure would settle approximately 0.2 in., and most of this settlement would occur during construction.

Figure 26. Axial load versus settlement for 14-in. H-pile (USACE 1956).

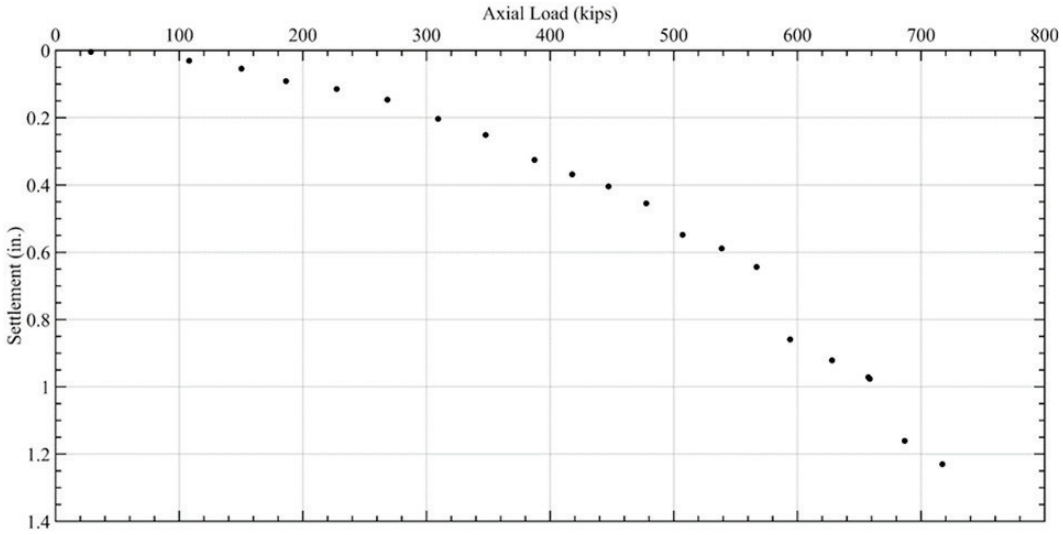

Shear strengths of the foundations soils were also assigned based on the results of the strain measurements during the load test. Based on direct shear tests on samples from the silt stratum, it was shown that full shear strength was mobilized at 0.2 in. of displacement; therefore, it was assumed that the same displacement would lead to full mobilization of shear strength along the pile. The average skin friction for the silt was computed for each pile from the portion of total load carried by the silt stratum. The skin friction developed in the silts during the load test and calculated values of skin friction are shown in Figure 27.

The friction angle calculated based on bearing capacity of the sand and Terzaghi's formula for tip resistance in a pile was found to be 33 deg, which is less than that measured in CD triaxial tests, and was attributed to the maximum shear strength mobilized at the maximum safe movement of the pile.

Figure 27. Skin friction measured from pile load test compared to assumed values, USACE (1956).

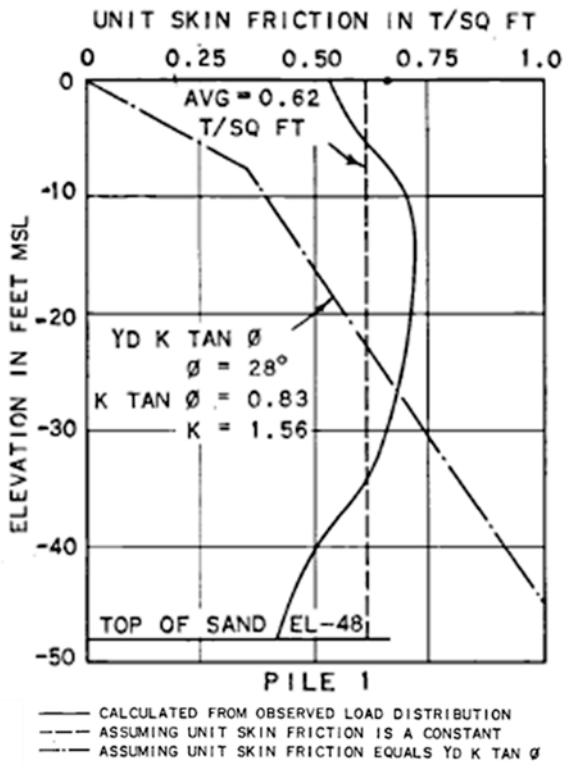

4.4 Numerical analysis of pile stability

Numerical modeling was performed in three stages. The first stage was performed to calibrate the model parameters of a single pile to the results of the pile load test. The second and third stages were used to assess the response of the pile groups in the low-flow and weir monoliths. Three material property cases were used in the second and the third models. These material property cases incorporated the results of the first model in addition to a conservative case.

4.4.1 Pile load test model

Results of the pile load test described in USACE (1956) were used to calibrate a numerical model to assess the conservativism of the design parameters recommended from the results of the pile load test. The numerical model simulated the pile load test and the software used for this assessment was TZPILE, version 2014, distributed by ENSOFT. Table 7 shows the properties of the 14-in. H-beam pile used in the model. During the load test, piles were driven vertically as opposed to at a batter due to cost and loading difficulties. The designers felt that the battered

piles would not have appreciably less resistance and could be driven through the clay stratum based on experience from pile load tests at the Morganza Floodway control structure (USACE 1956).

Table 7. Pile properties, 14-in. H-beam.

Weight (lb/ft)	Area (in²)	Depth (in.)	Flange Width (in.)
73	21.4	13.61	14.59
E_s (psi)	AE (lb)	A_t* (in²)	L_{emb} (in.)
29,000,000	6.206E8	198.5	966

Note: *tip area was taken as a rectangle due to probable plugging of web during driving, E_s is the Young's modulus of steel, A_t is tip area, L_{emb} is embedment length, AE is area times Young's modulus

The numerical model of the pile load test was conducted in two different cases. The first case considered the foundation to consist of a silt layer and a sand layer. The two-layer model used load transfer curves generated using Mosher's sand model (Mosher and Dawkins 2000). Results from the two-layer model adequately matched the load settlement curve from the 1956 load test, but the load distribution diverged. Therefore, a four-layer model was developed, with three layers in the silty layer above the aquifer and one layer for the aquifer. In addition to splitting the foundation into four layers, the API sand model was adopted as this soil model is available for use in the 3-D model, while Mosher's model is not. Both models are available in TZPILE. Figure 28 shows the unit skin friction along the pile in the silt layer compared to the ultimate skin friction assumed for the model.

Figure 28. Skin friction measured in pile load test (discrete points), and the assumed skin friction in numerical model (solid line).

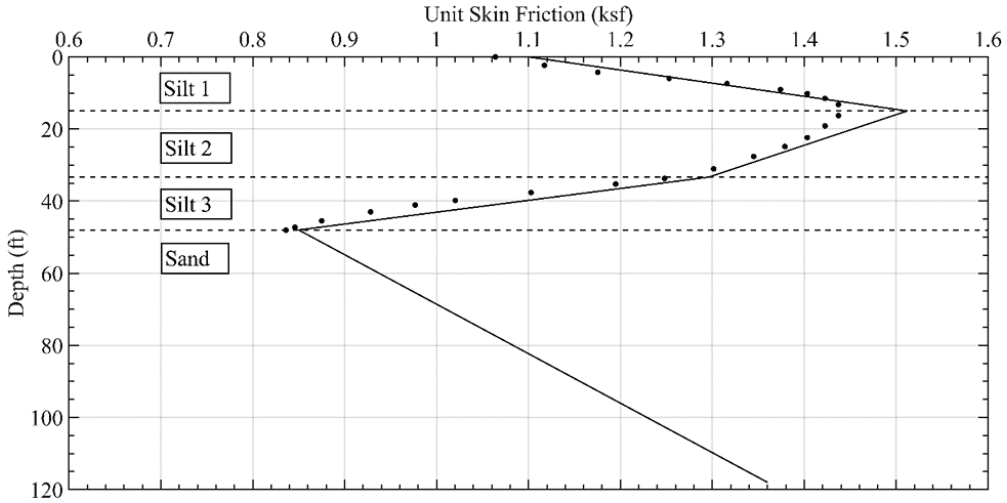

Soil properties used in the model are shown in Table 8 and are the result of SPT correlations and laboratory testing. The ultimate side friction at depths between the top and bottom of a layer was attained by linear interpolation between the top and bottom values. The pile tip load versus displacement (Q-w) relationship measured during the load test and that used in the model are shown in Figure 29.

Table 8. Soil properties used in the numerical model.

Layer	Depth (in.)	γ_b (lb/in^3)	φ' (deg)	Side friction (psi)	Tip resistance (psi)
Silt 1 (top)	0	0.033	33	7.3	-
Silt 1 (Bot.)	180	0.033	33	10.5	-
Silt 2 (top)	180	0.033	33	10.5	-
Silt 2 (Bot.)	400	0.033	33	9	-
Silt 3 (top)	400	0.033	33	9	-
Silt 3 (Bot.)	576	0.033	33	5.5	-
Sand (top)	576	0.033	36	5.5	2200
Sand (Bot.)	966	0.033	36	5.15	2200

Figure 29. Axial load versus displacement from load test and that assumed in the model.

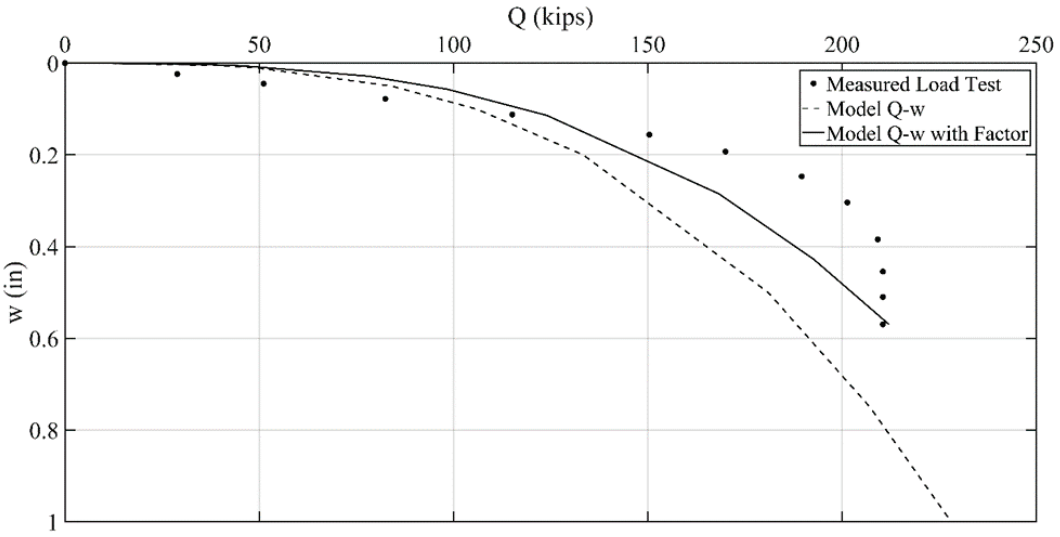

The Q-w relationship derived from the material properties is shown in Figure 29. This relationship overpredicts the displacements under a given load compared to that measured in the field; therefore, scaling factors were applied for a more accurate representation of the values measured during the load test. The predicted load (Q) points were

multiplied by 0.93 and the settlement (w) points were multiplied by 0.57. These data are shown in Figure 29 as the "Model w/Factor" curve.

The axial load versus settlement relationship is shown in Figure 30 with results of the modeling effort. Case 1 in Figure 30 represents the results of the modeling effort using the recommended design values for skin friction and tip capacity. Case 2 represents the results using magnification factors for the tip load and skin friction. The difference in results represents the level of conservatism associated with the original design properties. Case 3 represents a lower bound case modeled in the 3-D model as part of a parametric analysis. The Case 2 results represent a best estimate of in situ conditions, and they are still slightly conservative, meaning that the predicted settlement under a given load would be larger than that measured in the pile load test.

Figure 30. Axial load versus settlement for load test and numerical model (4 layer).

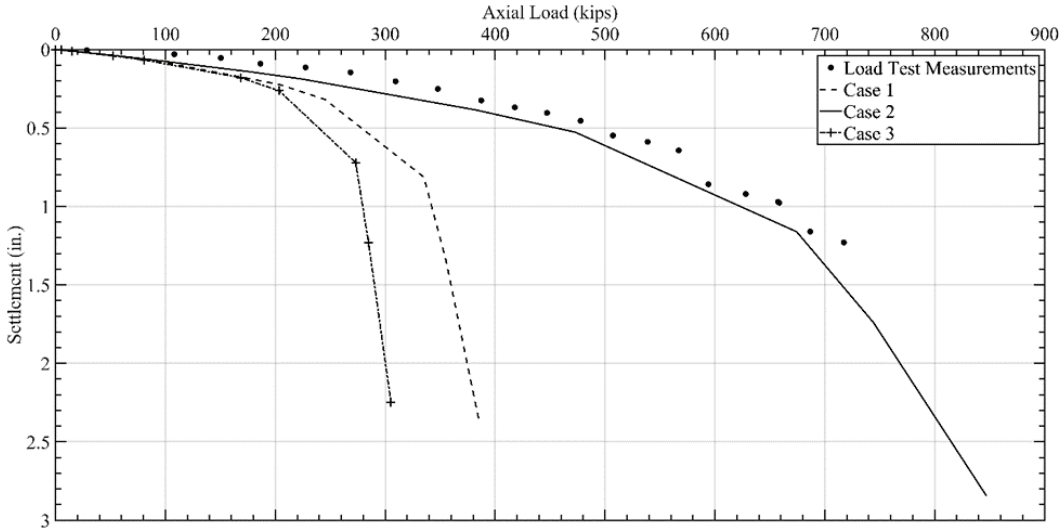

Load distributions along the pile are shown in Figure 31. Modification factors were applied to the t-z curves generated from the material properties. The factors varied with depth and are shown in Table 9. Generally, there is adequate agreement between the measured load distribution and the predicted load distribution, as shown in the results from the Case 2 model.

Table 9. t-z multipliers with depth.

Depth (in.)	t-multiplier	z-multiplier
0	1.85	0.55
240	1.75	0.65
600	1.8	0.9
966	0.4	1.3

Figure 31. Load distribution in pile, load test and model results; solid lines represent model results, and dots represent measurements.

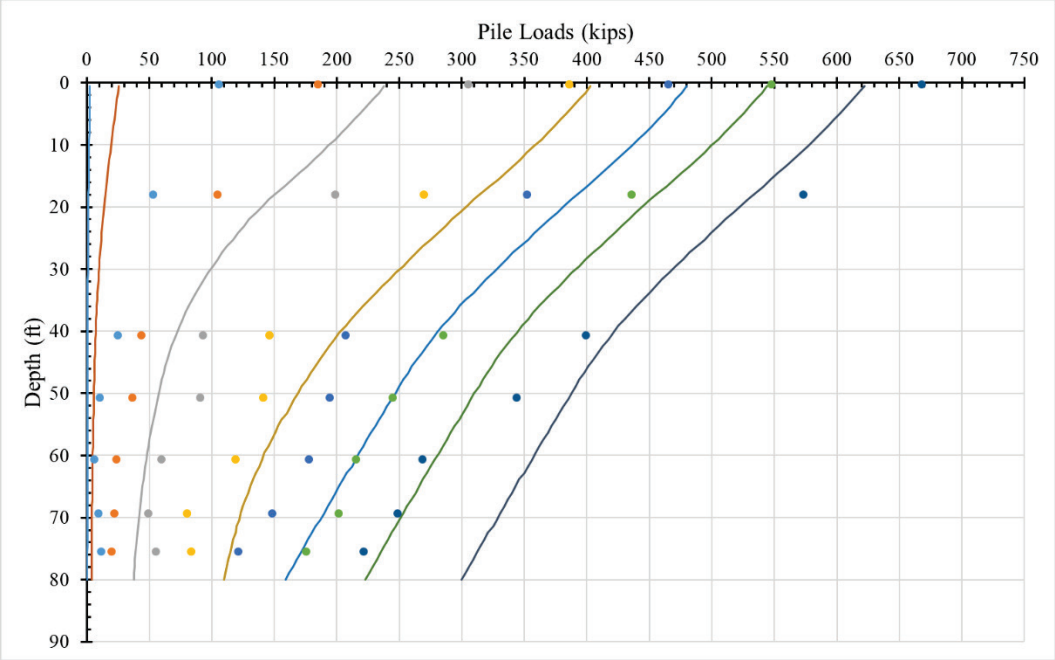

Results of the pile load test indicate that the original tip and side friction properties used for design were conservative. The term conservative in this case means that increased displacements would have resulted from their use for a given load. The threshold for settlement of the structure was deemed to be 0.2 in. based on the sensitive nature of the structure. In order to adequately model the pile load test results, magnification factors were necessary to match the load test results or in situ conditions.

4.4.2 Ultimate capacity

The allowable design loads used in the design of ORLSS were 200 kips compression and 80 kips tension. The allowable loads reported in USACE (1975) provide a factor of safety of 1.52 and 1.75 for compression and tension respectively. These loads were based on the ultimate capacities obtained from the pile load tests (USACE 1956). The piles in the tests were

driven to a tip elevation of -80.0 ft, msl, while the average pile tip elevations of those driven for the structure were -90.0 ft, msl (USACE 1975). As shown in Figure 23, there is a definite increase in shear strength with depth; therefore, the ultimate capacity of the pile foundation of the structure was taken as 304 kips compression and 140 kips tension (USACE 1975a). The capacity was selected based on the allowable pile displacement of 0.2 in.

To investigate the reasonableness of the selected foundation properties, axial capacities were calculated using Nordlund's method as described in U.S. Department of Transportation (2006). The Nordlund method was derived based on field observations of load tests performed in cohesionless soils. The method takes into account pile shape and its soil displacement in calculating the pile shaft resistance. It also accounts for the differences in pile material to soil friction. The length of embedment used in the calculation was 81.0 ft, and the friction angles of the silty soils and sands were 33 deg. The results of these calculations were 99.4 tons tip resistance and 239 tons of shaft resistance with 79.3 tons in the silty soils and 160 tons in the sand. The ultimate capacity is the sum of the tip and shaft resistance and was found to be 338.7 tons. The ultimate capacity of the pile measured in the pile load test was found to be 344 tons at a net pile displacement of 1.18 in. There is reasonable agreement between the two methods. Results of this calculation and the modeling of the pile load test indicate that the selected foundation properties are representative of the site and are reasonable and appropriate for use in the 3-D structural model.

4.5 Summary of previous analyses

There have been six analyses performed on the pile foundation of ORLSS. These analyses range from using classical methods, such as Culman's method, to the linear 3-D analysis performed using Hrennikoff's method. The level of complexity increased through time and can be attributed to the availability of computing equipment capable of performing increasingly complex computations. Culman's method was performed in the original design analysis described in USACE (1954). Often classical methods, such as Culman's method, assumed the pile cap was rigid and all loads were resisted only by axial forces in the piles, and no attempt was made to calculate the deformations of the system (Mosher and Dawkins 2000). Classical methods can be unconservative depending on the attachment of the pile head to the structure.

The method developed by Hrennikoff is a direct stiffness approach, which can be used in 2-D and 3-D. This method considers the interaction of the piles with the surrounding soil in addition to the compatibility of the pile head and pile cap displacements. The relationship between the pile head forces and the displacements of the point of attachment to a rigid pile cap is assumed to be linear (Mosher and Dawkins 2000).

The current stability analysis using nonlinear methods employs numerical methods to solve for the capacity and deformation. This method employs nonlinear relationships that give soil stiffness and resistance as a function of pile deflection along the pile length. The solutions of the resulting equations are then made to satisfy conditions of equilibrium and compatibility (Van Impe and Reese 2010).

The ORLSS was designed for a maximum water surface elevation of 67.0 ft, msl. The project flood discharge is 620,000 cfs for both the overbank and ORLSS for the 1950 channel conditions (USACE 1954). The load cases used in the design analysis are shown in Table 10. Culman's method of analysis was used in the foundation design assuming 200 kips compression and 80 kips tension. The low-flow monolith was constructed with results of load cases IIa, III, and VI. The required load capacity for the Group A piles was 60 kips compression, Group B piles were 26 kips tension and 52 kips compression, and Group C piles were 128 kips compression. The weir monoliths required load capacities of 50 kips compression for Group A piles, 38 kips tension and 48 kips compression for Group B, and 120 kips compression for Group C piles (USACE 1954). Results of the design analysis showed only Group B piles incurring tension; therefore, this pile group was installed with tension connectors.

Table 10. Load cases considered for design of ORLSS (USACE 1954).

Load Case	Headwater (ft, msl)	Tailwater (ft, msl)	Uplift Condition	Note:
I	NA	NA	NA	Structure complete, dewatered condition
II	35	0	Design	Gates closed, bridge live loads
IIa	35	0	TW over entire base	Bridge live loads
III	67	40	Design	Bridge live loads
IIIa	67	40	TW over entire base	Bridge live loads
IV	67	40	Design	Bridge live loads, all gates open
IVa	67	40	TW over entire base	Bridge live loads, all gates open
V	67	40	Design	One gate per monolith open, all bridge live loads
VI	23	38	TW over entire base	Bridge live loads

Note: design uplift = $0.5\Delta h+h_{TW}$, applied at the upstream edge

$=0.1\Delta h+h_{TW}$, applied at the downstream edge

TW = tailwater elevation

The resulting pile layout from the design analysis is shown in Figure 25. A follow-up analysis was conducted for the first periodic inspection in 1967. This analysis was conducted to inspect the design uplift assumptions. Piezometer data from 2 June 1961 were used, and the uplift was calculated. The piezometers used for this analysis were B-3, B-4, and B-10 and are located upstream, centerline of structure, and downstream, respectively (USACE 1967). These piezometers are located near the centerline of the channel. The results of this analysis agreed well in terms of percent difference; the upstream pressure was 0.5 percent greater than the design value, 2.5 percent smaller at the centerline, and 0.2 percent greater at the downstream edge. With these results, no further calculations were necessary, and it was concluded that the structure was operating as designed.

Another stability review was conducted for the second periodic inspection conducted in 1969. The critical design load cases, IIa, III, and VI were investigated. These cases were reanalyzed using uplift pressures

extrapolated from observed piezometer readings. This analysis was conducted using Culman's method. Results of this analysis are shown in Table 11. Review of Table 6 shows that load case III results in a small amount of tension developed in the Group A piles. Again, only Group B piles were fitted with tension connectors. This analysis assumed that the small magnitude of the tension load for Group A, with the capacity to carry no tension, would be redistributed to the Groups A and C piles without a problem. The remaining pile loads were within capacity of the structure with the largest compressive load occurring in Group C piles with load case III. This load was greater than that assumed for design but was only 3.5 percent more and still less than capacity.

Table 11. Results of Periodic Inspection #2, stability review.

Load Case	Group A Piles (kips)	Group B Piles (kips)	Group C Piles (kips)
IIa	183	52	153
III	-6.7	-27	207
VI	49	198	5

Note: positive pile load for compression, negative for tension

An amendment to the 1972 periodic inspection was made as Appendix E and was completed after USACE analysis (1972). This appendix resulted from a recommendation made after review of the periodic inspection report within MVN and the USACE Lower Mississippi Valley Division, where it was requested that the design analysis be updated using Hrennikoff's method for a 3-D analysis This updated analysis was conducted on the low-flow weir and transition monoliths. Loading conditions for this analysis consisted of IIa, IIIa, VI, and III. Table 12 shows the results of the analyses conducted for the 1972 periodic inspection.

Table 12. Results of the analysis using Hrennikoff's method conducted for the 1971 periodic inspection recommendation (USACE 1972).

Monolith	Load Case	Group A Piles (kips)	Group B Piles (kips)	Group C Piles (kips)
Low-Flow	IIa	198.7	92.6	173.3
	IIIa	79.2	-9.2	206.9
	VI	60.3	-10.4	176.8
	III	40.7	-44.6	205.4
Weir	IIa	186.3	95.6	173.9
	IIIa	70	-27.1	203.3
	VI	48.1	176.1	-20.6
	III	32.9	-59.8	202.2

Note: positive pile load for compression, negative for tension

The results of 1972 analyses were judged to match the original analysis conducted using Culman's method of analysis. The maximum axial load was calculated to be 206.9 kips and represented a 3.5-percent overstress. This overstress was for one row of piles in Group C, and it was felt that neighboring piles would be able to carry the excess. A maximum tensile load of 20.6 kips was also found in the Group C piles, and it was felt that the original design was in error on this regard. Meaning that additional pile groups should have been fitted with tension connectors. A calculation of the bond between the pile and the concrete base was made, and the results of this analysis showed a tensile capacity of 45 kips for piles without formal tension connectors. Therefore, it was felt that the piles in Group C would accommodate that small tensile load calculated in the analysis. The results of the analysis of the transition monolith were all within the allowable axial pile loads. The conclusion drawn from this analysis was that the original design of the pile foundation was compatible with the updated methods of analysis.

In the spring of 1973, a flood event resulted in the failure of the left abutment approach wingwall and a large portion of the silty sand foundation beneath the south monoliths of ORLSS with scour to EL -55.0 ft, msl. Figure 32 shows the lateral extent of the scour beneath the structure, and Figure 12 shows extent at the deepest section from upstream to downstream. A remediation program was initiated during and following the flood event as a result of the scour. The remediation included a grouting program, increased instrumentation monitoring, construction of a riprap training dike, and subsequent stability analysis. The stability analysis was outlined in USACE (1975), and the purpose of the stability analysis was reported to provide an evaluation of ORLSS for existing and predicting future design cases, include an evaluation of the structure for stability and alternative evaluation, and address the question of risk.

The stability future design cases were investigated, and allowable operating conditions were developed. The stability analysis consisted of load cases from the original design memorandum (USACE 1954), as well as future design cases developed from predicted channel elevations and river hydraulics upstream and downstream of the structure. Table 13 shows the additional load cases. The original design load cases were each assigned four subcases, which included assumptions about the grouted foundation. It should be noted that the 1975 load cases do not agree with the original design (USACE 1954) load cases. For example, in

USACE 1954 load case VI had a headwater elevation of 23 ft and a tailwater elevation of 38 ft while USACE 1975a reported load case VI with a headwater elevation of 70 ft and a tailwater elevation of 51.3 ft. Therefore, each load case throughout this document is reported with headwater and tailwater elevations to avoid further confusion.

Figure 32. Scour beneath the structure because of the 1973 spring flood (USACE 1975).

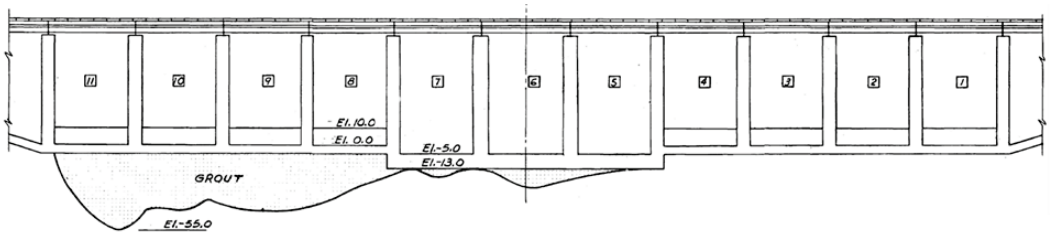

Table 13. Predicted future load cases from USACE (1975).

Load Case	Headwater (ft, msl)	Tailwater (ft, msl)	Uplift Condition	Note:
VI	70	51.3	Full HW, base of slab	No horizontal load on grout, no crane live load, all gates closed
VII	62.5	40.8	Full HW, base of slab	No horizontal load on grout no crane live load, all gates closed
VIII	62.5	40.8	Full TW uplift	Grout load on piles, horizontal load on piles, highway and crane live loads
IX	NA	NA	No uplift	Dewatered condition, all live and dead loads

Note: design uplift, = $0.5\Delta h+h_{TW}$, applied at the upstream edge

= $0.1\Delta h+h_{TW}$, applied at the downstream edge

TW = tailwater elevation, HW = headwater elevation

The subcases identified above considered the condition where the grout bonded to the piles and acted as an additional dead load on the piles. The other conditions include the uplift located either at the base of the grout or directly beneath the structure. The following list outlines these subcases further (USACE 1975):

a. No grout load, full headwater uplift applied at the base of the slab, no horizontal load on the grout, and no crane live load. It was felt that this case would result in a maximum tensile load in the piles, with the assumption that the grout did not bond to the piles.

b. Grout load assumed acting on the piles, headwater uplift applied at base of grout, horizontal load on the grout, no crane or highway live load. This load case was assumed to represent the lower limit of the tensile load on the piles.

c. Grout load assumed acting on the piles, full tailwater uplift applied at base of slab, horizontal load on grout, highway and crane live load. This case was considered to represent the maximum compressive load on the piles.

d. No grout load, full headwater uplift applied at base of the slab, no horizontal load on grout, no crane or highway live load, no Group A piles. This case represents the condition where the Group A piles are neglected due to their inability to carry a tensile load.

The ultimate pile capacities used to assess the factor of safety were 304 kips compression and 140 kips tension for the piles unaffected by scour and 200 kips compression and 80 kips tension for those affected by scour. Pile groups B and C noted in USACE (1975) are switched when compared to USACE (1954). In the 1975 stability analysis, pile Group C were the piles fitted with tension connectors, originally noted as Group B. The method of analysis used to assess the stability was based on Hrennikoff theory and is similar to the analysis presented in USACE (1972). The stability criteria used in the assessment were the following (USACE 1975):

1. Tension in either Group A or B piles.
2. Tension load greater than 80 kips in Group C.
3. Compression loads greater than 200 kips.
4. Axial and lateral loads such that the combined stress formula exceeds a value of one.

Results of the analysis indicated that unstable conditions existed for most cases considered for the south weir monoliths and the low-flow monolith. The two worst conditions per load case of the stability analysis are shown in Table 14 and 15. The worst conditions were defined as the largest compressive or tensile load.

This analysis represents a conservative approach aimed at providing a basis for operating the structure safely in the future (from 1975 onward). Results for the low-flow monolith were similar, albeit the calculated loads in the piles were lower in magnitude. Table 14 shows the results of the stability analysis for the low-flow monolith. No displacements or load distributions were presented. One of the primary factors impacting these results were the assigned uplift conditions, with lower uplift conditions causing higher compressive loads as can be seen in the subcase C results. High tensile loads resulted from the subcase A results, where full headwater uplift conditions were assigned.

Table 14. Results of stability analysis south weir monolith (USACE 1975a).

Load Case	Subcase	Group A	Group B	Group C	Group Exceeded Failure Criterion
I	A	-51.2	149.6	-107.2	A,C
I	C	152.7	282.9	28.9	B
II	A	-4.01	96.3	-57.6	A
II	C	201.8	252.2	70.9	A,B
III	C	257.7	237.6	126.6	A,B
IV	B	153.6	208.8	-75.9	B
IV	C	292	287	121.8	A,B
V	B	199.4	78.6	338.4	C
VI	NA	-36.8	148.5	-73.7	A
VII		-21	136.6	-84.2	A,C
VIII		256.8	227.6	132.9	A,B
IX		335.4	202.8	381.1	A,B,C

Table 15. Results of stability analysis low-flow monolith (USACE 1975a).

Load Case	Subcase	Group A	Group B	Group C	Group Exceeded Failure Criterion
I	A	-42.3	161.6	-122.3	A,C
I	D	NA	222.9	-216.5	B,C
II	D	NA	131.9	-84.9	C
IV	A	61.8	105.8	-102.7	C
IV	C	218.7	196.4	96.5	A
V	C	82.9	-2.6	185.1	B
VI	NA	-237	156.5	-97.7	A,C
VII		-9.4	145.7	-107.4	A,C

Results of the 1975 stability analysis led to construction of the auxiliary structure and a 13-ft head differential operating condition. Another analysis was conducted for the 1986 dewatering of the structure. This analysis was conducted in a similar manner as the 1972 and 1975 analyses, except that the loading conditions considered were focused on headwater elevations up to 40.0 ft with dewatered conditions on the tailwater side of the structure. It was found that the low-flow monolith was critical due to high tension in the piles. Considering the load redistribution, a headwater of 30.0 ft was considered safe for dewatering. The uplift conditions considered for this analysis were assessed based on piezometric interpretations, full headwater and design uplift, and conditions assumed for the 1975 analysis.

At the time of the 1986 dewatering analysis, the maximum differential head on the structure was increased to 22.0 ft. The increase took into account the 1975 analysis, in addition to allowable pile overloading, and it was stated that this limitation was coincidental with both a hydraulic limitation, based on scour considerations, as well as anticipated future head requirements for flow distribution (USACE 1986). Historically, ORLSS was subjected to differential heads of 35.0 ft in 1964 and 33.5 ft in 1966, both loadings coincided with marine salvage operations (i.e., removal of barges).

Using the Hrenikoff method of pile analysis, three load cases were investigated for the 1986 dewatering analysis. The first case considered that the grout provided confinement pressure to the piles but did not bond to the piles. The second case assumed the grout provided confinement and bonded to the piles, and the buoyant weight of the grout mass was applied as an additional load. The lateral water pressure for Cases I and II was applied to the base of the slab, while for Case III, the lateral water pressure was applied to the base of the grout. Uplift pressure was applied based on piezometer assessment and full headwater was applied on the upstream side with a reduction applied across the base of the slab.

The differential heads applied ranged from 8.0 to 12.0 ft for the 1986 dewatering analysis. Results shown in Table 16 represent either maximum compression or tension (negative values). The maximum pile compression that resulted from this analysis was for piles in Group B for Case III, with a headwater of 30.0 ft, msl and a 12.0 ft head differential. For this analysis, the results showed that 7 percent of the piles would be overstressed, and no tension was developed in Group A piles.

Table 16. Results of 1986 dewatering analysis (USACE 1986).

Load Case	Headwater (ft msl)	ΔH (ft)	Group A (kips)	Group B (kips)	Group C (kips)	% piles overstressed
II	15	8	213	145	198	3
II	15	10	194	140	186	-
II	20	8	210	151	182	2
II	25	8	202	157	166	-
II	25	8	194	153	161	-
III	30	12	202	214	-18	7
III	30	12	196	198	57	-
III	30	12	188	195	96	-
II	30	8	189	159	148	-
II	30	8	182	155	144	-
II	35	8	175	166	129	-
II	35	8	168	162	124	-

The 1986 dewatering analysis was limited to the conditions pertinent to the planned dewatering of the stilling basin. Noteworthy was the continued use of Group C piles, oriented to the upstream side in their batter direction, which was first noted in the 1975 analysis where the original design for these piles was noted as Group B piles. Figure 33 shows the difference between the original and 1975 pile nomenclature. It appears that the number of piles and batter orientation are correct, but it is worth pointing out the change in nomenclature to avoid any confusion for future reference. The original pile nomenclature will be referenced (USACE 1954, Figure 33). This nomenclature indicates that Group B are the piles fitted with tension connectors and battered toward the upstream direction.

Figure 33. Original design (USACE 1954) nomenclature and 1975 pile nomenclature (USACE 1975).

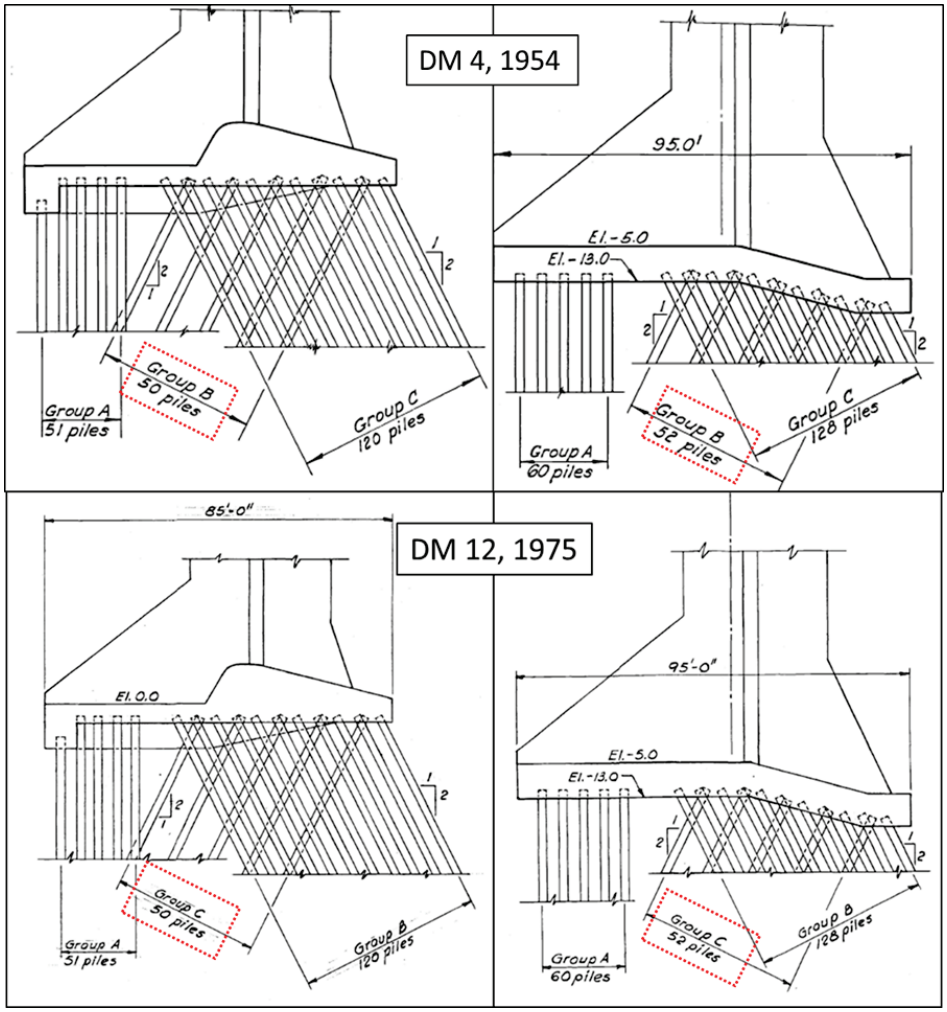

4.6 2021 updated ERDC pile stability analysis

An updated analysis of the pile response was conducted for this study for both the low-flow and weir monoliths. Each of the monoliths was analyzed for the design condition as well as for the post-scour conditions. Table 17 shows the loading conditions for the design, Table 18 shows loading conditions for the post-1973 cases for the low-flow monolith, and Table 19 shows the post 1973 cases for the weir monolith. Note that load case VI from Table 17 changes to V in Table 19. The design condition was analyzed to compare how the nonlinear software GROUP would compare to the linear analysis methods used previously. The headwater-tailwater, uplift, and additional loadings are shown in Table 17. The stability of the low-flow monolith was also investigated. The loading conditions for this analysis are shown in Table 18. The uplift condition assumed for this analysis was full headwater.

Table 17. Load cases considered for the design condition for both the low-flow and weir monoliths.

Load Case	Headwater (ft, msl)	Tailwater (ft, msl)	Uplift Condition	Note:
IIa	35	0	TW over entire base	Bridge live loads
III	67	40	Design	Bridge live loads
IIIa	67	40	TW over entire base	Bridge live loads
VI	23	38	TW over entire base	Bridge live loads

Note: design uplift, = $0.5\Delta h+h_{TW}$, applied at the upstream edge

= $0.1\Delta h+h_{TW}$, applied at the downstream edge

TW = tailwater elevation

Table 18. Loading and modeling assumptions for low-flow monolith, post-scour event. Note the USACE (1975a) load cases were used.

Load Case	Headwater (ft, msl)	Tailwater (ft, msl)	Uplift Condition
I	67	40	Full HW
IV	35	0	Full HW
VI	70	51.3	Full HW

Note: HW = headwater elevation

Loading conditions for the post-scour condition of the weir monolith were analyzed with similar sub-cases as those used in the 1975 analysis. Loadings for the post-scour condition of the weir monolith and modeling assumptions are shown in Table 18. Two uplift conditions were considered: a full headwater and uplift distribution assumed during design of the structure as shown in Table 19. Analysis of the designed uplift assumption was validated in periodic inspection numbers 1 and 2 by comparison to measured values. The uplift condition is important for this analysis as it can impose additional tension on the piles. Additionally, an assumption regarding how the grout interacts with the piles was simulated, whether the grout is bonded to the piles or not bonded. To simulate a grout-to-pile bond, an additional dead load was applied, and its magnitude corresponded to the assumed weight of the grout injected in the foundation.

Table 19. Loading and modeling assumption for weir monolith, post-scour event. Note the USACE (1975a) load cases were used.

Load Case	Gates	Headwater (ft, msl)	Tailwater (ft, msl)	Loading details
I	closed	67	40	Full HW, no grout load Design, no grout load Full HW, grout load Design, grout load
IV	closed	35	0	
V	closed	23	38	
VI	closed	70	51.3	

To build the 3-D model of the low-flow and weir monoliths, it was necessary to map out the locations of the pile head and tips. This was made possible by using the information available in the as-built plans (USACE 1959). The location of the pile heads is shown in Figure 34 with solid symbols, and the pile tips are shown with open symbols. The sign convention of this figure is positive towards the left abutment and upstream locations. The location of the data shown in Figure 34 is at the intersection of the weir and channel centerline. The 3-D models constructed using the digitized as-built data are shown in Figure 35. Material properties used in this analysis are shown in Table 7. The pile heads were modeled in the pinned condition.

Figure 34. Pile head and tip locations for ORLSS; solid symbols are head, and open symbols are tip.

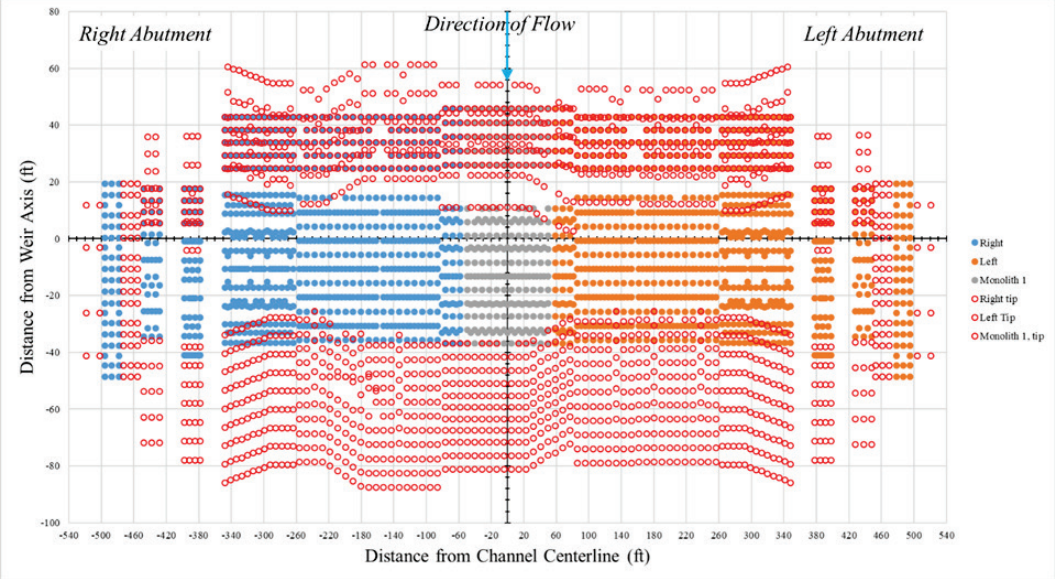

Figure 35. Low-flow monolith 3-D model, (a) section and (b) isometric view. Note that vertical piles occur at the upstream side of the structure.

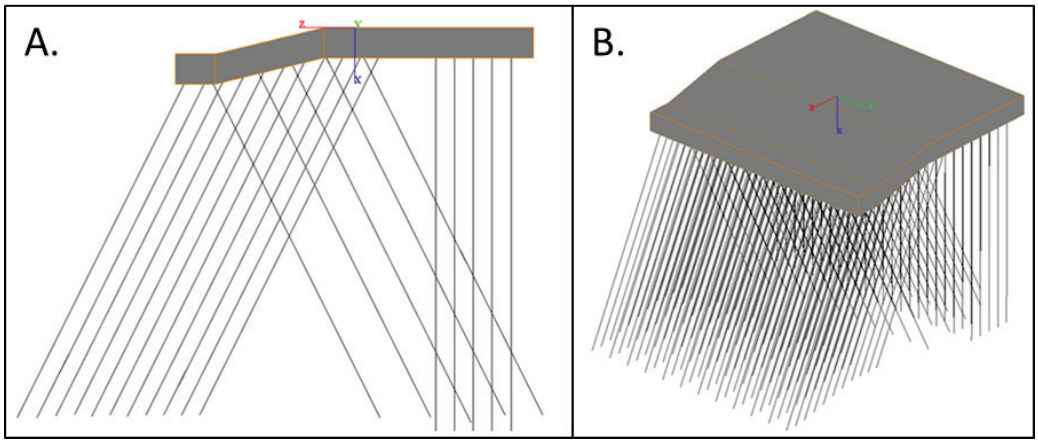

4.6.1 Modeling results low-flow monolith

Analysis of the low-flow monolith included the pre- and post-scour event conditions. The pre-scour or design condition was assessed using four loading conditions (Table 17). There were three loading conditions considered for the post-scour event. The results using the best estimate of material properties are presented in Table 18. Results of other property cases were within a few kips of the results presented. The most critical loading condition was for pile Group A, with a maximum displacement of 0.16 in. and an axial force of 199.3 kips. Headwater and tailwater elevations for load case IIa were 35.0 ft and 0 ft, respectively. The location of the maximum axial force for this analysis is shown in Figure 36 and was in the second row of Group A piles. These results are similar to those presented in the 1972 analysis. The results of the 1972 linear analysis are presented in the final column of Table 20 for comparison.

Comparison of the results between the two analyses for load case IIa is very reasonable, with the current analysis having higher compressive loads in pile Group A and lower in Group B. The largest discrepancy between the two analyses is for load condition VI, where reverse loading was considered (i.e., higher head on the stilling basin side from Red and Atchafalaya river flooding). For load condition VI, the 1972 analysis resulted in tension occurring in Group C piles, while the minimum load in these piles for the current analysis remained compressive. The differences between two analysis methods are judged reasonable, and the foundation properties and method of analysis are considered appropriate.

Table 20. Results of the low-flow monolith considering design conditions; negative values are tension, and positive values are compression.

Load Case	HW Elevation (ft, msl)	TW Elevation (ft, msl)	Group	Max Disp. (in.)	Min Disp. (in.)	Max Axial Force (kips)	Min Axial Force (kips)	1972 App. E Max Axial Force (kips)
IIa	35	0	A	0.16	0.14	199.3	172.2	198.7
			B	0.12	0.07	110.6	64.7	92.6
			C	0.12	0.07	144.0	91.4	173.3
IIIa	67	40	A	0.07	0.07	87.0	63.6	79.2
			B	0.12	0.08	94.9	44.8	-9.2
			C	0.13	0.08	163.9	122.1	206.9
VI	23	38	A	0.04	0.03	56.1	47.1	60.3
			B	0.06	0.05	91.3	78.5	176.8
			C	0.06	0.05	45.7	23.0	-10.4
III	67	40	A	0.04	0.01	49.3	14.8	40.7
			B	0.11	0.06	84.7	17.5	-44.6
			C	0.12	0.05	159.9	102.4	205.4

Figure 36. Axial force distribution for load Case IIa from the design condition analysis; length of bar is relative to axial load, and left side of plot is upstream side.

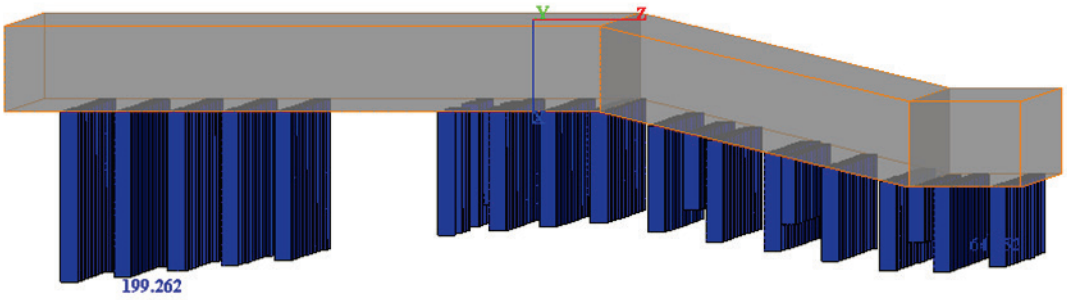

Results of the post-scour condition analysis for the low-flow monolith with full headwater uplift are shown in Table 21. The critical load case for this analysis was load Case I, with a headwater and tailwater elevation at 67.0 ft and 40.0 ft, respectively. The distribution of axial forces in the pile group from load Case I is shown in Figure 37. Tension developed in Group A piles with a magnitude of 12.7 kips. This condition is likely caused by the applied full headwater uplift condition. The grout used beneath the low-flow weir was the capping grout, mixture OR-23 (Table 4). No grout losses were reported in this vicinity during grouting operations. Measured

displacements remain elastic for the low-flow structure, and only minor increases in uplift pressure have occurred. Therefore, results of the post-scour analysis show some tension developing in pile Group A, but this is minimal and would not exceed the 45-kip threshold previously calculated for piles without tension connectors. Results of the post-scour analysis for the low-flow monolith indicate that for the design loading conditions, this monolith will perform as designed. Note the minor displacements predicted for these different load conditions.

Table 21. Results of the low-flow monolith considering post-scour conditions; negative values are tension, and positive values are compression (critical case in red). Note the USACE (1975a) load cases were used.

Load Case	HW Elevation (ft, msl)	TW Elevation (ft, msl)	Group	Max Disp. (in.)	Min Disp. (in.)	Max Axial Force (kips)	Min Axial Force (kips)
I	67	40	A	0.01	-0.01	9.1	-12.7
			B	0.05	0.02	8.9	-35.4
			C	0.06	0.02	110.6	77.9
IV	35	0	A	0.07	0.07	91.7	69.4
			B	0.03	0.00	1.5	-36.9
			C	0.04	-0.01	77.5	27.1
VI	70	51.3	A	0.02	0.01	31.2	14.4
			B	0.06	0.03	32.2	-3.0
			C	0.06	0.03	101.3	74.6

Figure 37. Axial force (kips) distribution resulting from pile group analysis for load case I post-scour conditions; red indicates tension, and blue indicates compression.

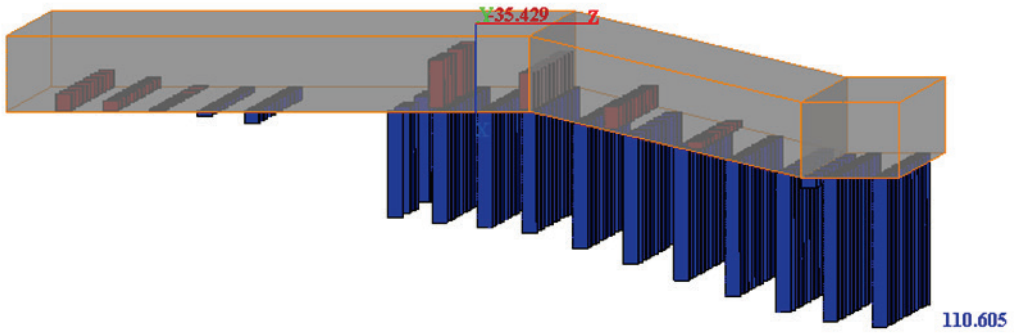

4.6.2 Modeling results weir monolith

Results of the design condition analysis for the weir monolith are shown in Table 22 and Figure 38. Results show that the weir monolith was well within the design standards. Also shown in Table 21 are the results of the 1972 analysis. Similar magnitudes of axial force were found for load Case IIa. The largest difference between the two analyses was for load case VI, which is a reverse loading condition. The 1972 analysis calculated 20.6 kips in tension in Group B piles while the current analysis calculated a minimum of 84.9 kips in compression. Additionally, larger magnitude compression was found in Group C piles, compared to the present analysis. This load distribution highlights the possible differences in the method of solutions. With these differences considered, the current results followed similar trends, and it appears that the modeling assumptions are correct.

Table 22. Analysis results for weir monolith with design conditions; negative values are tension, and positive values are compression.

Load Case	HW Elevation (ft msl)	TW Elevation (ft msl)	Group	Max Axial Disp. (in)	Min Axial Disp. (in)	Max Axial Force (kips)	Min Axial Force (kips)	1972 App. E Max Axial Force (kips)
IIa	35	0	A	0.15	0.13	186.5	165.8	186.3
			B	0.12	0.08	103.9	66.3	95.6
			C	0.12	0.08	148.8	103.2	173.9
IIIa	67	40	A	0.06	0.04	77.2	57.0	70.0
			B	0.11	0.07	54.6	15.4	-27.1
			C	0.11	0.07	165.1	124.4	203.3
VI	23	38	A	0.03	0.02	44.9	25.7	48.1
			B	0.07	0.04	113.7	84.9	-20.6
			C	0.08	0.04	45.0	3.5	176.1
III	67	40	A	0.03	0.01	42.9	13.3	32.9
			B	0.10	0.05	40.5	-11.6	-59.8
			C	0.10	0.04	159.8	105.4	202.2

Figure 38. Distribution of axial forces (kips) in the weir monolith piles, load Case III.

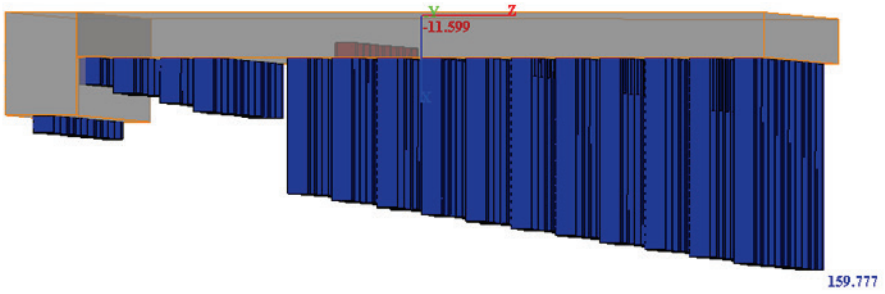

The post-scour condition analysis for the weir monolith was performed with four subcases (Table 19) for each load case. Subcase ‘a’ represents the full headwater uplift condition with no additional grout load applied. Subcase ‘b’ had the design uplift pressures applied with no grout load; this subcase represents a design condition. Subcase ‘c’ had a full headwater uplift condition with the additional grout load applied. Finally, subcase ‘d’ was with a design uplift condition with an additional grout load. These assumptions were investigated in USACE (1975b) and were performed with a nonlinear analysis method. Results for load Case I are presented in Table 23, and axial force distribution is shown in Figure 39.

Results for load Case I illustrate the impact of using a full headwater uplift condition and the grout load. If subcases ‘a’ and ‘c’ are considered, using full headwater uplift with no additional grout load applied results in tension developing in the Group A piles. If the additional grout load is applied in subcase ‘c’, tension does not result in pile Group A, and compressive loads are increased for all pile groups. These results are also illustrated in subcases ‘b’ and ‘d’; the difference being that the compressive loads are greater for these subcases compared to the full headwater uplift, as no large uplift force counteracts the additional grout load. The assumptions made in the subcases represent the extremes that could have resulted from the scour event. Load Case I results indicate that, according to these models, the weir monolith would be quasi-stable but very close to exceeding the design load capacity. Maximum tension in the Group A piles was near the threshold of 45 kips, although a small percentage exceeded this threshold. The compressive force exceeded 200 kips for subcase Id, but likely the surrounding piles would be able to handle the extra load.

Table 23. Post-scour conditions weir monolith load Case I; results exceeding design conditions are shown in red.

Load Case (see Table 19)	HW Elevation (ft msl)	TW Elevation (ft msl)	Group	Max Disp	Min Disp	Max Axial Force (kips)	Min Axial Force (kips)	% piles overstressed
Ia	67	40	A	-0.017	-0.039	-23	-51.5	100%
			B	0.049	0.001	-12.1	-62.3	-
			C	0.055	-0.005	115.9	59.9	-
Ib	67	40	A	0.025	-0.002	34.8	-2.8	21.57%
			B	0.108	0.048	74	8.9	-
			C	0.115	0.04	154.2	85	-
Ic	67	40	A	0.055	0.034	73.5	47.5	-
			B	0.117	0.072	75	26.5	-
			C	0.122	0.066	167.3	115.7	-
Id	67	40	A	0.1	0.074	127.8	96.5	-
			B	0.179	0.121	151.3	98.4	-
			C	0.186	0.114	206.3	143.5	18.33%

Figure 39. Axial force distribution of the post-scour condition analysis for the weir monolith, load Case Ia.

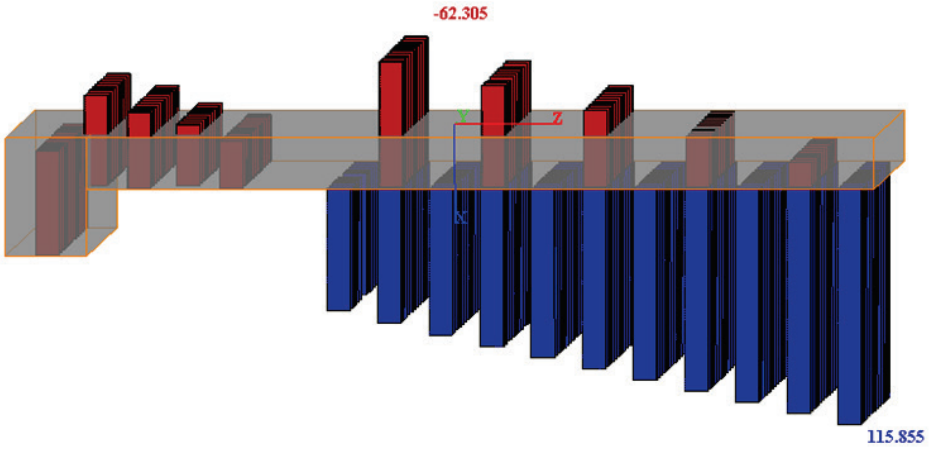

Results of the post-scour condition analysis for the weir monolith with load condition IV are shown in Table 24. Results of this load case were within the design thresholds, and the weir monolith responded with minimal displacements.

Table 24. Post-scour conditions weir monolith, load case IV.

Load Case	HW Elevation (ft msl)	TW Elevation (ft msl)	Group	Max Disp	Min Disp	Max Axial Force (kips)	Min Axial Force (kips)	% piles overstressed
IVa	35	0	A	0.0137	0.0058	19.1	8.1	-
			B	0.0382	0.0205	14.5	-5.3	-
			C	0.0404	0.0183	71.5	48.5	-
IVb	35	0	A	0.0597	0.0518	80	70.4	-
			B	0.0828	0.0658	80	52.8	-
			C	0.0849	0.0637	107.7	70.8	-
IVc	35	0	A	0.0873	0.0816	112.6	106.2	-
			B	0.1031	0.0911	94.6	82.7	-
			C	0.1046	0.0897	122.8	109.3	-
IVd	35	0	A	0.1401	0.1349	173.7	168.4	-
			B	0.1525	0.1425	147.9	138.2	-
			C	0.1537	0.1413	160.4	149.5	-

Results of the post-scour analysis for load case V, reverse loading, are shown in Table 25. The design conditions were exceeded for load case Vc, full headwater uplift with the grout load applied. Pile Group B exceeded the compressive load threshold of 200 kips. The distribution of axial forces for load case Vc are shown in Figure 40. The compressive load results appear counter-intuitive to results discussed for load case I but with the water loads reversed on the structure, the change in moments resulted in an increased compressive force on pile Group B, which are battered upstream and are the primary piles resisting the reversed loading.

Table 25. Post-scour conditions weir monolith, load case V (results exceeding design conditions are shown in red). Note the USACE (1975a) load cases were used.

Load Case	HW Elevation (ft, msl)	TW Elevation (ft, msl)	Group	Max Disp	Min Disp	Max Axial Force (kips)	Min Axial Force (kips)	% piles overstressed
Va	23	38	A	0.063	0.048	84.1	66.3	-
			B	0.106	0.074	143.8	114.2	-
			C	0.109	0.07	77.6	36.5	-
Vb	23	38	A	0.028	0.016	39.2	22.4	-
			B	0.064	0.038	99.8	38.9	-
			C	0.067	0.034	99.9	3.5	-
Vc	23	38	A	0.145	0.131	179	164.4	-
			B	0.184	0.154	227	203	100.00%
			C	0.187	0.15	128.4	96.2	-
Vd	23	38	A	0.105	0.094	133.8	121.4	-
			B	0.134	0.112	182.6	161.2	-
			C	0.137	0.109	90.6	63.4	-

Figure 40. Axial force distribution of the post-scour condition analysis for the weir monolith, load case Vc.

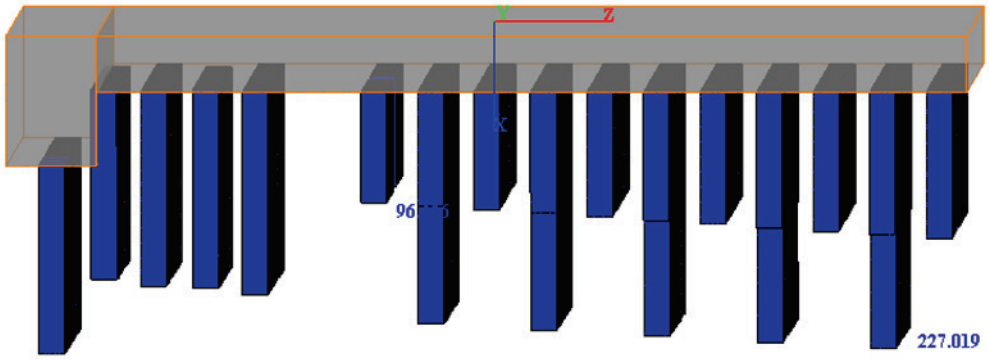

Results of the weir post-scour analysis for the load condition VI are shown in Table 26. Tension developed in Group A piles but did not exceed the 45-kip threshold for load case VIa with full headwater uplift no grout load. While in load condition VId, with design uplift and grout load, the compressive forces in pile Group C exceeded 200 kips. Although displacements approached the limiting value of 0.2 in., they did not exceed this value. Results for this extreme loading condition are similar to those found for load case I.

Table 26. Post-scour conditions weir monolith load case VI, results exceeding design conditions shown in red. Note the USACE (1975a) load cases were used.

Load Case	HW Elevation (ft msl)	TW Elevation (ft msl)	Group	Max Disp	Min Disp	Max Axial Force (kips)	Min Axial Force (kips)	% piles overstressed
VIa	70	51.3	A	-0.005	-0.025	-7.2	-34.4	100.00%
			B	0.056	0.012	-4	-51.6	-
			C	0.062	0.006	122.1	70.7	-
VIb	70	51.3	A	0.019	-0.009	27	-12.3	33.30%
			B	0.106	0.043	76.4	8.3	-
			C	0.114	0.036	149.7	76.4	-
VIc	70	51.3	A	0.067	0.048	88.2	65.5	-
			B	0.124	0.082	82.4	38.2	-
			C	0.129	0.077	173.7	126	-
VId	70	51.3	A	0.094	0.066	120.2	87.1	-
			B	0.177	0.116	153.2	97.2	-
			C	0.185	0.109	202.4	135.1	-

Results from load case I and VI were similar in magnitude, so this load case was chosen to find out if the stresses in the piles exceeded allowable limits. If these limits are exceeded, the piles could fail structurally and reduce the capacity of the pile foundation to sustain loading. Failure of a pile or group of piles could potentially lead to failure of the structure by either sliding, overturning, or losing the ability to operate the gates, due to differential settlement. Therefore, the combination of both axial and bending stresses were calculated and checked using Equation 1.

$$\frac{f_a}{F_a} + \frac{f_b}{F_b} < 1 \qquad \text{(Eq. 1)}$$

Where f_a is the axial unit stress, f_b is the bending unit stress, F_a is the limiting axial stress taken as 50 percent of the steel yield stress, and F_b in the bending stress threshold taken as 60 percent of the yield stress of steel. The stresses were calculated from load case I results. Results of these calculations are shown in Table 27, where M_y is the moment about the local axis and σ_b is the pile bending stress. Inspection of the results shown in Table 27 show the stresses are well below the failure criteria.

Table 27. Results of calculations checking pile stresses.

Load Case	Max total stress (kip/in^2)	Pile #	M_y (kip-in.)	σ_b (kip/in^2)	Failure Criteria Check
Ia	2.44	208	716.34	6.69	0.48
Ib	1.63	210	380.66	3.55	0.28
Ic	9.01	221	16.32	0.15	0.55
Id	4.58	1	324.41	3.03	0.43

4.6.3 Discussion of pile stability results

Results of the pile analysis indicate that the condition of the grout beneath the structure is of primary concern. If the grout is competently filling the 1973 scour void with no gaps or cracking, then less than full headwater uplift conditions will persist. If this condition is the case, then subcases 'a' and 'c' investigated in the weir monolith, post-scour condition analysis, would not be representative. Investigation of this assumption was performed in a separate report of investigation from the historic piezometer data. This study is still in review, but the results indicate that measured uplift conditions following the scour event are less than the full headwater uplift. Further discussion of piezometer results is presented in Chapter 5.

Material properties used in this model were derived from the original design investigation conducted in the 1950s, and more modern testing might result in slightly different shear strengths. However, it is uncertain whether a large enough deviation from the design shear strengths would result in an unstable condition.

The pile foundation was designed to be primarily end-bearing, and the sampling and testing methods used in the design investigation were conducted competently compared to current methods. Sampling from the underlying sands was planned to collect both disturbed and undisturbed samples via freezing techniques, which were unique at the time. Compared to published values for these soil types, the shear strengths measured were conservative. Modeling of the pile load test using these shear strengths further established that the selection of the shear strength values was conservative. This condition was apparent in that magnification factors were applied to match the measured load versus settlement curve.

Analysis of the low-flow monolith showed that for load case I Group A piles developed a small amount of tension. This amount may be small enough that the surrounding piles might be able to carry the extra load and operation could continue undeterred. The critical conditions were found for the weir monolith. Although, the results of this updated analysis were smaller in magnitude compared to the results presented in USACE (1975b). The luxury of this analysis was greater than 40 yr of operational records that showed no plastic deformation under large flood loads. However, the differential heads observed were smaller than those seen prior to the scour event.

The assumption of the grout adhering to the piles seems overly conservative, considering the grout mixes used were more in line with a soil-cement than a grout. The grout mix was designed to have a modulus that matches the surrounding soils and should likely respond similarly. The bond condition that the grout has on the piles is an important assumption that has considerable impact on the current results as well as those from the 1975 analysis (USACE 1975a, 1975b). Results of the pile analysis conducted for this study showed that for extreme design loading conditions, the axial pile loads were less than those found in the 1975 analysis. The 1975 analysis used a linear analysis method while the current method allows for nonlinear response, which may have allowed for different load distributions in the pile cap and piles. However, a central question is the bond relationship between the grout and the batter piles in the grout-filled void. Physical samples from the grout mass may better define the bond relationship and the in situ properties of the grout mass beneath the structure's foundation.

5 2021 ERDC Seepage and Limit Equilibrium Analysis

Seepage and stability analyses were performed using a finite element and limit equilibrium software, SLIDE, distributed by RocScience. This portion of the analysis was conducted to assess the global factor of safety for stability of the structure. In addition, the seepage analysis should provide a better understanding of the potential uplift conditions by calibrating to the piezometric response from a flood loading that occurred on 11 May 2011. The seepage analysis was performed uncoupled from the mechanical loadings. An uncoupled analysis considers only the impact of changing hydraulic boundary conditions when performing calculations. Impacts of flood loading on effective stress were ignored. The analysis was performed using steady-state conditions, meaning it was independent of time.

Material properties were chosen based on those used in the pile analysis and derived from the site characterization of the structure performed pre-design (USACE 1953, 1954, 1963; ASCE 1956). Global stability of the structure was investigated using Spencer's method for both linear and nonlinear search methods. Material properties used in the seepage and stability analyses are shown in Table 28.

Table 28. Material properties for seepage and stability analyses.

Material	γ (psf)	c (psf)	ϕ	k_s (cm/s)	k_{rat} (k_2/k_1)
Aquifer	120	-	33	1.00E-02	1
Channel Fill	118	200	28	1.80E-04	1
Grout	115	3300	-	5.00E-06	1
Riprap Fill	130	-	40	1.00E-03	1

Note: γ is unit weight, c is cohesion, φ is friction angle, and k is the saturated hydraulic conductivity

Stratigraphy of the site was characterized using the 2016 bathymetric survey of the channel, supplemented with results from the scour limits defined in previous sections of this report, and the design site investigations (USACE 1953, 1954, 1963; ASCE 1956). The location of the representative cross section is shown in Figure 41 and overlain on the 2016 bathymetric survey contour map. A deep scour hole is shown in Figure 41 just downstream of the weir structure (dark blue color).

The scour hole resulted from turbulent outflows during high outflow periods. The scour hole is approximately 100 ft deep, and its deepest point is nearly 500 ft from the centerline of the structure. The location of this depression represents the downstream boundary of the model. The depth of this feature, shown in Figure 42a, should allow for communication between the foundation soils and the tailwater. The upstream boundary of the model was selected as the centerline of the Mississippi River, nearly 3,000 ft upstream of the structure's centerline. The cross section used in the model is shown in Figure 42.

Figure 41. Location of the cross section (A-A') used in seepage and stability analysis.

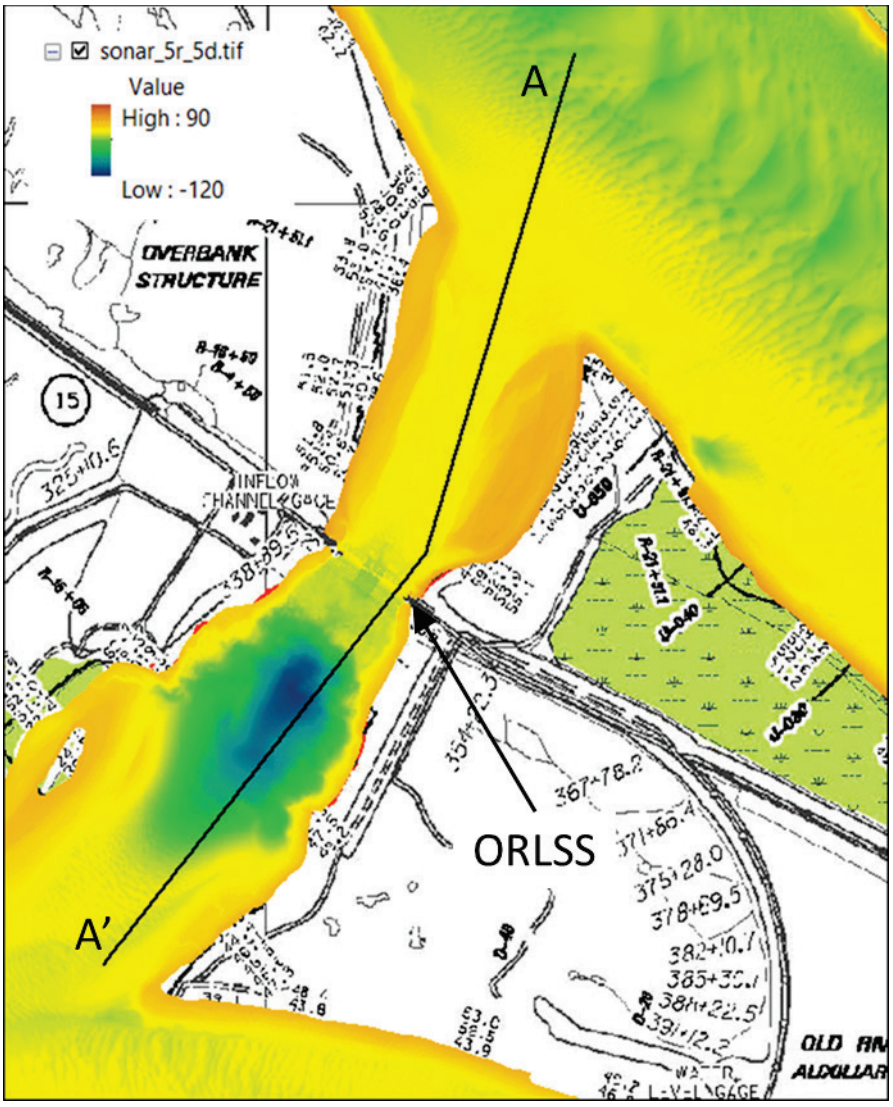

The cross section shows the pile groups and limits of the scour beneath the structure. The superstructure of ORLSS was not included, but the weight was applied during the limit equilibrium analysis as an applied

surcharge. The hydraulic conductivities of the foundation soils were considered isotropic. In the original design, the channel fill was considered anisotropic, but a sensitivity analysis conducted during model calibration revealed that this had minimal impact on the results. Four load cases were analyzed in the seepage and stability analyses as shown in Table 29. Three of the load cases were derived from 1975 stability analysis (USACE 1975b). An additional load case was considered from a flood event that occurred in May 2011 where the structure underwent a significant loading. This load case was used to calibrate the seepage model against piezometer readings collected during the flood event.

Figure 42. Cross section and stratigraphy used in seepage and stability analysis: (a) full model extents, (b) close-up of weir.

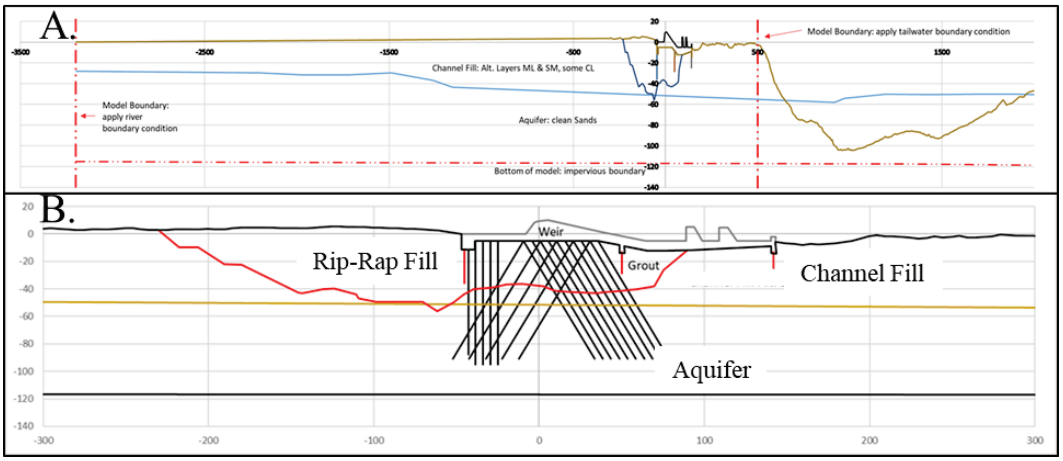

Table 29. Load cases used in seepage and stability analysis.

Load Case	HW (ft)	TW (ft)
I	67	40
IV	35	0
VI	70	51.3
5/23/2011	65.2	50.9

5.1 Seepage analysis results

Calibration of the seepage model was performed by first constructing the model and assigning material properties. The properties and certain geometric aspects were adjusted until the closest match to the measured pore water pressures was found. The geometric aspects considered were boundary locations and the connection between the scour hole upstream of the structure and the pervious aquifer. Results of the calibration are shown in Figure 43. The results of the calibration showed that a direct

connection between the upstream scour containing riprap and the aquifer was unlikely. The interpreted depths of the scour hole were reported in USACE (1975); this report indicated that the 1973 scour event reached sufficient depths to encounter the pervious aquifer sands. There is no reason to believe that the scour hole did not originally encounter the aquifer, but it is likely this connection has since silted in.

The results of the model calibration are shown in Table 30, which shows the comparisons between piezometric readings and the seepage model results. Piezometers B-6, B-8, and B-11 are located near the contact between the structure and foundation. These piezometers were used to calculate the uplift pressures. Piezometers RP-10 and RP-11 are in the grout, and piezometers A-8 and A-2 are in the pervious aquifer upstream and downstream of the structure, respectively. A plan view of the piezometers used in this analysis are shown in Figure 43. Annotations of piezometer locations are made in Figure 44. These piezometers were found to have a percent difference less than 4 except for B-1. Piezometer B-1 is located at the centerline of the channel, upstream of the structure outside of the scour area, but was included for reference.

Figure 43. Plan view of instrumentation at ORLSS.

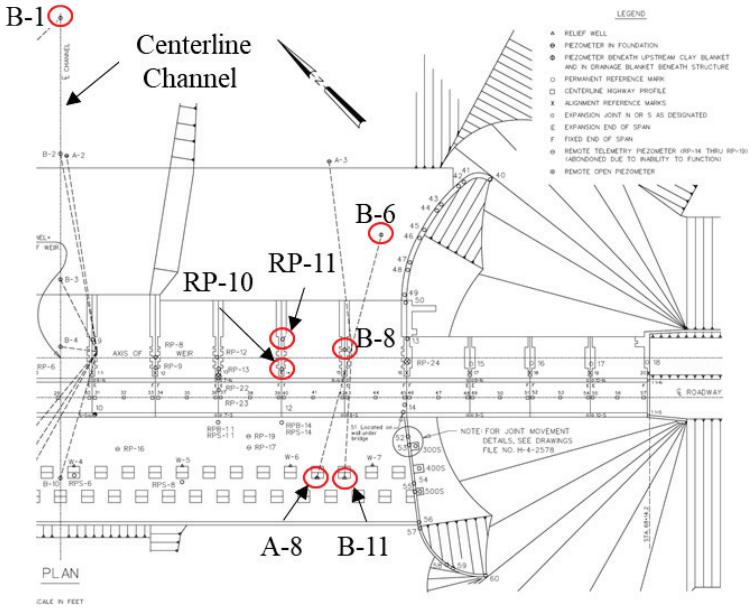

Figure 44. Total head contours resulting from the calibration of the seepage model.

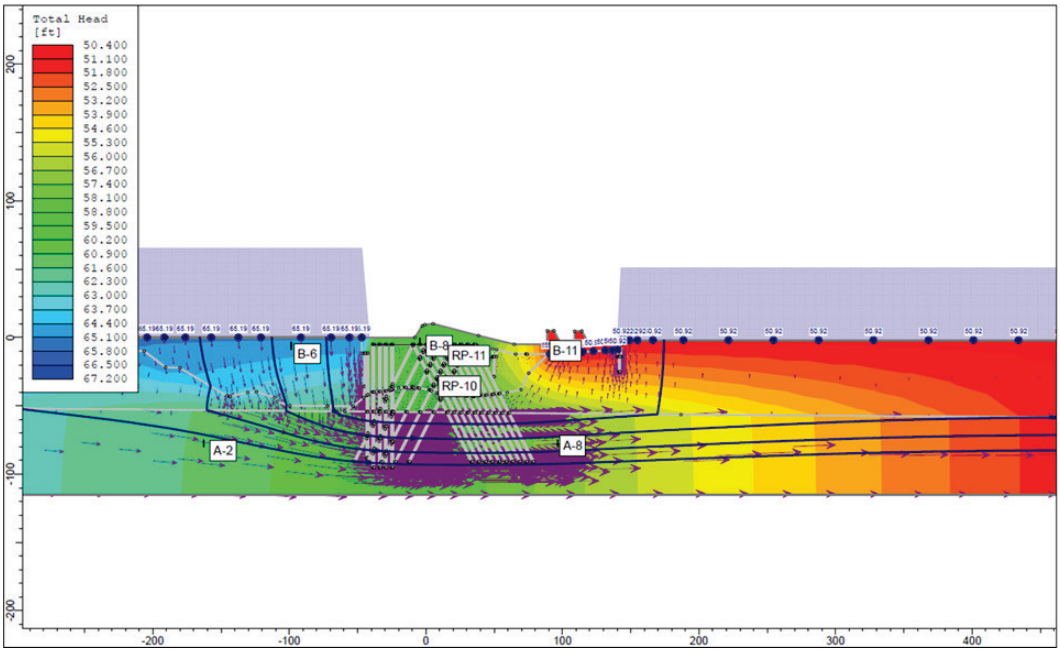

The calibration results shown in Table 30 show the largest difference between the measured and modeled values occurred for piezometer B-1 with the model over predicting the total head. Piezometer B-1 is well outside of the scour zone, located at the centerline of the channel, as shown in Figure 44. Piezometer B-1 was included as a reference and was not considered when calibrating the model. The remaining comparisons fall below 4 percent difference of each other. Figure 45 shows the different methods used to calculate uplift beneath the weir. The most conservative uplift condition was to use full headwater, as was used in the 1975 stability analysis. A regression analysis was performed to assess the uplift conditions using piezometric readings following the 1973 scour event. Additionally, Figure 45 shows the results of a regression analysis of piezometer data collected after the 1973 scour event and is described in Breland et al. (2021*). The upstream conditions providing a good match between the regression and measured total head, while downstream the results are more conservative. The measured and model uplift conditions are greater than the original design although nearly the same rate of decrease in pressure was found across the structure. These results show that the current

* Breland, B. R., L. A. Walshire, and J. B. Dunbar. 2021. *Piezometer assessment through time for Old River Low Sill structure*. ERDC/GSL TN-DRAFT, in review.

conditions are less than full headwater but still greater than the original design uplift. These results impact the pile loads, as was shown in the pile analysis. Larger uplift values resulted in increased tension, while decreased uplift pressures resulted in larger compressive loads.

Table 30. Calibration results compared to piezometric measurements, May 2011 flood event.

Piez. #	Measured (ft)	Model (ft)	Error (ft)	% Difference
B-6	64.67	64.74	-0.07	-0.11%
B-8	60.15	59.18	0.97	1.62%
B-11	49.96	51.06	-1.10	-2.20%
A-8	55.15	57.05	-1.90	-3.45%
RP-10	59.10	58.87	0.23	0.39%
RP-11	60.10	58.74	1.36	2.26%
B-1	59.84	64.74	-4.90	-8.19%
A-2	63.90	61.47	2.43	3.80%

Figure 45. Comparison of different methods used to calculate uplift beneath the weir; the weir is shown for reference.

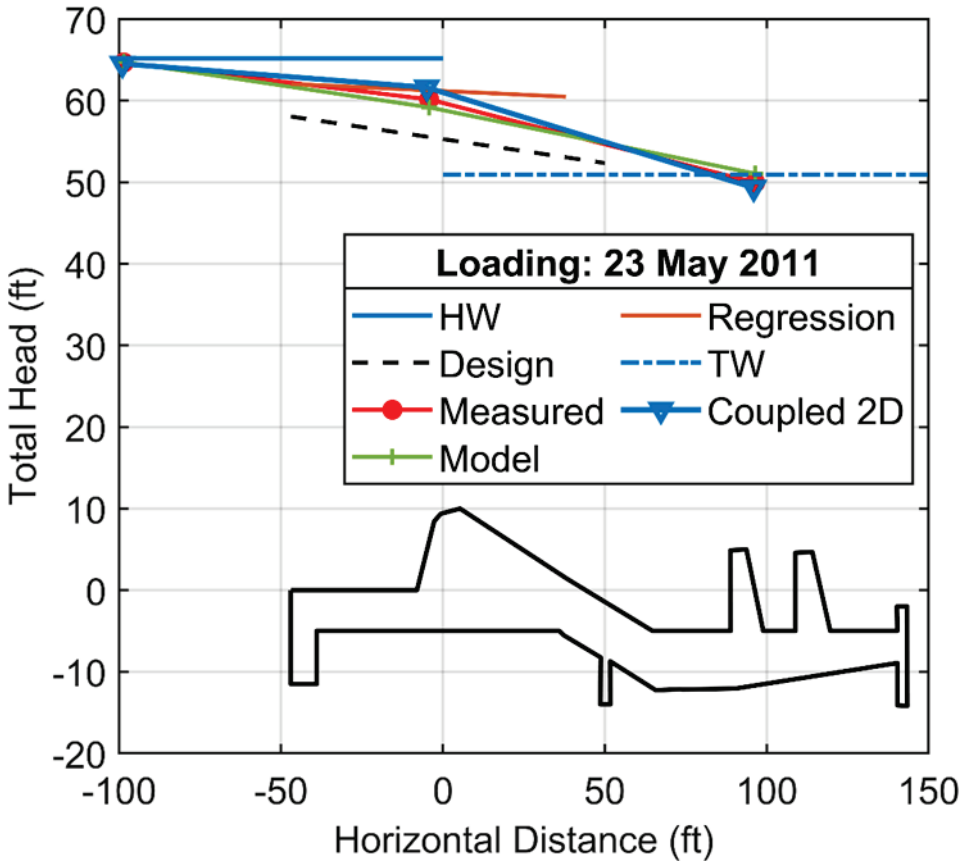

5.2 Stability analysis results

A stability analysis of the weir was conducted using limit equilibrium and Spencer's method with the pore water pressures imported from the seepage analysis. For each hydraulic loading condition, a steady-state seepage analysis was conducted. When steady-state equilibrium was reached, these pore water pressures were imported into the limit equilibrium software and circular and noncircular searches were used to find the critical failure surface. The result of this analysis provides a good reference for the global stability of the structure. Material properties shown in Table 28 and the loading conditions from Table 29 were used in these analyses. The critical factors of safety from this analysis for the different hydraulic load cases are shown in Table 31.

The critical factor of safety (FoS) for load case VI was found to be the most critical. This load case has a headwater of 70 ft and a tailwater of 51.3 ft. The critical surface is shown in Figure 46 and was found using a nonlinear search. Figure 46 shows the different material types and pile locations used in the analysis. The nonlinear search method captured the critical failure surface, shown in green in Figure 46. The failure surface extends beneath upstream battered and vertical piles and extends to a depth of 100 ft. The upstream portion of the failure surface passes through the riprap fill and exits just downstream of the stilling basin. The failure surfaces were not allowed to pass through the pile group or the sheet pile walls.

Table 31. Results of the limit equilibrium stability analysis.

Load Case	FoS
I	1.99
IV	3.8
VI	1.8
5/23/2011	1.96

Figure 46. Critical failure surface for load case VI.

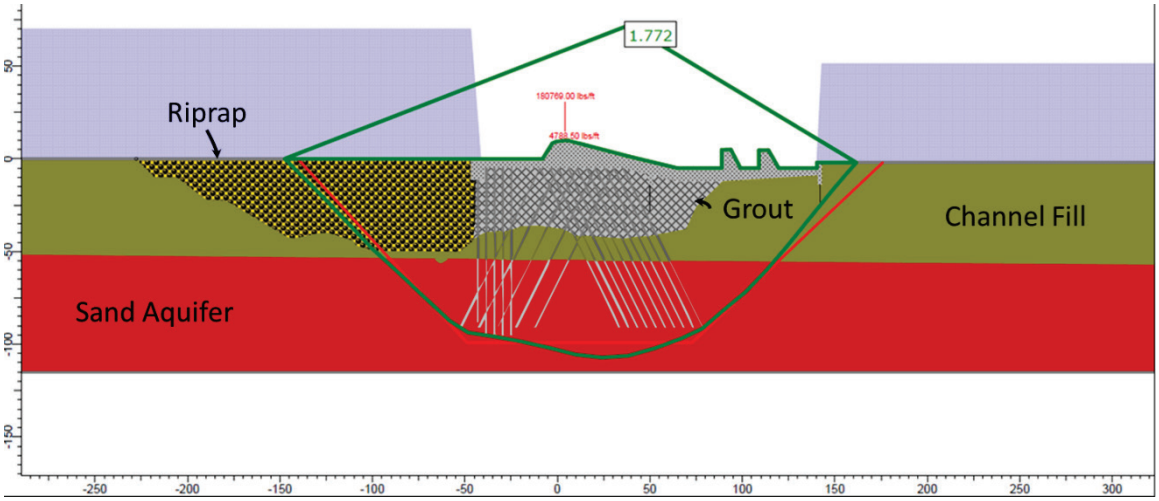

The factors of safety reported in Table 31 represent the critical factors of safety for each load condition. The stability analysis was performed for each load case considering both circular and non-circular search methods. For each search method, at least three different methods of implementing the search were employed. All critical surfaces were found using the non-circular method, meaning the non-circular factors of safety were always lower than the circular factors of safety. Both search methods were employed using Spencer's procedure, which satisfies both force and moment equilibrium. The magnitude of the factors of safety are greater than 1.0 and the structure would be considered stable under the loading conditions analyzed.

A review of USACE (2003) reported that for extreme pools, a factor of safety of 1.4 was acceptable for new dams. The same document reported that for existing dams, the factor of safety may be less considering the actual performance of the dam could be observed over time. Other factors of safety recommended for gravity dam stability were made in USACE (1995). The factor of safety recommended in this document for extreme loadings was 1.3. Considering both manuals, the structure would be stable from a limit equilibrium perspective. A further understanding of the response of the structure to these loadings was required, so an analysis was conducted by varying material properties to understand the impact of shear strength on the stability.

A review of the laboratory data presented in USACE (1954) showed that the channel fill exhibited some variation in shear strength across different drained tests. The shear strength of the pervious sand aquifer

did not vary much between tests, and it was determined that a relatively adequate value had been used in design. The shear strength of the riprap fill material had been assumed; therefore, a lower value was assumed to assess the impact. The shear strength values used in the analysis and the resulting factor of safety are shown in Table 32.

The impact of the different shear strength values used in the analyses is minimal, indicating that the model was fairly insensitive to the channel and riprap fill material. The greatest impact on the results is the shear strength of the aquifer sands. This outcome agrees with the original design of the structure, as the piles were designed to carry the weight of the flood loads and structure through pile end-bearing in the aquifer sands. Additional analyses were performed by neglecting the applied loads that corresponded to the weight of the superstructure and one without piles. The results of neglecting the weight of the superstructure show a marked decrease in factor of safety from 1.8 to 1.2. The decreased factor of safety shows that a change in confining pressure in the sands results in a lower shear strength of the aquifer sands. Another analysis was performed by completely neglecting the piles and only including the weir, with flood loads applied, a factor of safety was found that was much less than one indicating an unstable condition.

Table 32. Results and parameters varied in parametric analysis.

Material	Laboratory Test	c (psf)	φ' (deg)	FoS	Project/notes
Channel Fill	CU triaxial	200	20	1.7	LSS
	CD Direct Shear	0	33	1.8	LSS
	CD Direct Shear	0	30	1.8	Aux.
	Assumed	700	0	1.8	Increases 14 psf/ft
	Assumed	1050	0	1.9	Constant
Riprap Fill	Assumed	0	35	1.8	LSS
No Applied Loads	-	-	-	1.2	LSS

Results of these analyses show that besides providing confining pressure to the aquifer sands, the channel and riprap fill did not contribute significantly to the stability of the structure. The model was more sensitive to the shear resistance of the aquifer sands and, therefore, the load distribution along

the piles. These results show that for an uncoupled stability analysis the structure was considered stable under the conditions analyzed.

5.3 Coupled seepage and stability analysis

The software FLAC distributed by Itasca (2020) was used in this analysis and a semi-coupled approach was taken. The semi-coupled solution used in this analysis is accomplished by first bringing the model to equilibrium considering only mechanical equilibrium. Then a partial solution is found with only hydraulic equations partially solved and finally both mechanical and hydraulic conditions of equilibrium are satisfied simultaneously. This approach allowed for faster solution times with little impact on the results.

The coupled (or semi-coupled) analysis was conducted to understand the potential changes in effective stress and their impacts of consolidation on the stability of LSS. A 2-D FLAC analysis was performed using the material properties shown in Table 33. Additional properties were needed to estimate the displacement of the structure under the 23 May 2011 flood conditions, where the headwater (HW) was at elevation 65.19 ft and the tailwater (TW) was at 50.92 ft. The software required either the Young's modulus and Poisson's ratio or the bulk and shear modulus. Some modulus data were available from the design investigation of the auxiliary structure for similar soils. These data were used as an estimate for the LSS soils. The modulus data was estimated from consolidated undrained triaxial tests data. Data that were not available were assigned based on similar soils. The grout was assigned based on its similarity to soil cement grout designs used in grouted piezometers (Mikkelsen 2002).

Properties for the piles were shown previously in Table 7. The additional parameters needed for the FLAC deformation analyses are shown in Tables 33 and 34. The pile properties were collected from design data in USACE (1956b) and supplemented using H-pile specifications outlined in RW Conklin Steel (2020). The pile-to-soil interaction was modeled using shear and normal springs, and these properties were estimated based on recommendations from the program documentation and results of the pile load test conducted during design of ORLSS. For the initial 2-D deformation analysis, estimates of the spring parameters were used to gain a better understanding of the response of the coupled analysis. As a default, the program does not account for end-bearing effects of the pile. End-bearing was not considered for this analysis. Figure 47 shows the model's geometry near the weir.

Table 33. Material properties for 2-D FLAC analysis.

Material	Porosity	c (psf)	φ' (deg)	Bulk Modulus (psf)	Shear Modulus (psf)	Model
Aquifer	0.4	0	36	1.6E+06	5.2E+05	Mohr-Coulomb
Channel Fill	0.4	200	28	8.7E+06	8.7E+04	Mohr-Coulomb
Grout	0.4	3300	0	8.7E+06	8.7E+04	Mohr-Coulomb
Rip-Rap Fill	0.5	0	40	7.0E+06	3.2E+06	Mohr-Coulomb
Filter	0.4	0	36	1.6E+06	5.2E+05	Mohr-Coulomb
Concrete	0.4	-	-	2.4E+08	1.8E+08	Elastic

Table 34. Additional pile properties needed for the deformation analyses.

Property	Value
Perimeter (ft)	4.70
Cross-Sectional Area (ft^2)	0.15
Spacing (ft)	9.50
Pile head connection	pin
Moment of Inertia (ft^4)	0.04

Figure 47. Model geometry for the 2-D deformation analysis.

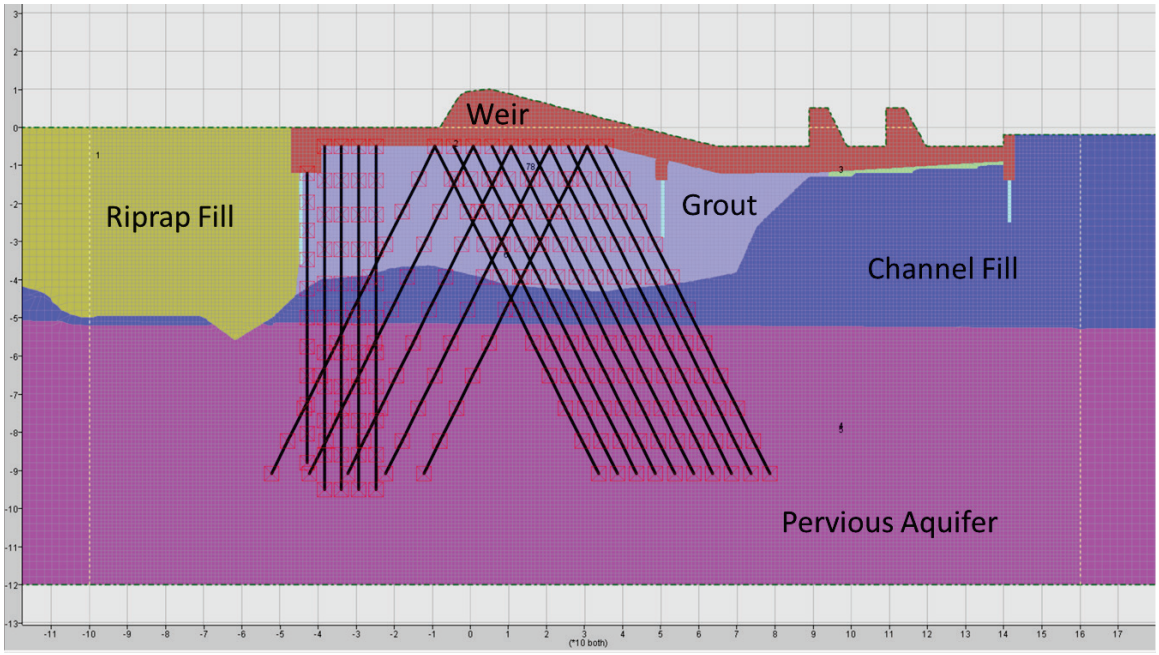

Figure 45 in Chapter 5 presents the uplift pressures as total heads. This figure allowed for a direct comparison of the piezometer readings taken during the flood event and those calculated using the design equations as well as the two modeling approaches. The modeling and the piezometer readings compared favorably. The uncoupled approach (model) slightly underpredicts, while the coupled model (coupled 2-D) slightly overpredicts the measurements.

Figure 48 shows the results as pressures with the piezometer readings being interpolated and only considered beneath the weir itself. The results show that the model is conservative but still well below a full headwater condition. The piezometer response was calculated by interpolating between the piezometer locations to better match the model locations. The results in Figure 48 show that the model matches the rate of pressure decrease over the same distance but overestimates the measured values. The same observation can be made for the original design equation. The uplift predicted using the regression equation does not match the rate of pressure decrease, although the upstream pressure is predicted more accurately than the model. The regression was constructed using available data following the scour event and subsequent grouting program. Therefore, both high and low water events were included. The regression equations represent the average seepage response including both high and low water periods. A change in behavior occurs between the average seepage response and the response during high water events. The difference between the regression predicted (purple dashed line) and piezometer measured (solid blue) uplift shown in Figure 48.

Figure 47. 2-D FLAC results comparing headwater and tailwater with predicted and measured uplift beneath the weir.

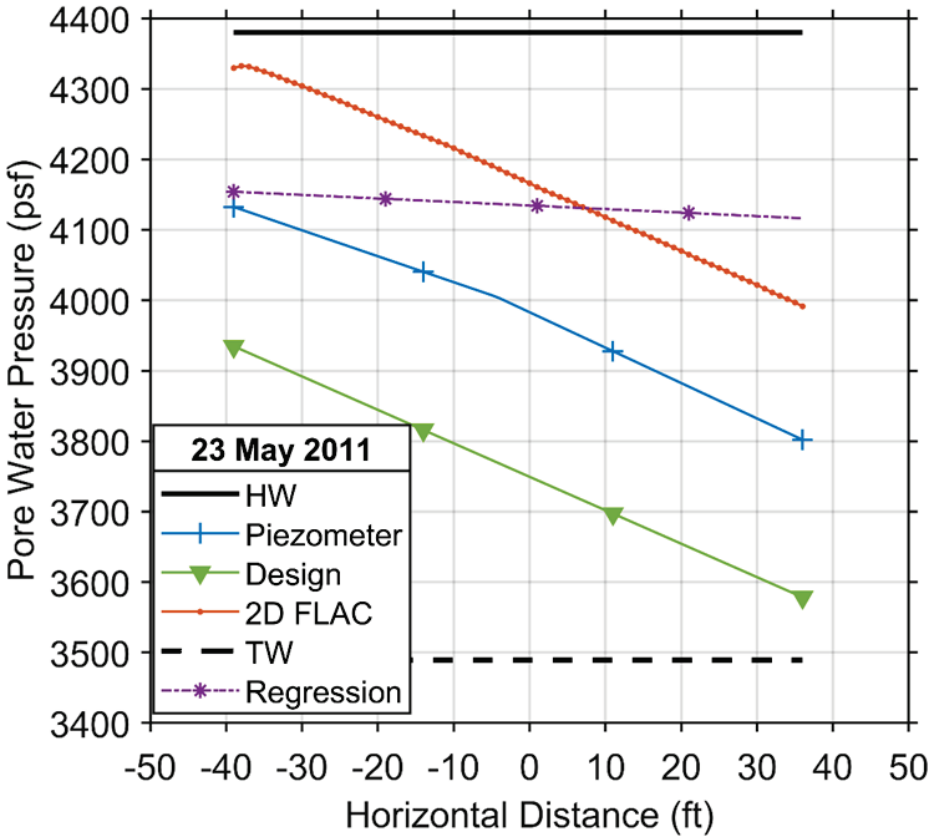

Displacements predicted from the 2-D deformation analysis beneath the weir are shown in Figure 49. The predicted displacement of the weir was 0.5 in. with a small differential of 0.05 in. from the upstream to downstream side. This displacement would have a minimal impact on the operation of the gates. The displacement contours are shown in Figure 50 with the largest displacements occurring in the riprap fill material in front of the weir structure. Displacements beneath the weir itself are relatively uniform.

Results of this analysis show that the predicted displacements beneath the weir are at about 0.5 in. during this event. Past displacements of the structure measured between 2006 and 2014 oscillate at +/- 0.5 in. at monolith 3 (south) based on centerline survey data. This displacement may indicate an elastic response to loading and unloading, which has been concluded by previous analyses of the measured settlement data at ORLSS (USACE 2016).

Figure 49. Vertical displacement predicted with the 2-D deformation model.

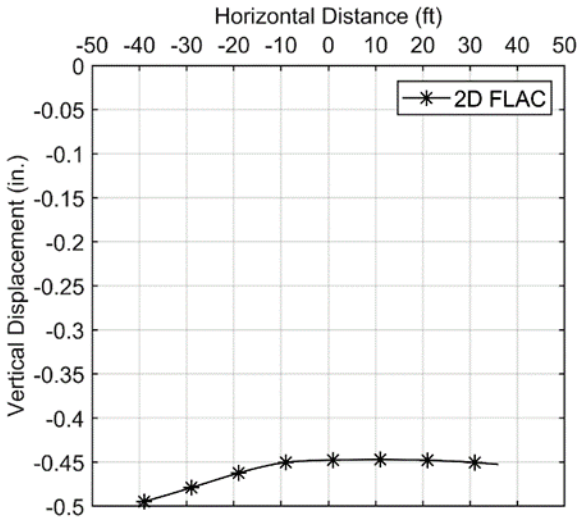

Figure 50. Vertical displacement contours predicted with 2-D deformation model, contours reported in feet (vertical piles located on upstream side).

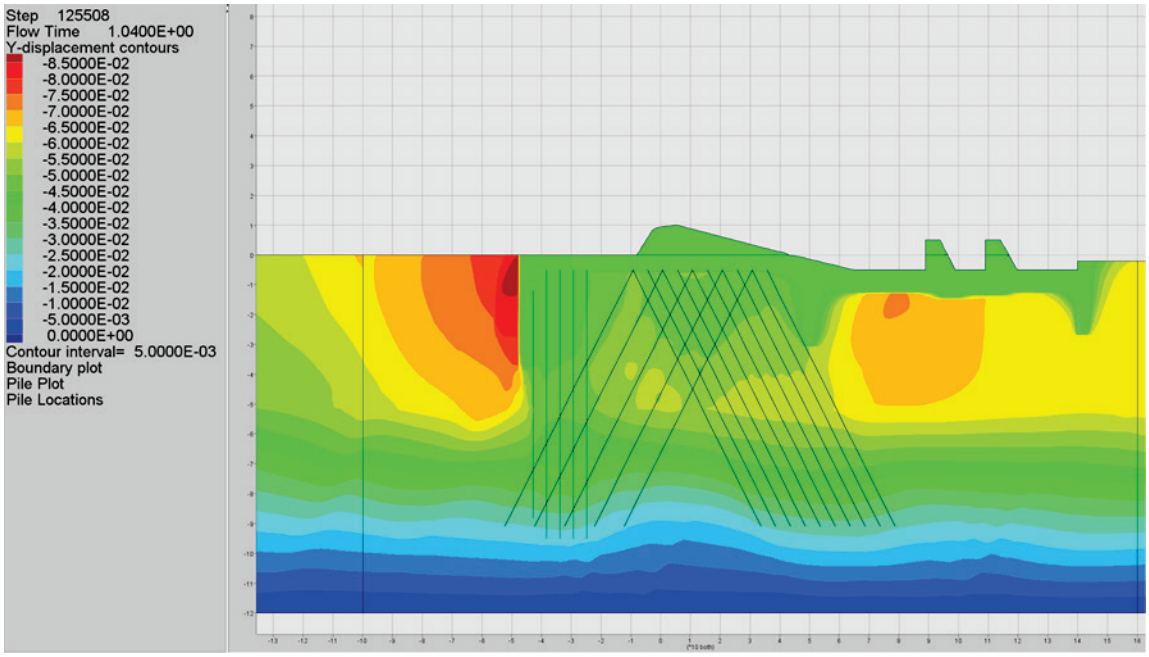

6 Conclusions and Recommendations

6.1 Summary

A stability analysis was performed on ORLSS under currently interpreted foundation conditions. The investigation was performed by first describing the events and identifying the extents of the foundation damage resulting from the 1973 flood event. A detailed investigation of the foundation geology was performed and described. Numerical models were employed to calculate pile stresses and loads, global factor of safety, and predicted uplift conditions. Design load cases were used, and no new geotechnical field investigations were conducted.

6.2 Conclusions

Following the 1973 flood and subsequent rehabilitation, a stability analysis was performed to assess future stability based on the newly rehabilitated foundation (USACE 1975). The results of the 1975 analysis resulted in operating restrictions in the form of differential head limitations to ensure stability. Over time, these head limitations have been increased from 13 to 22 ft with no appreciable settlement occurring as a result.

The current pile stability analysis showed that the structure was marginally stable under extreme loading conditions. Two modeling assumptions were the cause for the stability concern. There are two unknowns about the post-1973 foundation. One was increased uplift pressures; the other, the condition of the grout. Increased uplift can result in unacceptable tensile loads in the piles. If the grout is assumed to adhere or bond to the piles, an unacceptable compressive pile load occurs.

These modeling assumptions represent two extremes. If cracking exists in the grout, then full uplift conditions could exist and would result in unacceptable axial tensile loads. These large axial tensile loads would occur in piles without tension connectors. If it is assumed that the grout fully bonds to the piles, then an additional body load would occur on the structure and large compressive loads would result; often, these are in excess of the allowable compressive pile loads.

It was possible to investigate the uplift conditions through review and analysis of over 40 yr of piezometer data. The results of this review provided a regression analysis that could conservatively predict the uplift conditions. Seepage models compared well with field data and showed that

prediction of the uplift pressure was greater than that used in design, but much less than full headwater uplift. The stability analysis showed that global factors of safety were well within acceptable limits.

Investigation of the grout bonding to the piles is not possible at this time but review of current and historic periodic inspection reports showed that no appreciable settlement has occurred during the service life of this structure. Low displacements may indicate the grout is not fully bonded to the piles, indicating that the stability of the structure is likely between the two extreme conditions modeled in this study. It is not possible with the current information to fully understand the competence of the grout.

6.3 Recommendations

One of the objectives of this project was to assess whether modifications of the current operating conditions were appropriate. Based on the results presented, a decrease in the differential head restriction is not warranted. The results of this investigation indicate that the current operating conditions are appropriate. If increasing the differential head restriction is warranted, then the following recommendations apply to gain additional insight.

- A formalized monitoring plan, including data review and assessment, should be developed to monitor displacement during loadings that approach the differential head restrictions. This could be performed with remote monitoring methods (LiDAR surveys or remote sensing, such as robotic total stations).
- Results of the updated ERDC analyses presented in this report would support an increase in the differential head limitation with the following restrictions: These analyses were performed in a static condition; therefore, if an increase in the differential head was performed, it would need to occur incrementally with diligent observation and monitoring for signs of distress. Procedures similar to those undertaken for the first filling of a reservoir should be followed. Indications of structural distress would be found through increased displacements during loading or through apparent changes in piezometric head distribution across the structure, showing changes in foundation grout in the form of cracking. Prior to increasing the increment, performance data should be reviewed and approved by appropriate leadership. The incremental increases could be accomplished by increasing the head limitation in 0.5-ft increments

over time, where the structure was loaded at the current limitation over a period of time. The updated analysis was run for structural stability and did not include an analysis of flow conditions that would cause scour of the channel or foundation. Based on the presented results and past increases, an upper limit of 25 ft is possible, but this maximum loading will require years of incremental increases to reach with proper gate operation and monitoring.

If increased validation and decreased uncertainty are deemed necessary, then the following are suggested:

- Perform exploratory drilling into the grout at its deepest extent to gather grout samples for laboratory assessment. An area for consideration should be near bore hole 8c (grouting program) to detect presence/absence of a void in this location. The laboratory assessments should include strength, competency, and hydraulic conductivity. In situ grout testing in the form of packer testing would also give an indication of the competency of the grout.
- Perform soil borings and sampling in similar deposits with appropriate testing to assess shear strength and soil modulus. Performing CU triaxial testing on undisturbed sampling could accommodate this recommendation. Additional testing to validate the hydraulic conductivity values used in the model would be warranted. This recommendation could be achieved by one or two soil borings and common laboratory testing equipment.
- Incorporate drilling and testing results into a numerical analysis to validate increasing the differential head restriction.
- Increase collection and evaluation of continuous, accurate displacement measurements (spatial and temporal changes). Consider employing more modern methods such as LiDAR or robotic total station to accomplish these measurements.
- Consider more regular bathymetric or geophysical surveys of the forebay to look for changes or growth of anomalous areas.

Addressing these recommendations and using the results to modify the differential head restriction would need to be performed carefully. These recommendations will address the stability concerns, but additional analyses or operating plans may be needed to address scour of the approach channel.

References

American Society of Civil Engineers (ASCE). 1956. *Old River diversion control, a symposium, journal of the Waterways division*. Proceedings Paper 906. Reston, VA: ASCE.

Fisk, H. N. 1944. *Geological investigation of the alluvial valley of the Lower Mississippi River*. Vicksburg, MS: Mississippi River Commission.

_____. 1947. *Fine-grained alluvial deposits and their effects on Mississippi River activity, War Department, Corps of Engineers, Mississippi River Commission*. In two volumes. Vicksburg, MS: U.S. Army Engineer Waterways Experiment Station.

_____. 1952. *Geological investigation of the Atchafalaya basin and the problem of Mississippi River diversion*. Vicksburg, MS: USAE Waterways Experiment Station.

Graves, E. A., 1958. *Hydraulic requirements, Old River diversion control, a symposium, transactions*. Paper No. 2956, 1142-1159. Reston, VA: ASCE.

Kolb, C. R., and W. G. Shockley. 1957. Mississippi Valley geology – Its engineering significance. Miscellaneous Paper No. 3-208. Vicksburg, MS: U.S. Army Engineer Waterways Experiment Station.

Kolb, C. R. 1962. Distribution of soils bordering the Mississippi River from Donaldsonville to head of passes. Technical Report No. 3-601. Vicksburg, MS: U.S. Army Engineer Waterways Experiment Station.

Hardin, J. R. 1958. *The general problem, old river diversion control, a symposium, transactions*. Paper No. 2956, 1131-1141. Reston, VA: ASCE.

Itasca Consulting Group. 2020. *FLAC3D 6.0 documentation*. Minneapolis, MN: Itasca.

Latimer, R. A., and C. H. Schweizer. 1951. *The Atchafalaya River study, a report based upon engineering and geological studies of the enlargement of old and Atchafalaya rivers, in three volumes*. Vicksburg, MS: U.S. Army Corps of Engineers (USACE), Mississippi River Commission.

Mabrey, P. R., and W. B. Steinreide Jr. 1949. *Geology of old river closure control structures and lock sites*. Technical Memorandum No. 3-305. Vicksburg, MS: U.S. Army Engineer Waterways Experiment Station.

McGregor, J., and J. M. Duncan. 1998. *Performance and use of the standard penetration test in geotechnical engineering practice, report of CGPR*. Blacksburg, VA: Virginia Polytechnic Institute and State University.

Mikkelsen, P. E. 2002. Cement-bentonite grout backfill for borehole instruments. *Geotechnical Instrumentation News* 20(4):38–42.

Montgomery, R. L. 1974. *Correlation of engineering properties of cohesive soils bordering the Mississippi River from Donaldsonville to head of passes*. Miscellaneous Paper S-74-20. Vicksburg, MS: U.S. Army Engineer Waterways Experiment Station.

Mosher, R. L., and W. P. Dawkins. 2000. *Theoretical manual for pile foundations*. ERDC/ITL TR-00-5. Vicksburg, MS: U.S. Army Engineer Research and Development Center.

Reuss, M. 1998. *Designing the bayous, the control of water in the Atchafalaya basin 1800–1995*. Alexandria, VA: Office of History, U.S. Army Corps of Engineers.

RW Conklin Steel. 2020. RWCS catalogue H-piling. https://conklinsteel.com/wp-content/uploads/2020/04/H-Piling.pdf.

Saucier, R. T. 1969. *Geologic investigation of the Mississippi River area Artonish to Donaldsonville, LA*. Technical Report S-69-4. Vicksburg, MS: U.S. Army Engineer Waterways Experiment Station.

Saucier, R. T. 1994. *Geomorphology and quaternary geologic history of the Lower Mississippi Valley*. Vicksburg, MS: U.S. Army Engineer Waterways Experiment Station.

Sherman, W. C. 1962. Review of soils design, construction and performance observations low-sill structure, Old River. Technical report No. 3-601. Vicksburg, MS: U.S. Army Engineer Waterways Experiment Station.

Turnbull, W. J., and W. G. Shockley. 1958. *Foundation design, Old River diversion control, a symposium, transactions*. Paper No. 2956, 1160-1181. Reston, VA: ASCE.

U.S. Army Corps of Engineers (USACE). 1910. *Annual report of the chief of engineers, United States Army, improvements of rivers and harbors in the Vicksburg, Mississippi, district, Red River below Fulton, Ark.*, 578-581. Washington, DC: U.S. Army Corps of Engineers.

_____. 1953. *Soil and foundation studies low sill and overbank structures, Mississippi River Commission, U.S. Army Corps of Engineers, Vicksburg, MS*. Vicksburg, MS: U.S. Army Engineer Waterways Experiment Station.

_____. 1954. *Mississippi River and tributaries Old River control, detailed design memorandum–low-sill structure*. Design Memorandum No. 4. Washington, DC: USACE.

_____. 1956a. *Investigation of underseepage Mississippi River levees, Alton to Gale, Ill*. Technical Memorandum No. 3-430. Vicksburg, MS: U.S. Army Engineer Waterways Experiment Station.

_____. 1956b. *Mississippi River and tributaries Old River control, low-sill structure*. Design memorandum No. 1B supplement No. 3. Vicksburg, MS: U.S. Army Engineer Waterways Experiment Station.

_____. 1959. *Mississippi River and tributaries Old River control*. Completion report–Low-sill structure. Vicksburg, MS: U.S. Army Engineer Waterways Experiment Station.

_____. 1963. *Review of soils design, construction, and performance observations low sill structure, Old River control*. Technical Report No. 3-602, prepared for Mississippi River Commission. Vicksburg, MS: U.S. Army Engineer Waterways Experiment Station.

U.S. Army Corps of Engineers (USACE), New Orleans District. 1967. *Mississippi River and tributaries, Old River low-sill structure*. 1967 Periodic Inspection. New Orleans, LA: USACE.

_____. 1969. *Mississippi River and tributaries, Old River low-sill structure*. 1969 Periodic Inspection. New Orleans, LA: USACE.

_____. 1971. *Mississippi River and tributaries, Old River low-sill structure*. 1971 Periodic Inspection. New Orleans, LA: USACE.

_____. 1972. *Old River low sill control structure, analysis of pile foundation*. Old River low sill control structure report No 03, Appendix E. New Orleans, LA: USACE.

U.S. Army Corps of Engineers (USACE). 1973a. *Mississippi River and tributaries emergency repairs to Old River control structures, Concordia Parish, Louisiana*. Low sill structure forebay plan and section, DACW29-74-R-0035, drawing 3 of 7. New Orleans, LA: U.S. Army Corps of Engineers, New Orleans District.

_____. 1973b. *Placement of Derrick stone and riprap at Old River control structure*. Contract No. DACW29-73-C-0275. New Orleans, LA: USACE.

_____. 1975a. *Old river low sill and overbank structures, stability analysis, Volume 1 text and appendixes*. Design Memorandum No. 12. New Orleans, LA: U.S. Army Corps of Engineers, New Orleans District.

_____. 1975b. *Old river low sill and overbank structures, stability analysis, Volume 2 plates*. Design Memorandum No. 12. New Orleans, LA: U.S. Army Corps of Engineers, New Orleans District.

_____. 1986. *Old River low sill control structure dewatering analysis*, Mississippi River and Tributaries Old River Control, LA. New Orleans, LA: USACE.

U. S. Army Corps of Engineers (USACE). 1995. *Engineering and design-gravity dam design*. Engineering Manual EM 1110-2-2200. Washington, DC: Department of the Army, Corps of Engineers, Office of the Chief of Engineers.

_____. 2003. *Engineering and design-slope stability*. Engineering Manual EM 1110-2-1902. Washington, DC: Department of the Army, Corps of Engineers, Office of the Chief of Engineers.

_____. 2009. *Old River Control brochure*. New Orleans, LA: U.S. Army Corps of Engineers, New Orleans District. https://www.mvn.usace.army.mil/Portals/56/docs/PAO/Brochures/OldRiverControlBrochure.pdf.

_____. 2016. *Low sill control structure, Periodic inspection report no. 15*. New Orleans, LA: U.S. Army Corps of Engineers, New Orleans District.

U.S. Department of Transportation Federal Highway Administration. 2006. *Design and construction of driven pile foundations*. FHWA NHI-05-042, Courses No. 132021 and 132022, Reference manual Vol. 1. Washington, DC: Federal Highway Administration.

Van Impe, W. F., and L. C. Reese. 2010. *Single piles and pile groups under lateral loading*. London, UK: CRC Press.

Wilson, H. K. 1978. *Grouting of scoured foundation Old River Low Sill structure, Louisiana*. Miscellaneous Paper, C-78-19. Vicksburg, MS: U.S. Army Engineer Waterways Experiment Station.

Winkley, B. R. 1994. Response of the Lower Mississippi River to flood control and navigation improvements. In *The variability of large alluvial rivers*, ed. S. A. Schumm and B. R. Winkley, 45-74. New York, NY: ASCE Press.

Appendix A: Site Characterization

Figure A1. Log of borings along the centerline axis of the LSS with elevations for excavations of gated structure and stilling basin (USACE 1954).

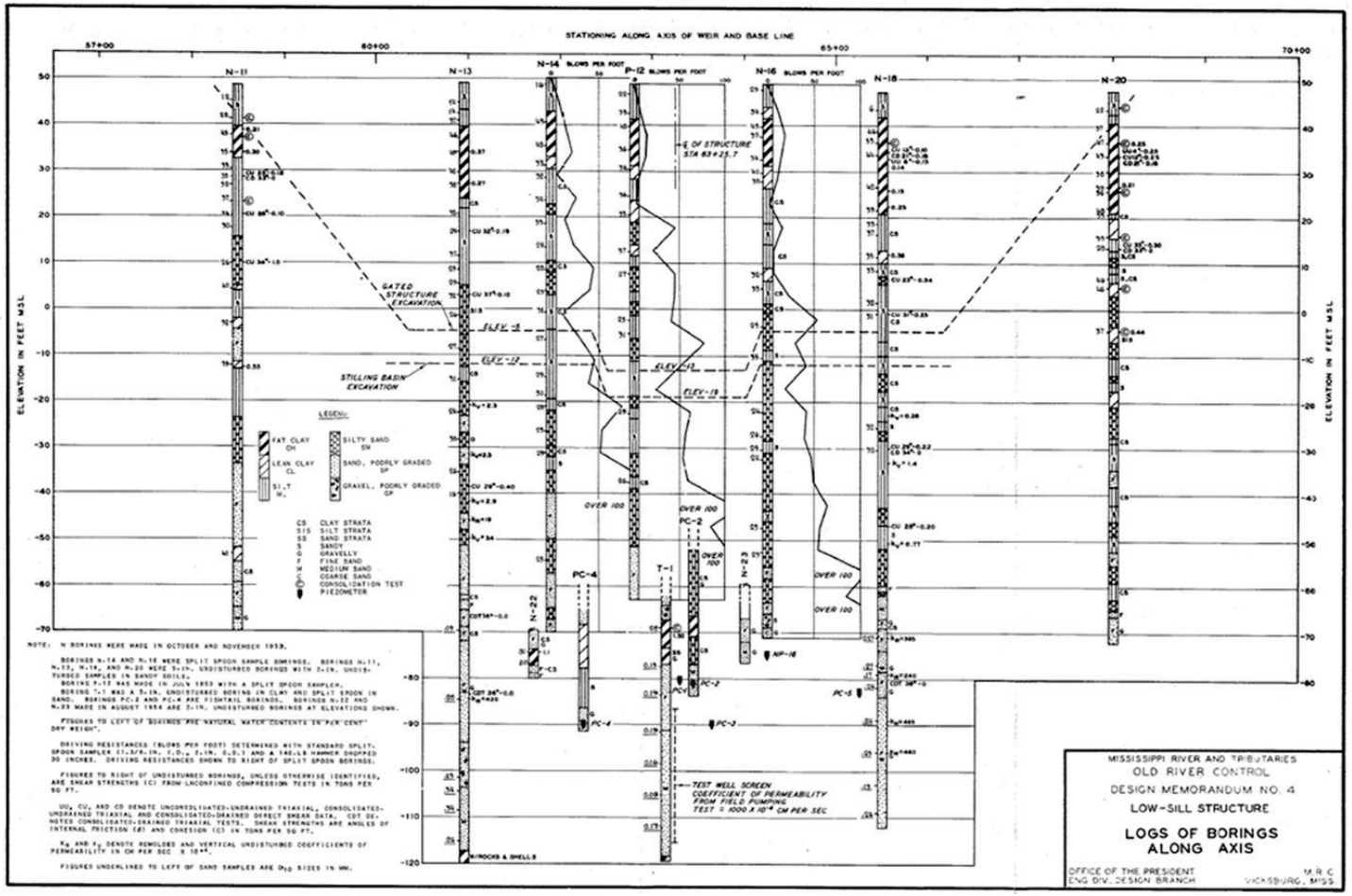

Figure A2. Log of borings along axis of overbank structure (USACE 1954).

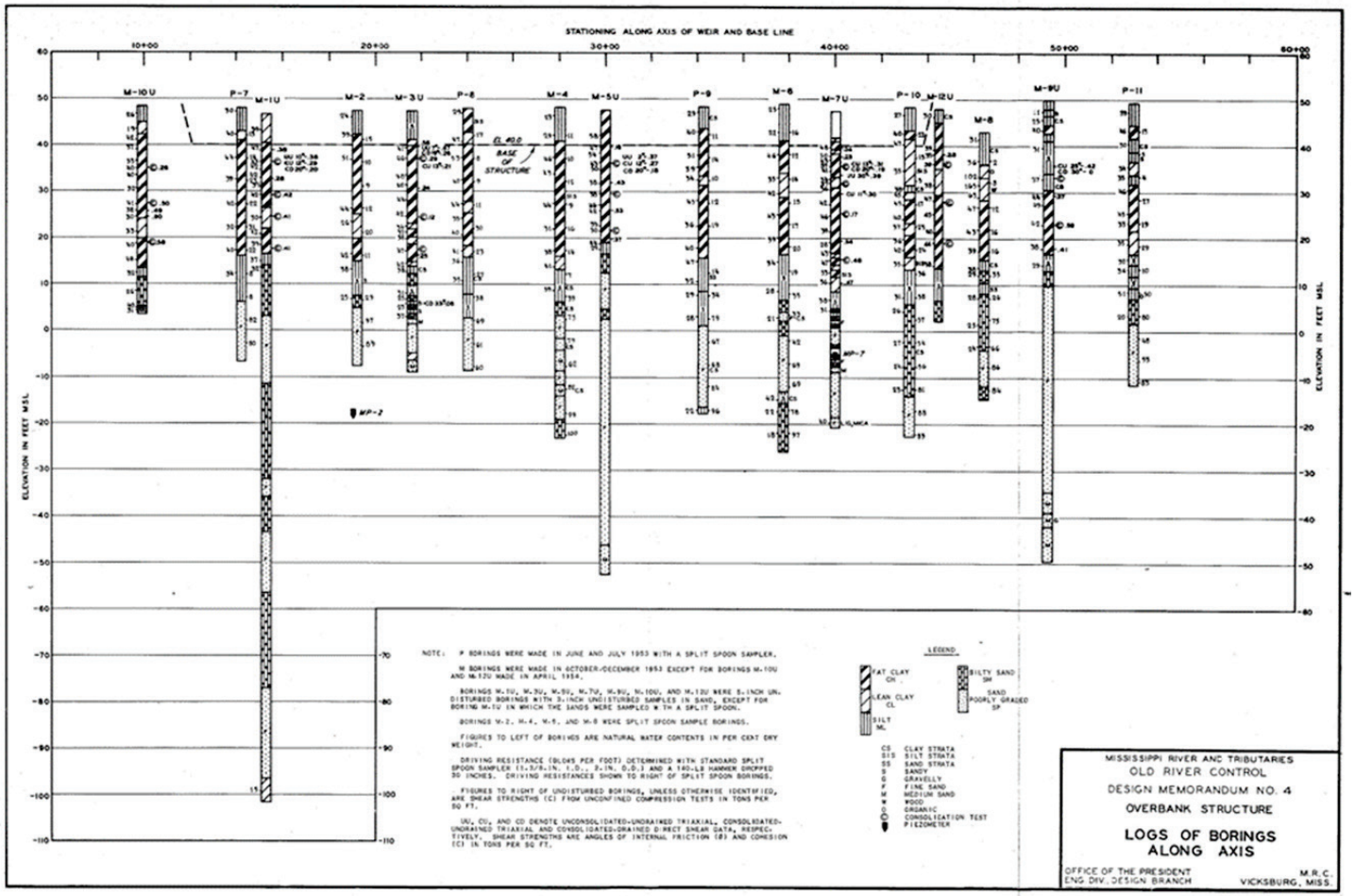

Figure A3. Generalized geologic profile along centerline of the channel showing depositional environments (USACE 1963).

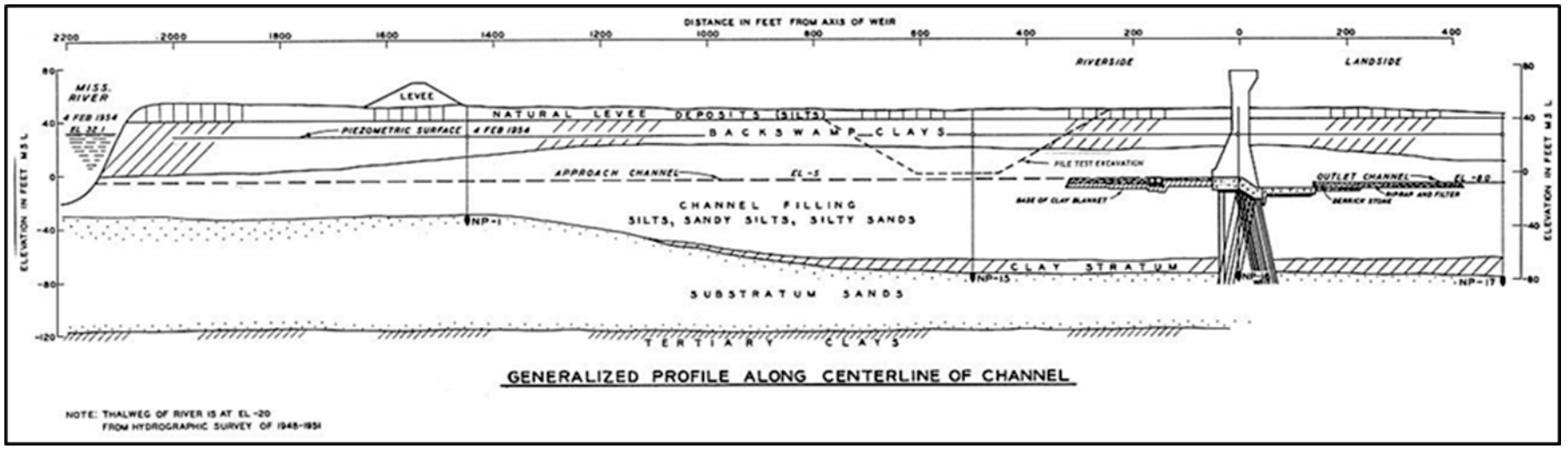

Figure A4. Log of borings along centerline of the channel showing USCS soils, water contents, and blow counts from spilt spoon samples (USACE 1954).

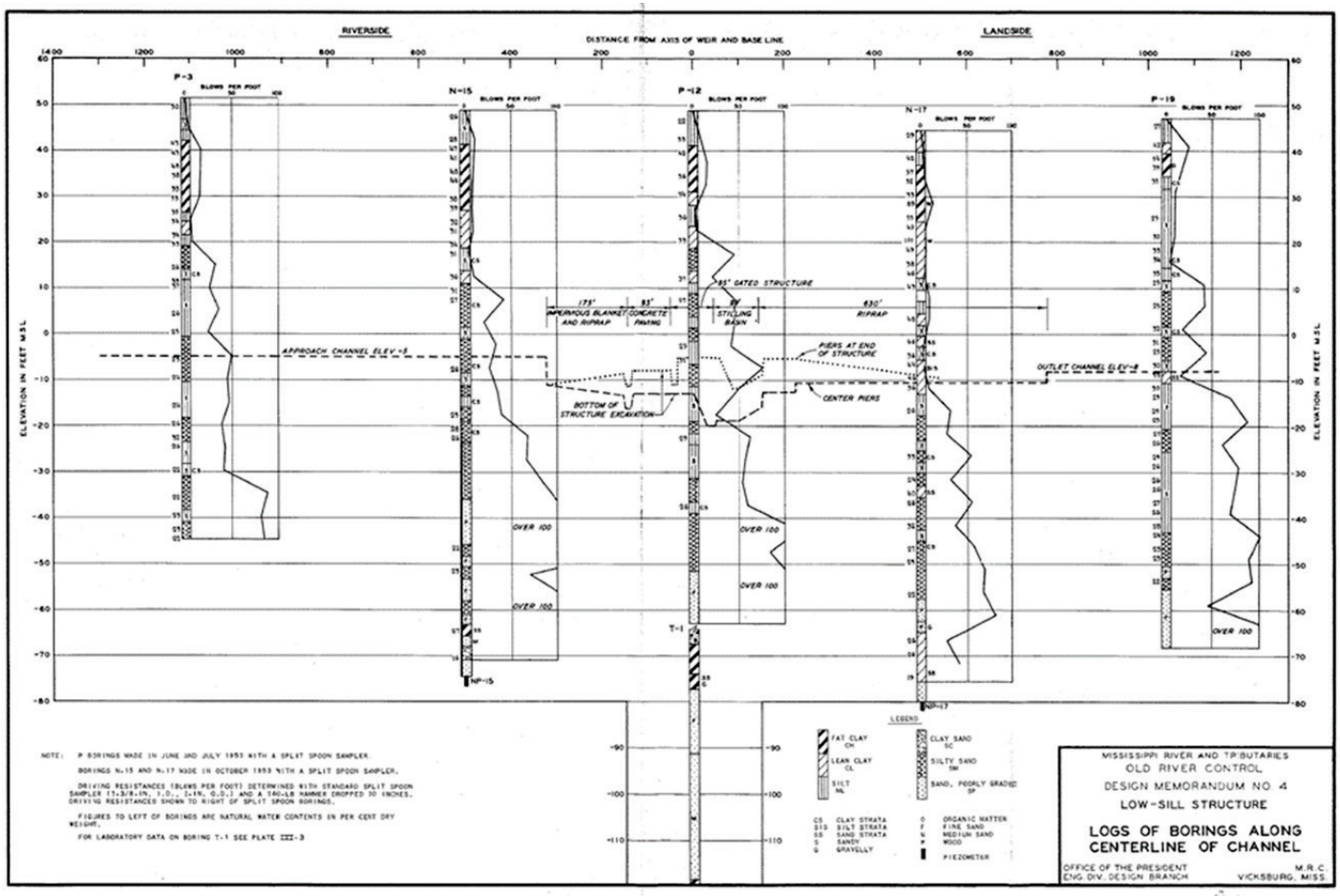

Figure A5. Summary of soil classification and compaction data (USACE 1954).

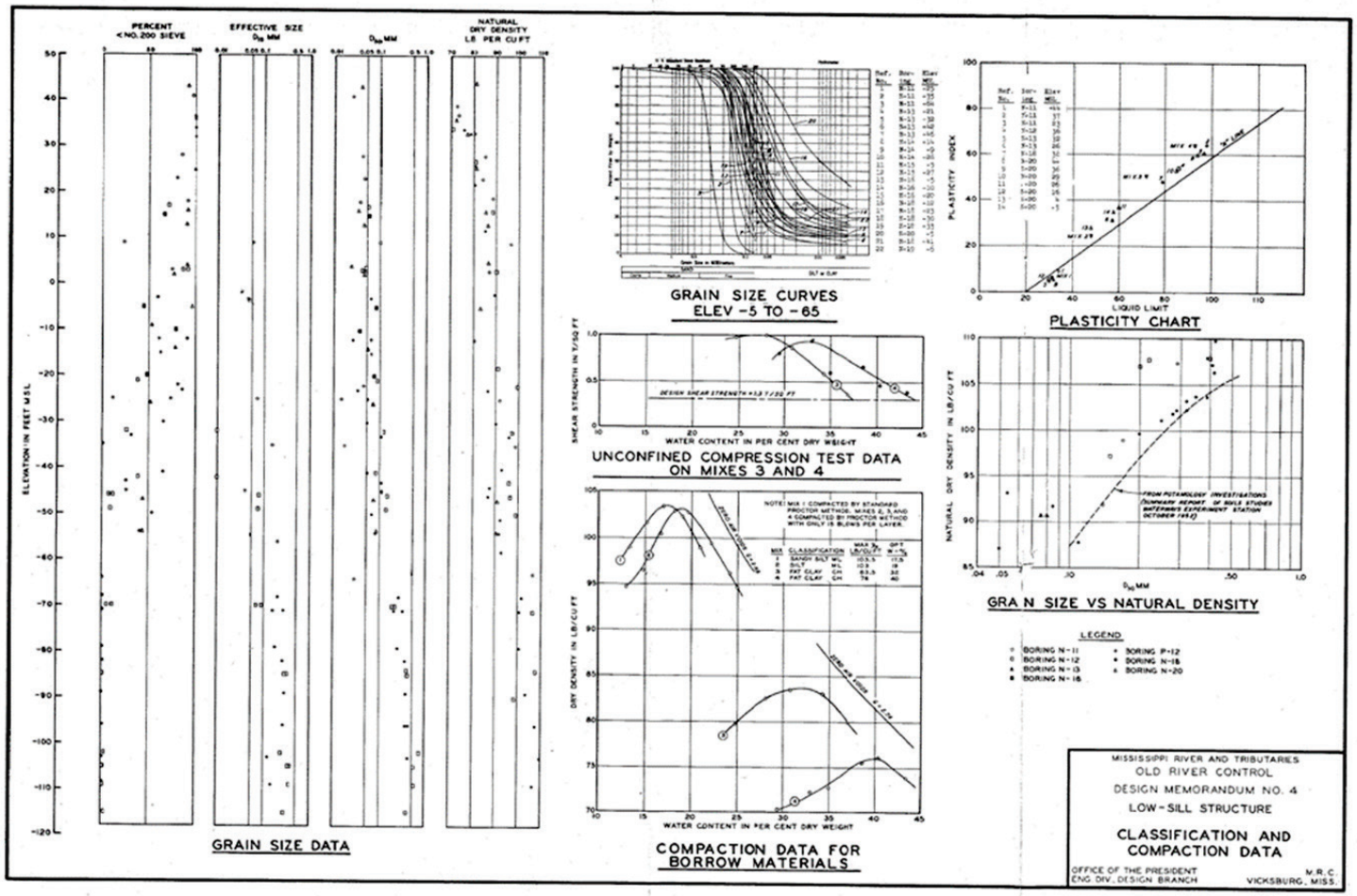

Figure A6. Summary of shear strength data (USACE 1954).

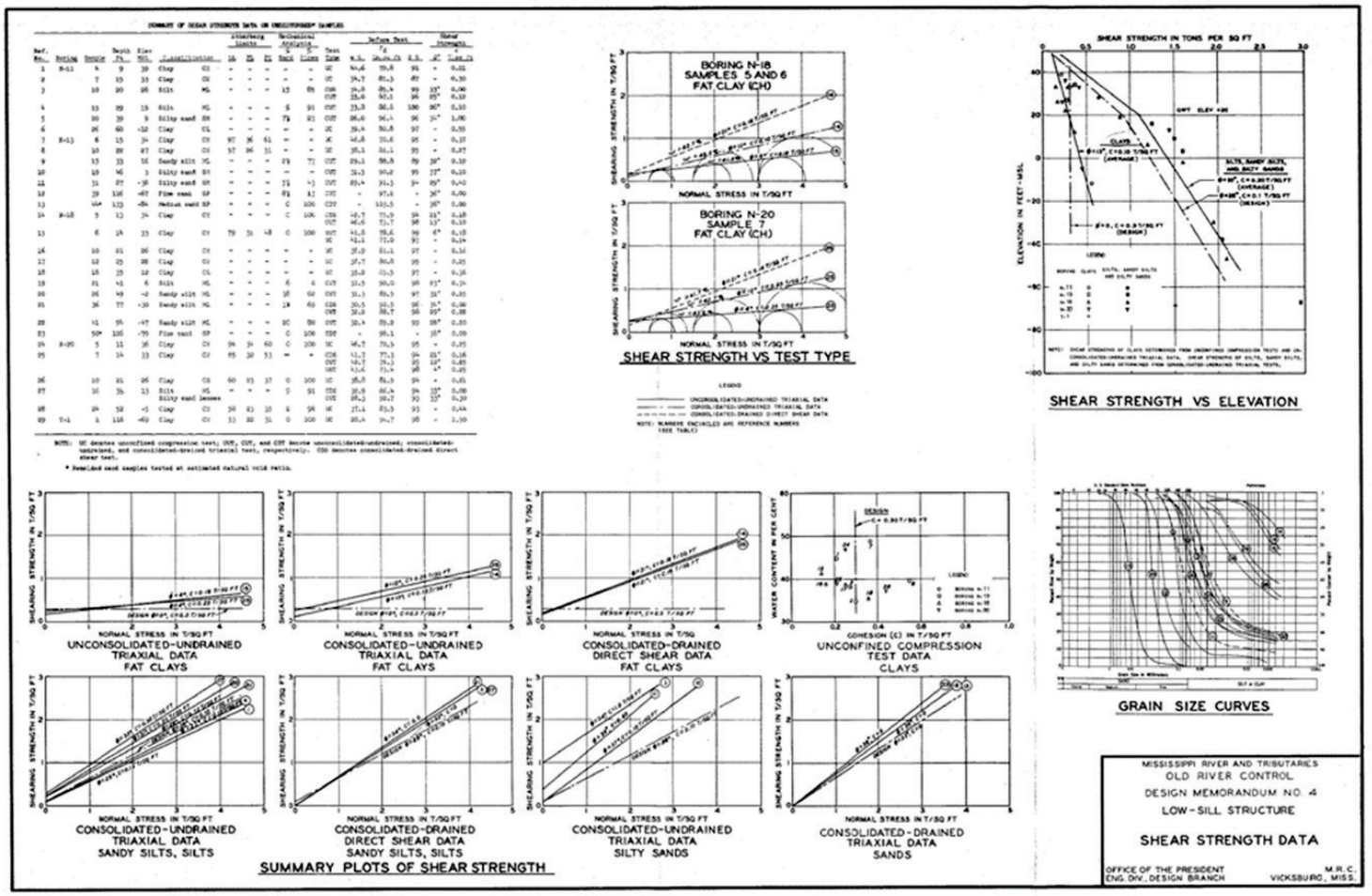

Figure A7. Summary of consolidation data (USACE 1954).

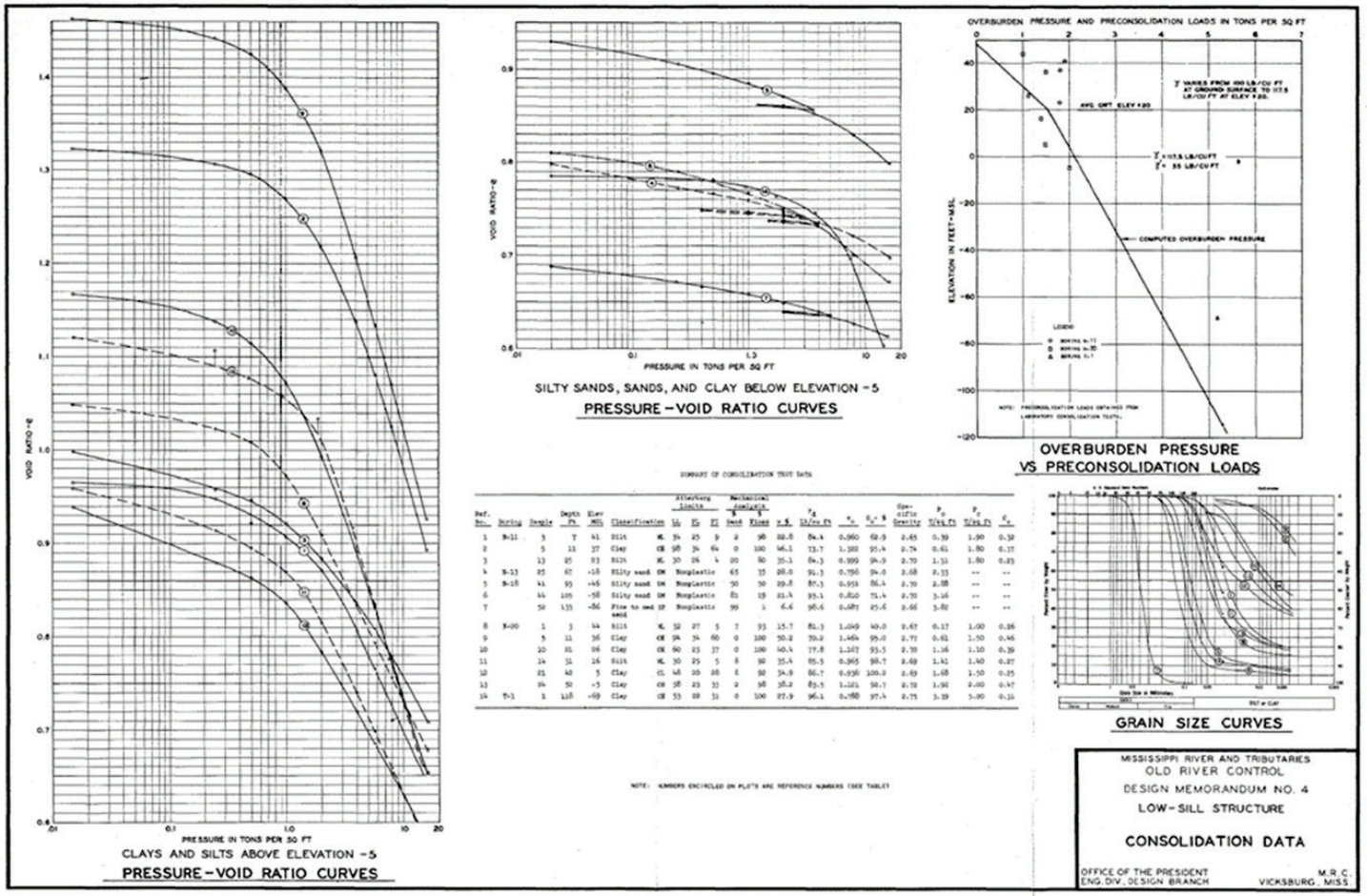

PLATE III-9

Figure A7. Summary of field pump test and permeability data (USACE 1954).

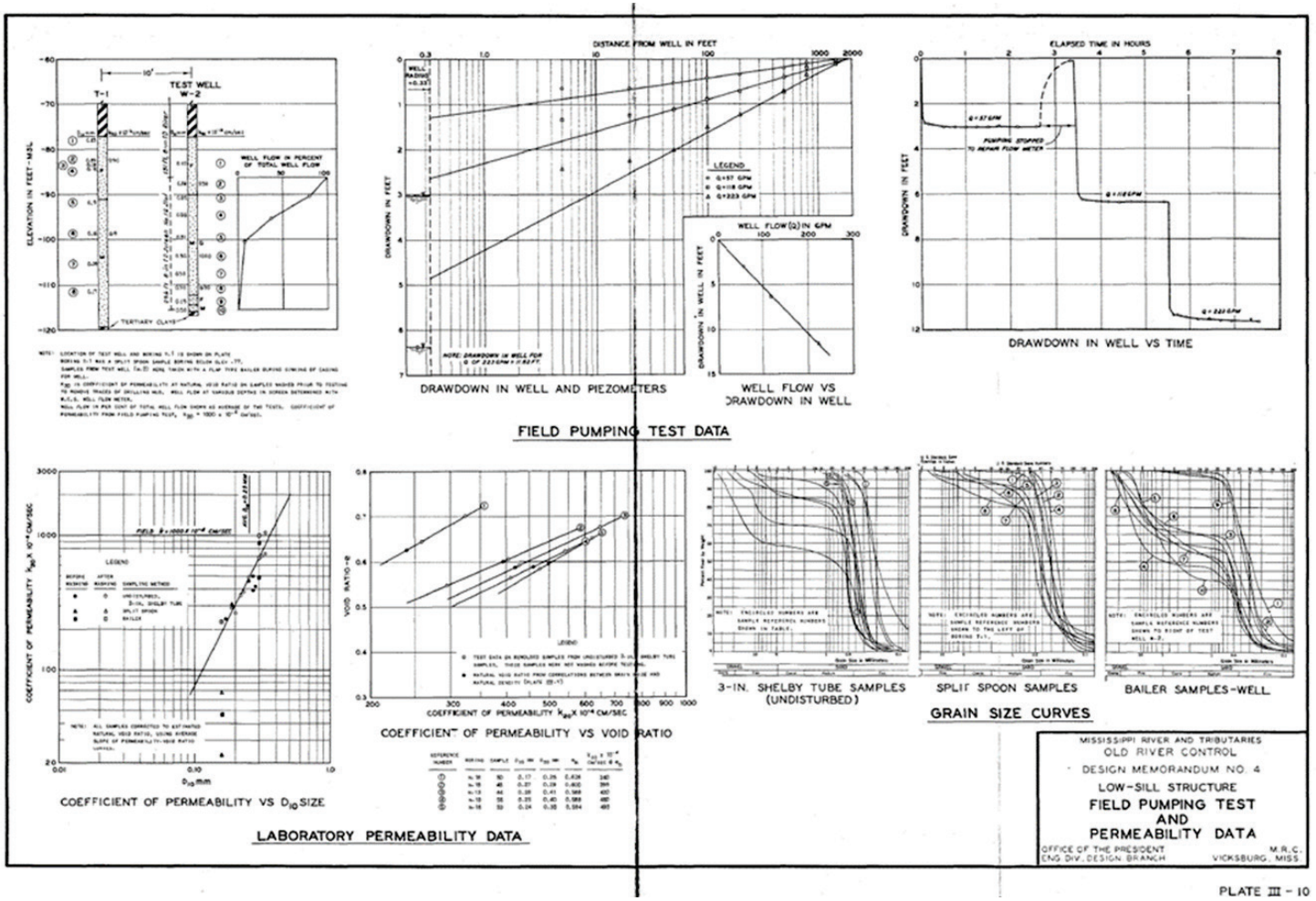

Figure A8. Profile along the B-line with important elevations noted (Wilson 1978).

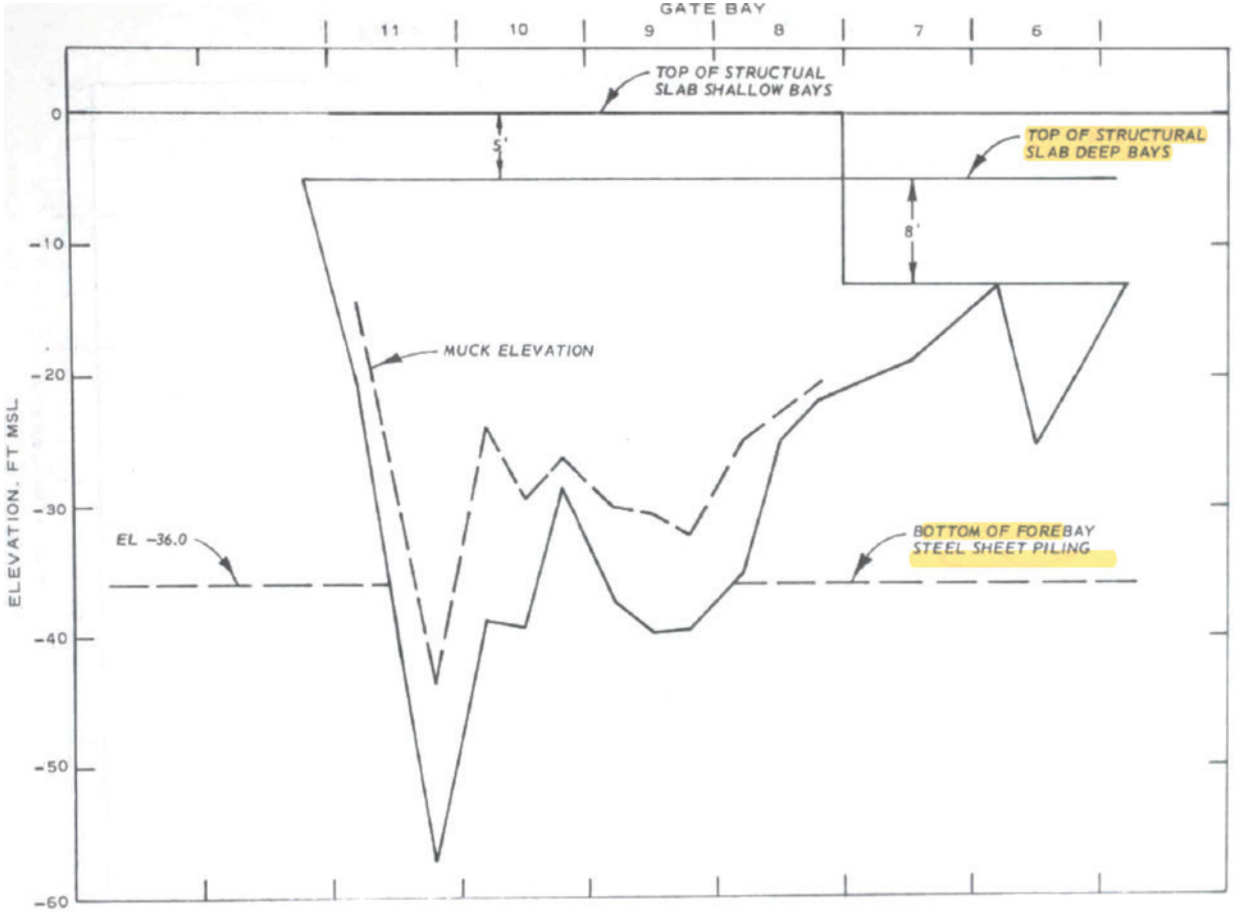

Figure A9. Profile along the C-line with important elevations noted (Wilson 1978).

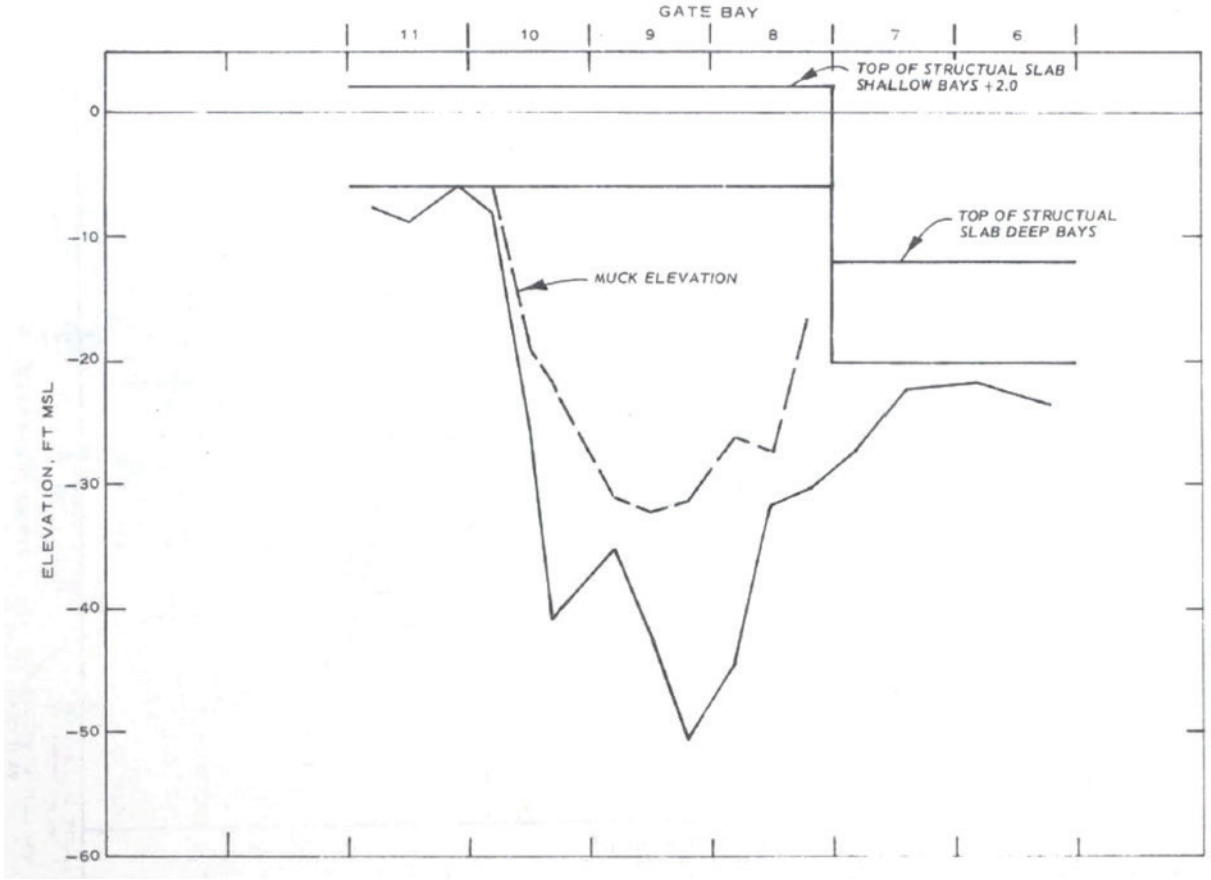

Figure A10. Profile along the D-line with important elevations noted (Wilson 1978).

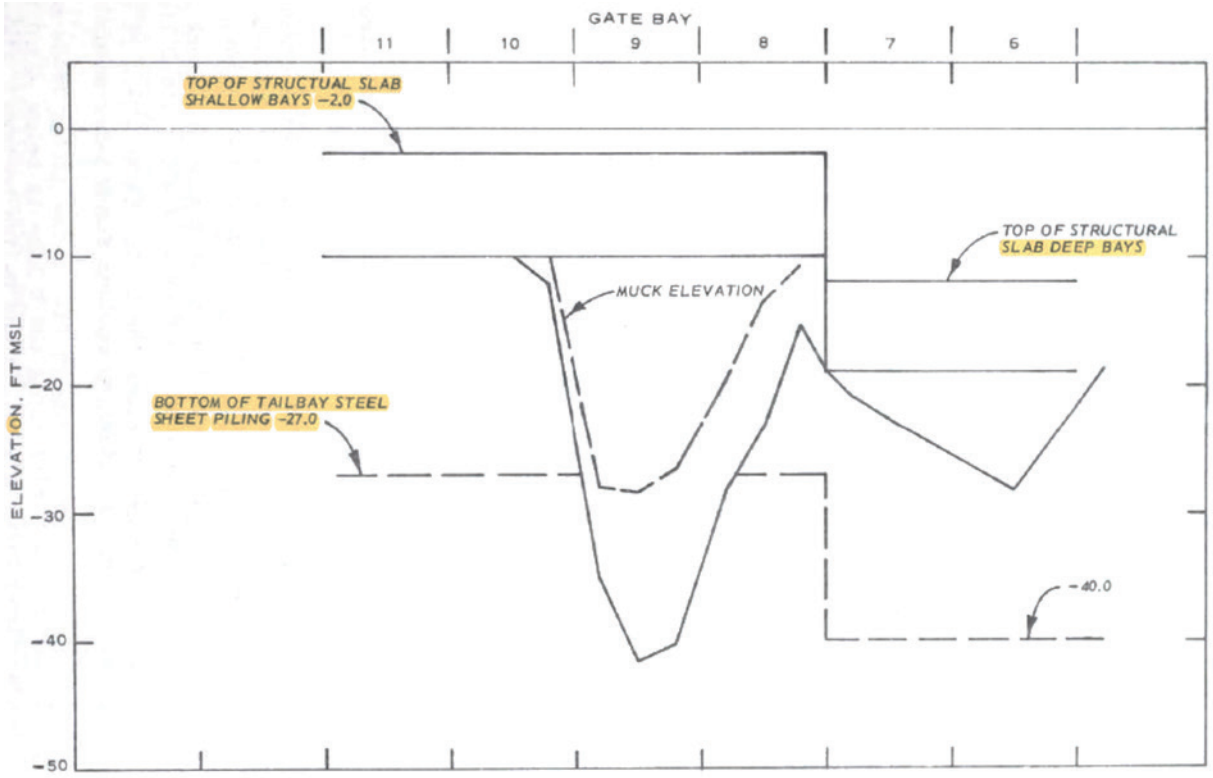

Figure A11. Boring locations and sheet pile elevations in profile used to determine void limits (Wilson 1978).

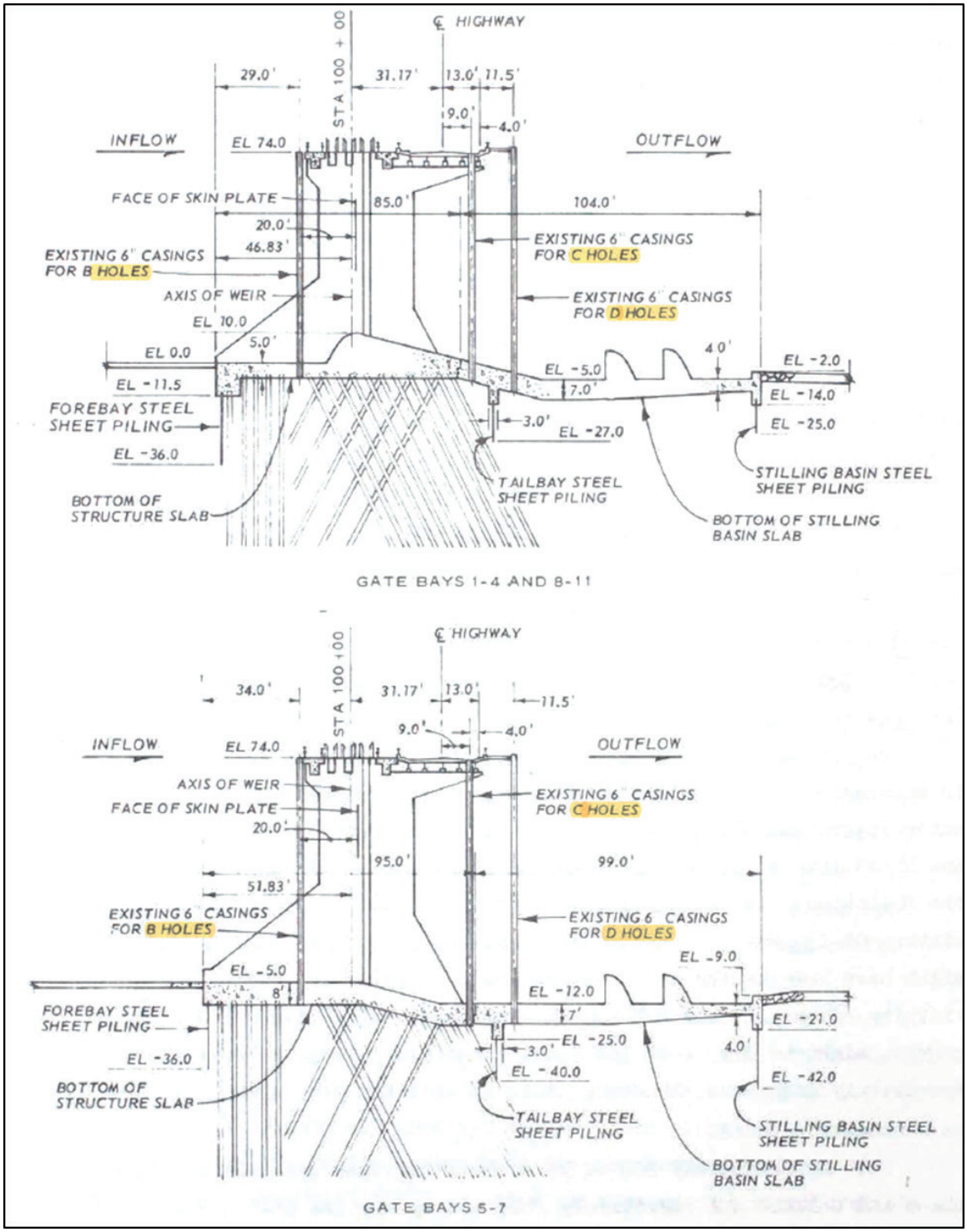

REPORT DOCUMENTATION PAGE

Form Approved
OMB No. 0704-0188

1. REPORT DATE *(DD-MM-YYYY)*	**2. REPORT TYPE**	**3. DATES COVERED** *(From - To)*
September 2022	Final	

4. TITLE AND SUBTITLE

Stability Analysis of Old River Low Sill Structure

5a. CONTRACT NUMBER

5b. GRANT NUMBER

5c. PROGRAM ELEMENT NUMBER

6. AUTHOR(S)

Lucas A. Walshire, Joseph B. Dunbar, and Benjamin R. Breland

5d. PROJECT NUMBER
478533

5e. TASK NUMBER

5f. WORK UNIT NUMBER

7. PERFORMING ORGANIZATION NAME(S) AND ADDRESS(ES)

Geotechnical and Structures Laboratory
U.S. Army Engineer Research and Development Center
3909 Halls Ferry Road
Vicksburg, MS 39180-6199

8. PERFORMING ORGANIZATION REPORT NUMBER

ERDC/GSL TR-22-22

9. SPONSORING / MONITORING AGENCY NAME(S) AND ADDRESS(ES)

New Orleans District (CEMVN)

New Orleans, LA 70160

10. SPONSOR/MONITOR'S ACRONYM(S)

11. SPONSOR/MONITOR'S REPORT NUMBER(S)

12. DISTRIBUTION / AVAILABILITY STATEMENT

Approved for public release; distribution is unlimited.

13. SUPPLEMENTARY NOTES

MIPR PA WI 1L8F7L

14. ABSTRACT

An updated stability analysis was performed on the Old River Low Sill Structure due to a change in the operating conditions from historic river sedimentation. Sedimentation of the Mississippi River channel since the 1973 spring flood has caused higher river stages at lower discharges. Numerical methods used included nonlinear analysis of pile group stability, seepage analyses, and limit equilibrium methods. The structure's foundation was compromised during the 1973 flood, and emergency repairs were conducted to prevent scouring and undermining of the foundation by the flood scour. Rehabilitation included the reconstruction of a failed wing wall on the left abutment, rock and riprap fill in the forebay channel, and emergency grouting to fill the scour hole beneath the structure. An operating restriction was emplaced to limit the differential head across the structure due to flood damage. Taking these conditions into account, results from an updated analysis showed that full headwater uplift caused increased tension in the piles, while the increased body load caused increased compressive loads in the piles. Review of piezometric monitoring and the seepage analyses showed that full headwater uplift is unlikely, indicating the foundation grouting adequately sealed the scour hole beneath the structure. Analysis results exhibited lower magnitude compression and tension loads in the piles with design load cases compared to previous analyses. Recommendations from these analyses indicate that increased monitoring and additional investigation may support increasing the differential head limitation.

15. SUBJECT TERMS

Stability
Dam
Low sill structure
Old River Low Sill Structure (La.)
Structural analysis (Engineering)
Hydraulic structures–Foundations–Stability

16. SECURITY CLASSIFICATION OF:			**17. LIMITATION OF ABSTRACT**	**18. NUMBER OF PAGES**	**19a. NAME OF RESPONSIBLE PERSON**
a. REPORT	**b. ABSTRACT**	**c. THIS PAGE**			**19b. TELEPHONE NUMBER** *(include area code)*
Unclassified	Unclassified	Unclassified	SAR	118	